JAERI-Review
94-008

JAERI TANDEM & V.D.G. ANNUAL REPORT 1993
April 1, 1993 ~ March 31, 1994

November 1994

Department of Reactor Engineering

日本原子力研究所
Japan Atomic Energy Research Institute

本レポートは，日本原子力研究所が不定期に公刊している研究報告書です。

入手の問合わせは，日本原子力研究所技術情報部情報資料課（〒319-11 茨城県那珂郡東海村）あて，お申しこみください。なお，このほかに財団法人原子力弘済会資料センター（〒319-11 茨城県那珂郡東海村日本原子力研究所内）で複写による実費領布をおこなっております。

This reports are issued irregularly.

Inquiries about availability of the reports should be addressed to Information Division Department of Technical Information, Japan Atomic Energy Research Institute, Tokaimura, Naka-gun, Ibaraki-ken 319-11, Japan.

© Japan Atomic Energy Research Institute, 1994

編集兼発行　日本原子力研究所

印　　刷　ニッセイエブロ株式会社

JAERI-Review 94-008

JAERI TANDEM & V.D.G.
Annual Report
1993
April 1, 1993 - March 31, 1994

Department of Reactor Engineering

Tokai Research Establishment
Japan Atomic Energy Research Institute
Tokai-mura, Naka-gun, Ibaraki-ken

(Received October 20, 1994)

This annual report describes research activities which have been performed with the JAERI tandem accelerator and the Van de Graaff accelerator from April 1, 1993 to March 31, 1994. Summary reports of 43 papers, and list of publications, personnel and cooperative researches with universities are contained.

Keywords: JAERI TANDEM, V.D.G., Nuclear Sturcture, Nuclear Reaction, Nuclear Theory, Atomic Physics, Solid State Physics, Radiation Effects in Materials, Progress Report

---

Editors: Yasuo SUZUKI, Hiroshi IKEZOE, Akira IWAMOTO, Yukio KAZUMATA, Nobuo SHINOHARA, Suehiro TAKEUCHI and Takashi OKABE

JAERI-Review 94-008

原研タンデム，バンデグラフ加速器
1993年度年次報告

日本原子力研究所東海研究所
原子炉工学部

（1994年10月20日受理）

本年次報告は，原研タンデム及びバンデグラフ加速器で，1993年4月1日から1994年3月31日までの間に東海研で行われた研究活動をとりまとめたものである。

(1) 加速器運転と開発研究 (2) 核構造 (3) 核反応 (4) 核理論 (5) 原子物理 (6) 固体物理及び材料の放射線効果の6部門にまたがる43編の研究報告，公表された文献，関与した職員及び大学等との協力研究のリストを収録している。

東海研究所：〒319-11 茨城県那珂郡東海村白方字白根2-4
（編集者） 鈴木康夫，池添 博，岩本 昭，数又幸生，篠原伸夫，竹内末広，岡部 隆

PREFACE

This report covers research and development activities during the period April 1, 1993 until March 31, 1994 at the tandem accelerator facility at JAERI, Tokai.

During this period, the tandem accelerator was operated over 4000 hours and supplied stable beams to experiments in the fields of : (1) Accelerator Development, (2) Nuclear Structures, (3) Nuclear Reactions, (4) Atomic Physics and (5) Solid State Physics and Radiation Effects in Materials. Forty-three research programs have been carried out by the JAERI staff and collaborators from universities and national laboratories; more than fifty researchers outside JAERI have collaborated with about fifty members of JAERI staff.

The JAERI superconducting booster for the tandem accelerator has been constructed and the commissioning test with ion beams from the tandem accelerator started from November 1, 1993, after the accomplishment of the cryogenic test, cavity test and RF test.

A recoil mass spectrometer for the tandem booster was under construction. It will be installed at the beam line of the tandem booster in April of 1995 and will be used for many kinds of experiments.

From this fiscal year, the activities at the tandem accelerator have been taken charge of, by Department of Reactor Engineering in place of Department of Physics due to the reformation of research divisions at JAERI.

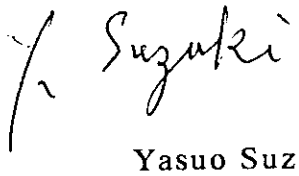

Yasuo Suzuki
Deputy Director
Departement of Reactor Engineering

Contents

1. Accelerator Operation and Development ····· 1
1.1 Tandem Accelerator Operation ····· 3
1.2 Superconducting Booster ····· 5
1.3 Control System for JAERI Tandem Accelerator ····· 7
2. Nuclear Structures ····· 9
2.1 Lifetimes of Excited States in ^{105,107}Sn ····· 11
2.2 Nuclear Moments of Radioactive Nuclide, ^{143}Pr($T_{1/2}$=13.6 d), by Collinear Laser-Ion-Beam Spectroscopy ····· 12
2.3 High-Spin States Above a High-Spin Isomer in ^{145}Sm ····· 14
2.4 High-Spin States of ^{147}Eu ····· 16
2.5 High-Spin States of ^{148}Tb ····· 18
2.6 Two-Phonon γ-Vibrational State in ^{166}Er ····· 20
2.7 Development of a New-Type Electron Spectrometer for Spectroscopy of Heavy Nuclei ····· 21
2.8 The Multiple-Target System for a Gas-Jet Type ISOL ····· 23
3. Nuclear Reactions ····· 25
3.1 Feshbach-Kerman-Koonin Model Analysis of Preequilibrium (p, p') and (p, n) Reactions at Low Incident Energies ····· 27
3.2 Measurements of Activation Cross Sections at 18-30 MeV by Using the ^{7}Li(p, n) Quasi-Monoenergetic Neutron Source at JAERI-TANDEM ··· 29
3.3 Observation of Nuclear Rainbow Scattering in the ^{16}O+^{16}O System at E_{lab}=124MeV and 145MeV ····· 31
3.4 Elastic and Inelastic Scattering of ^{58}Ni+^{60}Ni Near the Coulomb Barrier ····· 33
3.5 Investigation of the Multi-Nucleon Transfer Reaction (^{18}O, ^{14}O) for Neutron-Rich Nuclei ····· 35
3.6 Spin Assignments of Intermediate Structures in ^{12}C(^{16}O, ^{12}C(2_1^+)) ^{16}O Using the γ-Ray Recoil Method ····· 36
3.7 3-α Coincidence Measurements from the ^{16}O+^{12}C Reaction at 90 MeV ·· 38
3.8 Measurements of Capture Cross Sections between Heavy Ions ····· 40
3.9 Transition of the Fission Mechanism in the Proton-Induced Fission of ^{238}U Around E_x= 14MeV ····· 42
3.10 Study of the U + Li Reaction for the Synthesis of Americium Isotopes ····· 44

3.11 Entrance-channel Dependence of Sub-Barrier Fusion Cross Sections in Fermium (Z=100) Region ····· 45
3.12 Fragment Mass and Kinetic Energy Distributions in Fission of Z_{CN}=100 ····· 46
3.13 Heavy-Ion-Induced D-D Fusion in Deuteride Solid ····· 47
4. Nuclear Theory ····· 49
4.1 Applications of IBM-3 to the Z ∼ N ∼ 40 Nuclei ····· 51
4.2 Quantum Molecular Dynamics Calculation of Nucleon-Nucleus Reactions· 53
4.3 Improvement of Quantum Molecular Dynamics ····· 55
4.4 Generalization of Nucleus-Nucleus Potential ····· 57
5. Atomic Physics ····· 59
5.1 Projectile Charge State Dependence of Binary Electron Production for 1MeV/u Au^{q+} (q=12-37) Ion Impact on He ····· 61
5.2 Charge State Distribution of Neon Recoil Ion by Carbon Ion Impact in Coincidence with Projectile Final Charge States ····· 63
6. Solid State Physics and Radiation Effects of Materials ····· 65
6.1 X-ray Study of Irradiation Defects Caused by MeV Ion Implantation into Si Perfect Crystals II ····· 67
6.2 Electrical Conductivity Change of Synthetic Single Crystal Diamond by Ion Irradidtion ····· 69
6.3 Electrical and Structural Properties of Li-Ion Irradiated β-LiAl ·· 71
6.4 Ion Irradiation Effects on $EuBa_2Cu_3O_y$ Thin Films ····· 74
6.5 Effective Activation Energy of Proton Irradiated QMG-YBCO ····· 76
6.6 Effect of 180MeV Cu^{11+} Irradiation on $YBa_2Cu_3O_x$ and $Bi_2Sr_2CaCu_2O_y$··· 78
6.7 Bi2212 Tapes Irradiated by 120MeV Oxygen Ions ····· 80
6.8 Radiation Damage of UO_2 Implanted with 100MeV Iodine Ions up to Fluences Over an Extended Range ····· 82
6.9 Radiation Dameges in Li_4SiO_4 Irradiated by High Energy Oxygen Ions · 84
6.10 Radiation Damages in Vitreous Silicas Induced by High Energy N^{+5} and Cu^{+12} Ions Irradiation ····· 86
6.11 Single Event Effect in Power MOSFETS by High-Energy Carbon Ion ····· 88
6.12 Response of Silicon Suface Barrier Detector to Heavy Ions ····· 89
6.13 Effect of Gamma-Ray on Etching of Heavy Ion Track in Polyimide(2)··· 91
7. Publication in Journals and Proceedings, and Contributions to Scientific Meetings ····· 93
8. Personnel and Committees ····· 111
9. Cooperative Researches ····· 121

1. Accelerator Operation and Development

1.1 TANDEM ACCELERATOR OPERATION

Tandem Accelerator Group

The scheduled operation for experiments was performed through the past one year containing two short periods for the scheduled maintenance. Throughout the year, the accelerator ran smoothly. The accelerator running time was 4137.6 hours. The following are the summary of the operation from April 1, 1993 to March 31, 1994.

1) Time distribution by terminal voltage

>16 MV	75 days	38.7 %	11-12 MV	12 days	6.2 %
15-16	62	32.0	10-11	3	1.5
14-15	13	6.7	9-10	4	2.1
13-14	9	4.6	8- 9	3	1.5
12-13	10	5.2	< 8	3	1.5

2) Time distribution by projectile

^{1}H	11 days	^{18}O	6 days	^{54}Fe	3 days
$^{2}H2$	1	^{19}F	6	^{56}Fe	7
^{7}Li	7	^{28}Si	2	^{58}Ni	19
^{11}B	2	^{31}P	3	^{59}Co	9
^{12}C	9	^{32}S	5	^{63}Cu	9
^{13}C	11	^{35}Cl	17	^{79}Br	1
^{14}N	1	^{37}Cl	9	^{127}I	13
^{16}O	27	^{45}Sc	6	^{197}Au	6

3) Time distribution by activity

Operation for research		194 days
Atomic and solid state physics	(34 days)	
Radiation effects in materials	(19)	
Nuclear chemistry	(27)	
Nuclear physics	(86)	
Fast neutron physics	(8)	
Radiation chemistry	(4)	
Detector development	(3)	
Accelerator test	(11)	
Others	(2)	
Voltage conditioning		4 days
Operation training		2 days
Scheduled maintenance (2 tank openings)		85 days

Unexpected repair	(1 tank opening)	10 days
Holidays and vacation		70 days

A charging chain broke in May 13th 1993 when 14MV operation with beam acceleration. The chain was installed two months ago and had operated for 1,411 hours. Fortunately, damage was slight in the column components. It is obvious that the cause of trouble was shortage of the lubrication oil between the chain and the drive pulleys. Consequently, strong twist force attacked the nylon links of the chain. We presume that the automatic oil feeder stopped at least two months ago.

The construction of the tandem booster has almost completed in November 1993. The beam test is under going successfully. This item will be reported in later paragraphs.

1. 2 SUPERCONDUCTING BOOSTER

S. TAKEUCHI

The superconducting booster for the tandem accelerator was completed in October 1993 after 4 year research and development and 6 year construction since 1984. Beam testing has started with a successful result.

The booster is an independently phased linac composed of 46 superconducting resonators made of niobium and copper. The booster structure is illustrated in Fig. 1. Forty of them are used for acceleration and housed in ten cryostats, four for bunching in two cryostats and two for de-bunching. Forty-four resonators are all the same. Their frequency is 129.8 MHz. The bunching system is a double drift harmonic buncher. Two resonators for bunching have the frequency of 259.6MHz. The booster is equipped with two 250 watts helium refrigerators and liquid helium tranfer lines. By the end of FY 1992, all the resonators, their cryostats and refrigerators have been set ready for use.

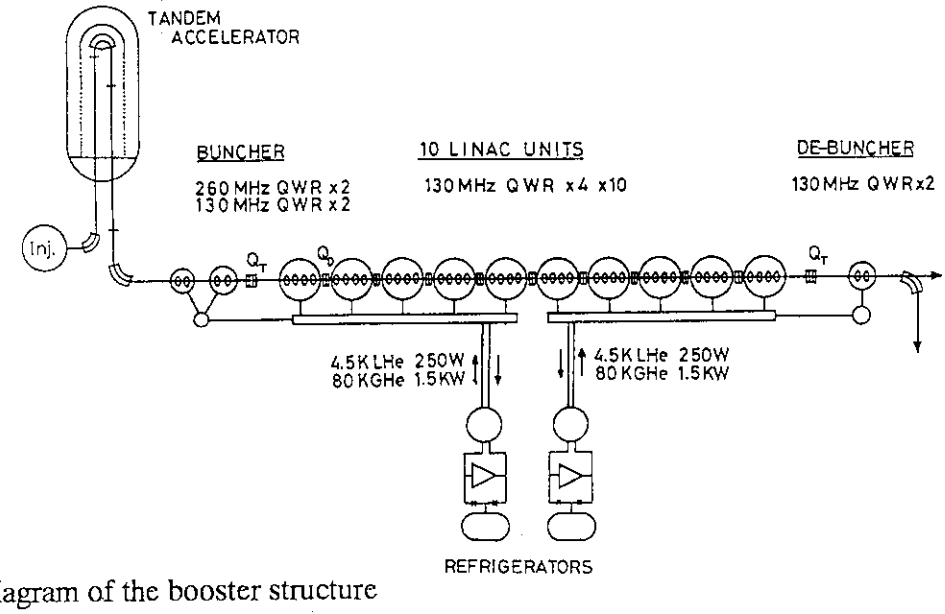

Fig. 1. Diagram of the booster structure

From the end of FY 1992 to October of this fiscal year, installation work of various components, such as beam line components, their control circuits, safety interlocks systems, resonator control modules, rf power amplifirs, rf cables and control cables, was done.
In the meantime, refrigerating systems with resonators were operated three times for learning operation, for opimizing control parameters of the systems and for resonator testing without beams. Several difficulties were found in the test runs. We could not have enough flow of liquid helium to the 5th unit of the linac. We had to open its flow adjusting valve much wider than others. The refrigerating system A had instability in the cold box; one of two expansion turbines continued a harmful oscillation of rotating frequency and was changed to a new one. The system B was troubled for a while with noise causing a big change of rotating frequency of turbines. In addition to the test runs, an annual inspection by ourselves, which is oblidged by regulation, was done for the first time with the whole high pressure system.

Resonator Q values were measured in the test runs of the refrigerating systems. In off-line tests, an appreciable Q-degradation occured with our niobium resonators, when the cooldown rate was smaller than 20K/h at about 120K[1]. With the refrigerators that cool down the resonators at a rate of 10 K/h, we found that the first 16 resonators had severe Q-degradation of 30 - 70 % compared to the fast cooldown data. But, the last 24 resonators, which were built one year later than the first 16 ones, had no severe Q-degradation. This is believed to be improved by feeding nitrogen gas bubbles into the electro-polishing solution in the final surface

treatment of niobium in order to prevent hydrogen from entering niobium walls[2]. The accelerating fields for the Q-degraded resonators were 3 - 5 MV/m with an rf input of 4 watts. We found another problem that many of the resonators had lower frequencies than the tunable range of 129.800-129.815MHz. The frequency adjustment we did at the room temperature was found to be not appropriate. The part which was deformed with too much stress recovered to some extent in thermal cycles.

On October 26, 1993, every thing had been completed for beam acceleration and the booster facility was inspected with respect to the radiation safety and approved by the authority for the safety law. The next day, beams of Cl^{10+} from the tendem accelerator were injected into the booster and passed through it, successfully. In November, beam acceleration test was carried out with beams of Cl^{10+} 164MeV(β= v/c= 0.1) from the tandem. The beams were bunched well. An energy-and-time spectrum was measured by a detector composed of Au target and Si detector located at the entrance of the linac. The spectrum showed that the beam bunch width was 0.3 nS and that 80 % of the incident beams were bunched. In acceleration, resonator field amplitudes and phases were set one by one by monitoring beam-bunch phases at beam-bunch phase detectors located after No.3, No. 6 and No.10 liniac units. The phase detectors worked very well in the resonator phase setting. As a result of the first acceleration test, we succeeded in accelerating the beams to 261 MeV by using 25 resonators operated at accelerating field gradients of 3 MV/m and at a frequency of 129.796 MHz . The energy spectrum measured at the end of the linac is shown in Fig. 2, in which every spectrum after resonator setting is superimposed.
The rest 15 resonators were not used mainly because their frequencies were lower than 129.796 MHz and partly because the 5th unit was out of liquid helium. The refrigerating system A had a big change of helium pressure on the resonator walls, when an rf power input was increased and liquid helium levels in the cryostats recovered to full after some decrease. It caused a big frequency change (nearly 100 Hz) to the resonators and made it difficult to lock resonator phases at high accelerating field gradients.
Then, all the cryostats except the 259.6 MHz sub-bunching unit were opened. With most of the resonators, frequencies were re-adjusted by a right method of deforming outer conductors. Frequency stabilizing supports were put on end-plates which are the most pressure sensitive walls of the resonators. They decreased the frequency change by a factor of 5. The work has finished by the end of FY 1993 and the cooldown for the second beam acceleration testing started.

We repeat testing with different heavy ions in the FY 1994. A complete test result will be presented in the next annual report.

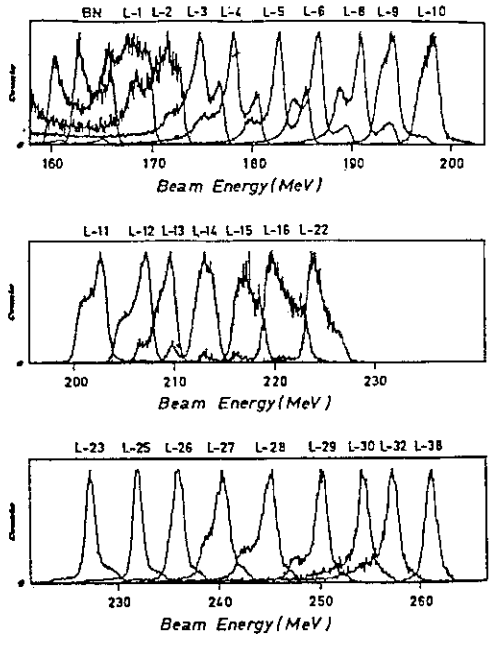

Fig. 2. Superimposed beam energy spectrum in resonator set-up

References
1) T. Ishii, M. Shibata and S. Takeuchi, Nucl. Instr. and Methods A328(1993)231-235.
2) M. Shibata, to be published in "Proc. of the 6th Workshop on RF Superconductivity, CEBAF, Oct. 1993"

1.3 CONTROL SYSTEM FOR JAERI TANDEM ACCELERATOR

S.HANASHIMA

Originally, control system for the JAERI tandem accelerator was based on mini-computers and a CAMAC serial highway system for I/O interface[1]. However we had some difficulties to stay on the base, such as the difficulty in maintenance of the old computers and shortage of the computing power for an expansion of the system. So we made renewal of control computer.

The new control system is utilizing transputer[2] and concurrent processing technology. We call the system ACCELL[3]. Figure 1 shows a block diagram of the new system. The new system is divided into 1)a host system using a work station, 2)a central system, 3)serial highway drivers, 4)a CAMAC serial highway system[4,5] and 5)two personal computers. The main roles of the host system are to support execution of the central system and to work as a part of man-machine interface. Data of the central system needed to control the accelerator are loaded from the host. A bit map display of the host is embedded in the operator console of the accelerator. Programs based on X-window system[6] are used on the display. Connection to the central system is an INMOS link[2] and a S-bus link adapter. The host system is also used as a file server. The central system is a multi processor of four T800 transputers[2] with local memory of one Mbytes to 16 Mbytes. It works as a main element of data processing. The serial highway drivers are front end processors of the central system to CAMAC system. Transputers are also used in the drivers. They have charge of low level control of the CAMAC serial

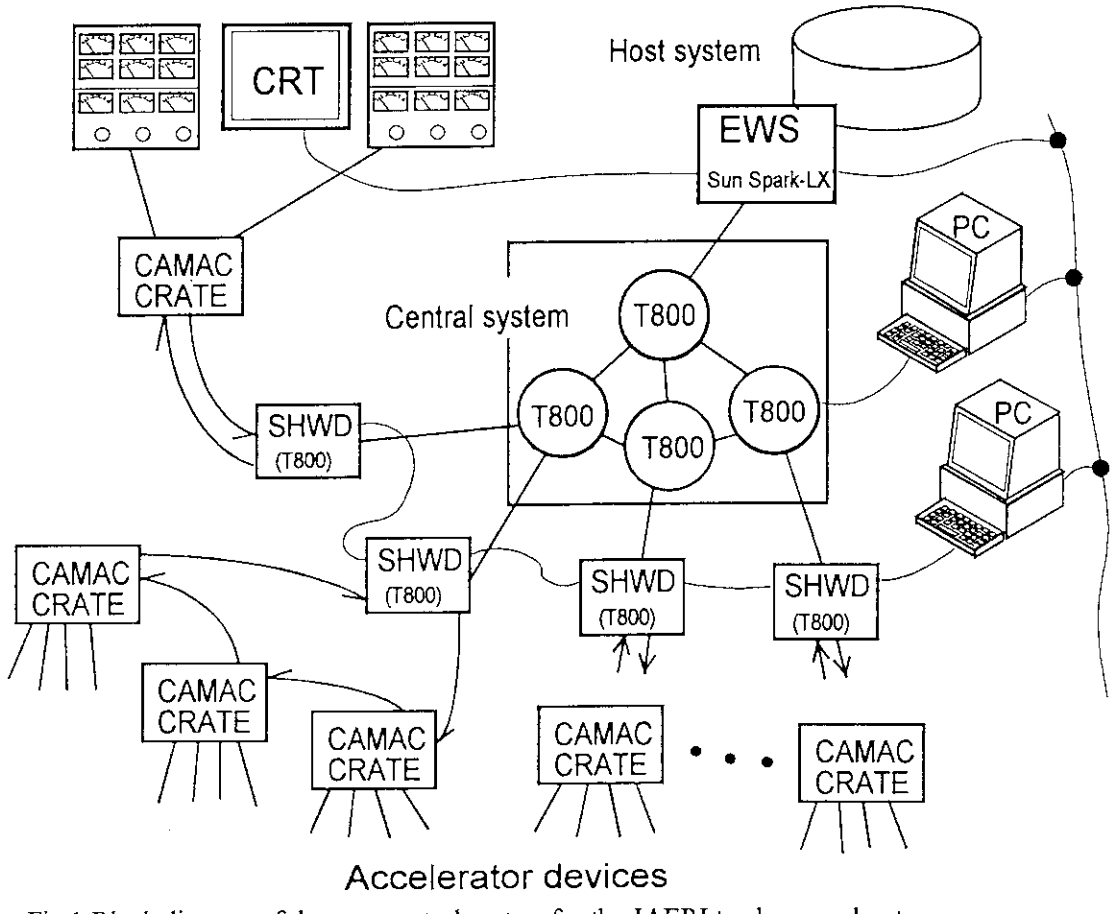

Fig.1 Block diagram of the new control system for the JAERI tandem accelerator

highways. CAMAC serial highway system is almost same as the old system. Seventeen CAMAC crates are distributed on the four serial highways. Two of the crates are dedicated to the control console. The control console has assignable valuators, which are called shaft encoders, assignable and dedicated meters etc. to control and monitor data points. Programming languages for the transputers are parallel C(INMOS ANSI-C)[7] and OCCAM2[8,9]. Programs of the transputers are developed on the personal computers. They are also used for monitoring a system operation.

The first version of the new system had started daily operation for the accelerator control in October of 1992. At that point, performance of message transfer between concurrent processes in the system was not so good as expected. It took about 2 milli-seconds for transfer of a message. It was the result of a bug fix of processes which relay communication messages in the central system(we call them monitor processes). In the last stage of the development of the first version, a deadlock problem was found in the processes. So we made additional mechanism for synchronization between processes. It caused the degradation of the performance.

In October of 1993, we had re-written the monitor processes. The performance of the message transfer was greatly improved from about 2 milli-seconds to about 0.3 milli-seconds per one message transfer. In the work, We analyzed program execution times of several instructions of the transputer and used new programming technic for better performance. So we could make the improvement without any change of external specifications of the monitors.

A new function of linked control using a virtual data points[3] was tested in March of 1994. The virtual data point named final energy(Ef) and its control process, scaling process, were installed in the test. It was intended to work as that a change of Ef reflects to several data points by the scaling rule[10] process, in the manner that beam transport of accelerated particle is maintained and the final energy is set equal to setting value of Ef. The mechanism follows not only to a step of the change but also to the continuous change of the virtual data point. Some mismatch between valuators of the control console and the new function was found by the test. On the other hand, it was shown that system performance of message passing and calculation were enough for smooth operation. Introduction of the function into daily machine operation should be suspended till improvement of the valuators.

References

[1]M.Maruyama, Proc. 3rd Int. Symp. on Electrostatic Accelerator Technology, Ork Ridge, Tennessee(1981),p17.
[2]INMOS Limited, The Transputer Data Book 2nd Edition, Prentice Hall, 1989.
[3]S. Hanashima et.al., The control system for the JAERI tandem particle accelerator using transputers, Transputer and OCCAM engineering series Vol. 35 (Proceedings of the 5th Transputer/Occam international conference 1993 Osaka, Japan) IOS Press, p69-81.
[4]IEEE Inc., Modular Instrumentation and Digital Interface System(CAMAC), IEEE Std 595-1976.
[5]IEEE Inc., Serial Highway Interface System(CAMAC), IEEE Std 595-1976.
[6]O.Jones, Introduction to The X Window System, Prentice Hall Inc., 1989.
[7]INMOS Limited, ANSI C toolset user manual, INMOS Limited 72 TDS 22400, 1990.
[8]INMOS Limited, Transputer Development System 2nd Edition Prentice Hall Inc.
[9]INMOS Limited, OCCAM2 Reference Manual, Prentice Hall, 1988.
[10]S.Hanashima and E.Minehara, Scaling of the optical parameters for the JAERI tandem accelerator, Rev.Sci.Instrum., 57(5), 1986, p787-788.

2. Nuclear Structures

2. 1 LIFETIMES OF EXCITED STATES IN ^{105,107}Sn

T. ISHII, A. MAKISHIMA[1], H. TSUCHIDA[2], M. OGAWA[2] and M. ISHII

We have measured the lifetimes of the $17/2^+$ and $7/2^+$ states in ^{105,107}Sn by the recoil distance method. In the previous experiments[1] the maximum recoil distance allowable had been 3 mm but it was improved to 9 mm. The nuclei ^{105,107}Sn were produced by bombarding the target ^{54}Fe, 0.8 mg/cm^2, with beams of 210 MeV ^{54,56}Fe ions. The Si box[2] helped us to select the reaction channel emitting two protons.

A schematic level ordering up to the $17/2^+$ state in both nuclei is illustrated in Fig. 1. The $5/2^+$ and $7/2^+$ levels are the seniority–1 states with the main configurations of $\nu d_{5/2}$ and $\nu g_{7/2}$, respectively. The higher states up to the $17/2^+$ level are the seniority–3 states. The halflives of the $17/2^+$ and $7/2^+$ states in these nuclei were determined from the decay curves for the $11/2^+ \rightarrow 7/2^+ \rightarrow 5/2^+$ transitions shown in Fig. 2:
$T_{1/2}(17/2^+) = 0.38(5)$ ns and $T_{1/2}(7/2^+) = 0.33(8)$ ns for ^{105}Sn;
$T_{1/2}(17/2^+) = 0.40(6)$ ns and $T_{1/2}(7/2^+) = 0.9(2)$ ns for ^{107}Sn.
The $17/2^+ \rightarrow 15/2_2^+$ M1 transitions turned out rather fast. These transitions are owing to the configurations $[\nu d_{5/2}(\nu g_{7/2})^2{}_{6^+}]_{17/2^+,15/2^+}$. The $7/2^+ \rightarrow 5/2^+$ transitions are l–forbidden by two orders of magnitude.

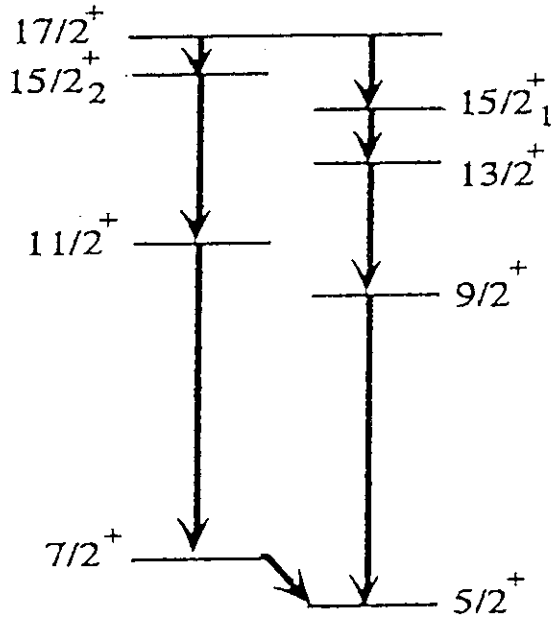

Fig. 1. Schmatic level structure in ^{105,107}Sn.

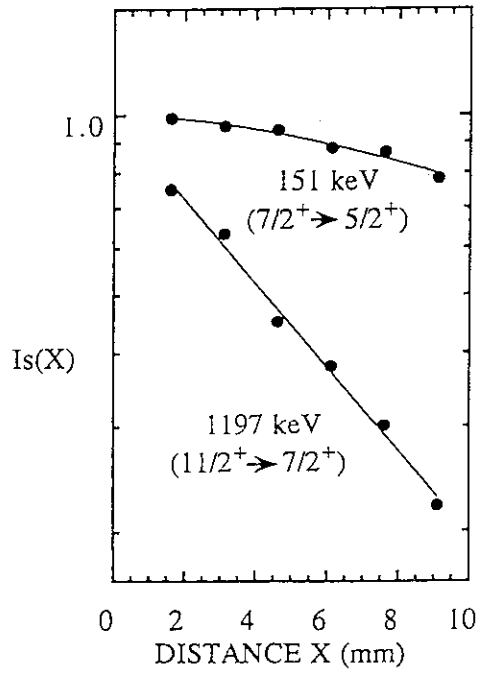

Fig. 2. Decay curves for the $7/2^+$ and $17/2^+$ states in ^{107}Sn

References
1)T. Ishii, A. Makishima, K. Koganemaru, Y. Saito, M. Ogawa and M. Ishii, Z. Phys. A347 (1993) 41.
2)M. Ishii, A. Makishima, M. Hoshi and T. Ishii, in Nuclei off the line of stability, edited by R.A. Meyer and D.S. Brenner(American Chemical Society, Washington D.C., 1986) pp.496–501.

[1]Center for Radioisotope Science, National Defense Medical College.
[2]Department of Energy Science, Tokyo Institute of Technology.

2.2 NUCLEAR MOMENTS OF RADIOACTIVE NUCLIDE, ^{143}Pr ($T_{1/2}$ = 13.6 D), BY COLLINEAR LASER-ION-BEAM SPECTROSCOPY

H.IIMURA, M.KUBOTA[1], Y.NAKAHARA, S.ICHIKAWA and T.HORIGUCHI[2]

The level structure in the odd-mass Pr (Z = 59) isotopes indicates a shape transition from "spherical" to "deformed" as the neutron number increases from 82 to 90, providing a good opportunity to test various nuclear models. Of these isotopes, the nucleus ^{143}Pr (N = 84) may be considered as a nearly spherical nucleus. It is interesting that the ground state of ^{143}Pr is $7/2^+$[1], since one expects the ground state of this nucleus to be $5/2^+$ from the simple shell model. This indicates the importance of the residual nucleon-nucleon interactions which must be incorporated into the shell model. There exist as yet, however, no experimental data on the nuclear moments of the $7/2^+$ ground state of ^{143}Pr. In this work, collinear laser-ion-beam spectroscopy was used for the measurements of the magnetic dipole and electric quadrupole moments of the ground state of ^{143}Pr. Outline of measurement of hyperfine structure has already been given in our previous report[2]. In this report, we describe results of the experiment.

Table I lists the values of magnetic-dipole constant A and electric-quadrupole constant B derived from measured hyperfine spectra of ^{143}Pr ($T_{1/2}$ = 13.6 d) and the stable isotope ^{141}Pr. The weighted mean of our measured ratios $A(143)/A(141)$ for the $^5H_3$ state and $^5G_2$ state gives the ^{143}Pr magnetic dipole moment, $\mu(143) = +2.701(4)\mu_N$. Here we used the value of $\mu(141)$ measured by Macfarlane *et al.*[3] ($\mu(141) = +4.2754(5)\mu_N$). No correction for a hyperfine anomaly was used. Such a correction is expected to be small, as there are no unpaired s electrons. For the quadrupole moment of ^{141}Pr, a value of -0.0589(42) eb was obtained from atomic-beam magnetic-resonance experiments[4], in which no Sternheimer corrections were made. Recently, Childs and Cheng[5] semiempirically obtained Sternheimer shielding factor R_{4f}. Taking their value of $R_{4f} = +0.23(2)$ gives $Q(141) = -0.077(6)$ eb. With the values of $B(143)/B(141)$ from the present work, we obtain $Q(143) = +0.77(16)$ eb.

Table I. Pr-II hyperfine structure constants measured in the present experiment.

	A(MHz)		B(MHz)	
Level	141	143	141	143
$4f^3(^4I^o)6p\ ^5H_3$	1029.5(7)	463.6(1.5)	-14(2)	150(22)
$4f^3(^4I^o)5d\ ^5G_2$	1703.6(7)	769.1(1.1)	-11(5)	95(11)

The magnetic dipole and electric quadrupole moments of ^{143}Pr are listed in Tables II and III, respectively. The experimental values for the ground state were determined in this work for the first time. They were compared with the calculation of Kisslinger and Sorensen (KS)[6] based on a pairing-plus-quadrupole model, and also compared with the predictions of intermediate coupling (IC) model[7]. In addition, the interacting-boson-fermion model (IBFM) calculation has been performed and the results were compared with the

[1]Department of Physics, Toho University.
[2]Department of Physics, Hiroshima University.

Table II. Magnetic moments of the ground and first excited states in ^{143}Pr.

Level (keV)	I^π	μ_{exp} (μ_N)	μ_{theor} (μ_N)		
			KS	IC	IBFM
0	$7/2^+$	2.701(4)[a]	2.12[b]	2.79[c]	2.21[d]
57	$5/2^+$	3.4(1)[e]	3.44[b]	2.99[c]	3.42[d]

[a]Present work.
[b]Reference [6]. Values for g_s = 5.58 and g_R = Z/A.
[c]Reference [7]. Values for g_s = 2.62 and g_R = Z/A.
[d]Present work. Values for g_s = 4.00 and g_d = 0.25.
[e]Reference [8].

experimental values. It was found that the theoretical value of the quadrupole moment has the wrong sign in the IC model. It was also found that the calculated quadrupole moment with the IBFM is considerably different from the experimental value. As for the magnetic moment of the ground state, the theoretical values with the pairing-plus-quadrupole model and the IBFM are smaller than the experimental value. Thus, it can be said that no overall agreement between the theories and experimental results for the nuclear moments of ^{143}Pr has been obtained as yet, and further studies to improve the theoretical predictions are expected.

Table III. Quadrupole moments of the ground and first excited states in ^{143}Pr.

Level (keV)	I^π	Q_{exp} (eb)	Q_{theor} (eb)		
			KS	IC	IBFM
0	$7/2^+$	0.77(16)[a]	1.22[b]	−0.73[c]	0.25[d]
57	$5/2^+$		−0.58[b]	−0.62[c]	−0.36[d]

[a]Present work.
[b]Reference [6]. Values for e_p = 2e.
[c]Reference [7]. Values for e_p = 2e.
[d]Present work. Values for e_B = e_F = 0.139 eb.

References

1) L.K.Peker, Nucl. Data Sheets 64, 429 (1991).
2) H.Iimura, M.Kubota, Y.Nakahara, S.Ichikawa and T.Horiguchi, JAERI Tandem & V.D.G. Annual Report 1992, 81 (1993).
3) R.M.Macfarlane, D.P.Burum and R.M.Shelby, Phys. Rev. Lett. 49, 636 (1982).
4) B.Bleaney, in Proceedings of the Third International Congress on Quantum Electronics, Paris, 1963, edited by P.Grivet and N.Bloembergen (Columbia Univ. Press, New York, 1964).
5) W.J.Childs and K.T.Cheng, Phys, Rev. A30, 677 (1984).
6) L.S.Kisslinger and R.A.Sorensen, Rev. Mod. Phys. 35, 853 (1963).
7) K.Heyde and P.J.Brussaard, Nucl. Phys. A104, 81 (1967).
8) G.Netz, W.Prieske, H.Daum, E.Gerdau, V.Lakshminarayana and P.Herzog, Hyperfine Interact. 3, 147 (1977).

2. 3 HIGH-SPIN STATES ABOVE A HIGH-SPIN ISOMER IN ^{145}Sm

A.ODAWARA[1],Y.GONO[1],S.MITARAI[1], E.IDEGUCHI[1],M.KIDERA[1],M.SHIBATA[1], T.MORIKAWA,T.KISHIDA[2],M.OSHIMA,H.IIMURA,M.SHIBATA,AND S.HAMADA

In ^{145}Sm, a 0.96 μsec high-spin isomer was reported without a detail level structure[1]. The decay scheme from the high-spin isomer in ^{145}Sm was constructed[2] based on the experimental data taken by using the ^{139}La(^{10}B,4n) reaction at Kyushu University combining those of the ^{136}Xe induced reactions, ^{16}O(^{136}Xe,7n) and ^{20}Ne(^{136}Xe,α7n) at RIKEN. The excitation energy of this high-spin isomer was determined to be 8.8MeV.

In order to study the states above the high-spin isomer in ^{145}Sm, prompt and delayed $\gamma\gamma$-coincidence measurements were performed using the ^{138}Ba(^{13}C,6n) reaction*. The ^{13}C beam of 95MeV was provided by the tandem accelerator at JAERI. Gamma-rays were detected by 5 HPGe detectors of 30% efficiency with BGO compton supression sheilds of RIKEN. New 12 taransitions and 11 levels above the high-spin isomer were found. The spin assignments were made by the γ-ray anglar distirbution measurement using the same reaciton at 98MeV. The HPGe detectors were placed at 30°, 60° and 90° with respect to the beam. The level scheme of ^{145}Sm has been extended up to the spin (65/2) state at 14.6MeV. The proposed level scheme above the high-spin isomer in ^{145}Sm is shown in Fig.1.

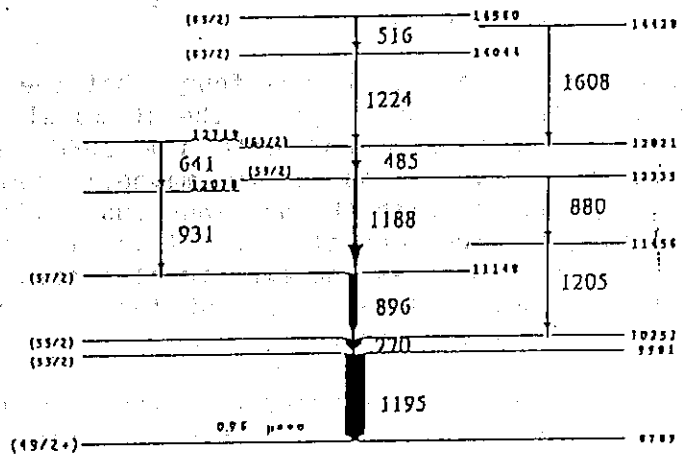

Fig.1 The level scheme above the high-spin isomer in ^{145}Sm.

The yrast configurations of ^{145}Sm and ^{147}Gd with N=83 were calculated by the deformed independent particle model (DIPM)[3]. The configuration of high-spin isomers in both nuclei were suggested to be $[\pi(h_{11/2})^2\nu(f_{7/2}h_{9/2}i_{13/2})]_{49/2+}$. The deformation parameters β of the yrast states were also calculated for both nuclei and are shown as a function of an angular momentum in Fig.2 with

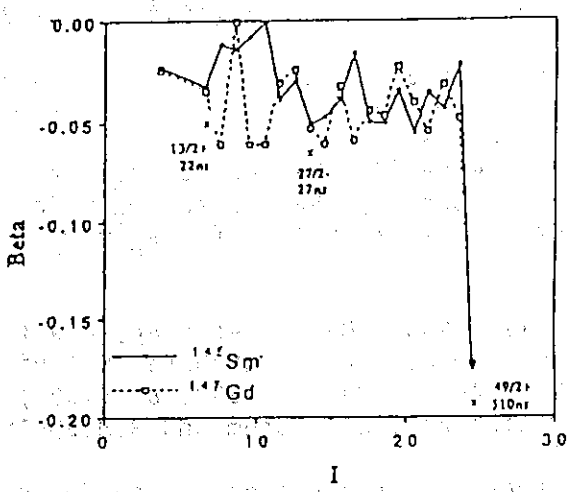

Fig.2 Deformation parameter β of the yrast states in ^{145}Sm and ^{147}Gd calculated by DIPM. Plots present experimental values of isomer in ^{147}Gd.

[1]Physics Department,Kyushu University,Hakozaki,Fukuoka,Japan
[2]RIKEN,wako-shi,Saitama,Japan
*The enriched material of ^{13}C was provided by KEK

the experimental values for isomers in ^{147}Gd. The DIPM calculation reproduces well these experimental values. At I=49/2, the dramatic increase of the deformation from $\beta \sim 0$ to about -0.2 is found in this figure. The high-spin isomers for these nuclei are considered to be caused by the sudden shape changes from near spherical to oblate deformation.

Average moments of inertia of ^{145}Sm and ^{147}Gd were deduced from the slope of the plots for experimental and theoretical yrast state energies vs I(I+1), shown in Fig.3(a) and (b). In case of experimental yrast states, there are two components in ^{147}Gd and the moment of inertia for I>49/2 is close to the rigid body value. On the other hand, there is only one component in ^{145}Sm. In case of theoretical yrast states, there are two components in both nuclei. The DIPM calculation could not reproduce experimental values.

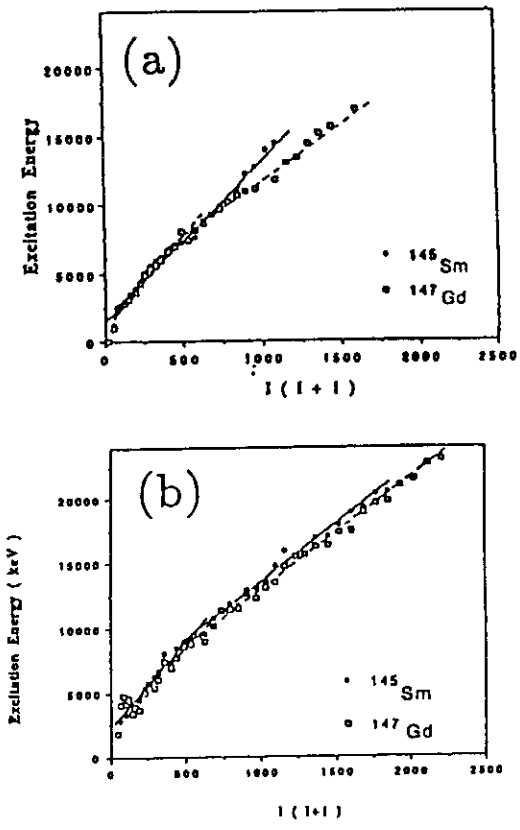

Fig.3 Plots of excitation energies vs I(I+1) for the experimental(a) and theoretical(b) yrast states in ^{145}Sm and ^{145}Gd.

References

1) A.Ferragut, Y.Gono, T.Murakami, T.Morikawa, Y.H.Zhang, K.Morita, A.Yoshida, M.Oshima, H.Kusakari, M.Sugawara, M.Ogawa, M.Nakajima, S.Mitarai, A.odawara, E.Ideguchi, T.Shizuma, M.kidera, J.C.Kim, S.J.Chae, B.J.Min and K.Kumagai, J.Phy.Soc.Jpn.62(1993)3343
2) A.odawara, Doctor Thesis(1994)
3) H.Sagawa, Private communication

2. 4 HIGH SPIN STATES OF ^{147}Eu

M.SHIBATA[1],Y.GONO[1],S.MITARAI[1],A.ODAHARA[1],E.IDEGUCHI[1],
M.KIDERA[1],M.OSHIMA,T.MORIKAWA,Y.HATSUKAWA,S.HAMADA,
H.IIMURA,M.SHIBATA,T.KISHIDA[2] and Y.KIMURA[3]

High-spin states of ^{147}Eu were studied by using in-beam γ-ray spectroscopy techniques. They were populated by the ^{139}La(^{13}C,5n)^{147}Eu reaction. The ^{13}C beam* of 98 MeV was provided by JAERI tandem accelerator. The target used was self-supporting ^{139}La foil of 11 mg/cm^2. The γ-rays were measured by using 6 sets of HPGe detectors with BGOACS of RIKEN which were placed at θ=-125°,-90°, -35°, 60°,150°(ϕ=0°) and θ=90°(ϕ=90°) with respect to the beam. The $\gamma\gamma$-coincidence data were taken in a 4 dimensional coincidence mode, i.e. Eγ-Eγ-T$\gamma\gamma$-Tγ-RF.

More than 10 new γ-rays were identified to be transitions in ^{147}Eu as can be seen in Fig.1. The level scheme of ^{147}Eu was known previously up to the (33/2+) state at 4.178 MeV[1]. Based on data analyses of the coincidence and angular distribution measurements, the level scheme was extended up to the (61/2) state at 8.935 MeV as shown in Fig.2. There was no high-spin isomer with a half-life of longer than 20 ns observed in this experiment.

The experimental results were compared with the deformed independent particle model calculation[2]. It was found in the calculation that the yrast states of this nucleus showed gradual shape change as the spin increases. This may be the reason why there is no high-spin isomer found as in the N=83 neighboring isotones in the experiment.

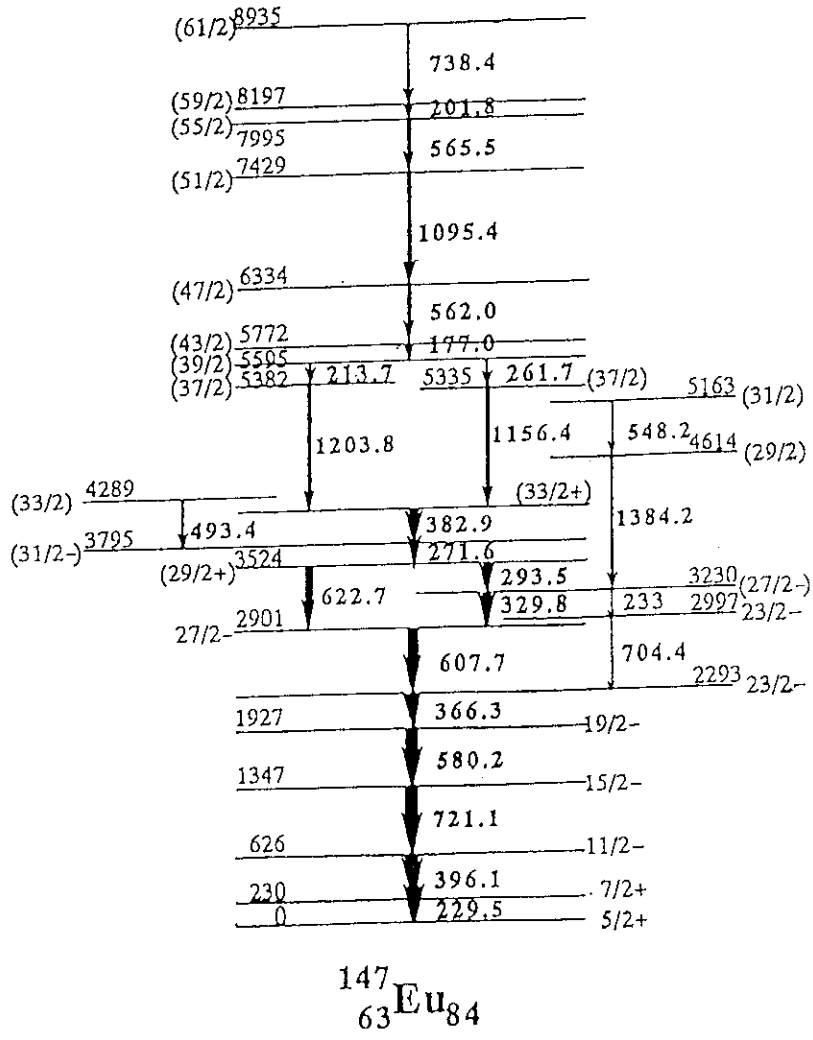

Fig.1 Level scheme of ^{147}Eu

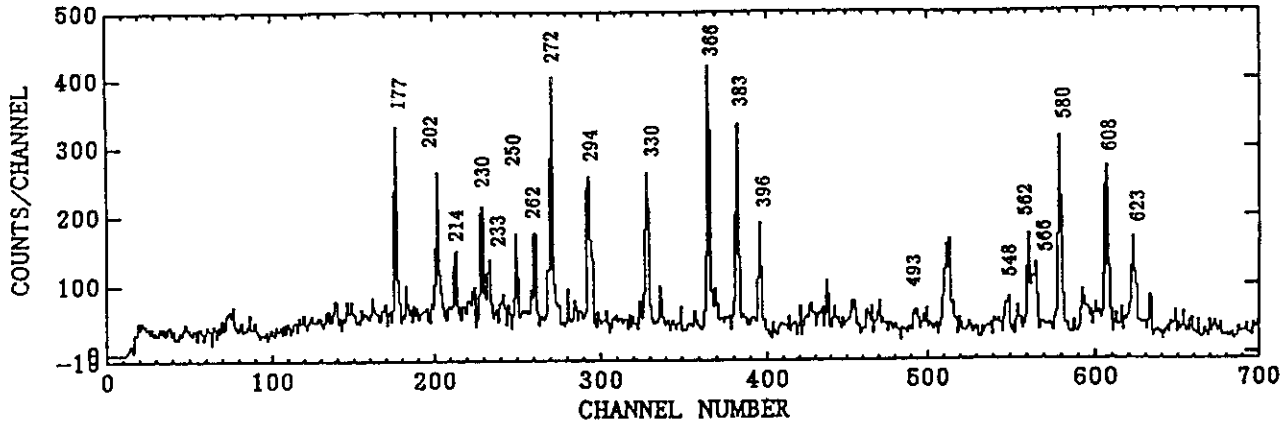

Fig.2 γ-ray coincidence spectrum gated on previously known γ-rays of ^{147}Eu

References
[1] E.der Mateosian and L.K.Peker,Nuclear Data Sheets 66(1992)705.
[2] H.Sagawa,private communication.

1.Department of Physics,Kyushu University.
2.Radiation Laboratory,RIKEN.
3.Department of Physics,Tohoku University.
* Enriched ^{13}C material was provided by KEK.

2.5 HIGH SPIN STATES OF ^{148}Tb

E.IDEGUCHI[1], Y.GONO[1], S.MITARAI[1], A.ODAHARA[1], M.KIDERA[1], M.SHIBATA[1], M.OSHIMA, T.MORIKAWA, Y.HATSUKAWA, S.HAMADA, H.IIMURA, M.SHIBATA, T.KISHIDA[2] AND Y.KIMURA[3]

High-spin isomers were systematically found in N=83 isotones[1]. Their excitation energies and half-lives are almost the same, i.e. ~8 MeV and ~1 μs, respectively. Among them, the level structure of ^{147}Gd was most extensively studied experimentally[2] and theoretically[3]. The calculation of deformed independent particle model (DIPM) reproduced well the experimentally determined deformation parameters β of three isomeric states of ^{147}Gd as shown in Fig.1. The configuration of the high-spin isomer was derived to be $[\pi(h_{11/2})^2,\nu(f_{7/2},h_{9/2},i_{13/2})]_{49/2^+}$ based on the g-factor measurement[4]. This configuration was further proved by the DIPM calculation. The results are shown in Fig.1 as well. Sudden increase of the deformation from β~0 to -0.2 are resulted by the DIPM calculations at spin 49/2 in ^{147}Gd and 27 in ^{148}Tb. This abrupt change of the shape may generate the relatively long-lived high-spin isomers in N=83 isotones.

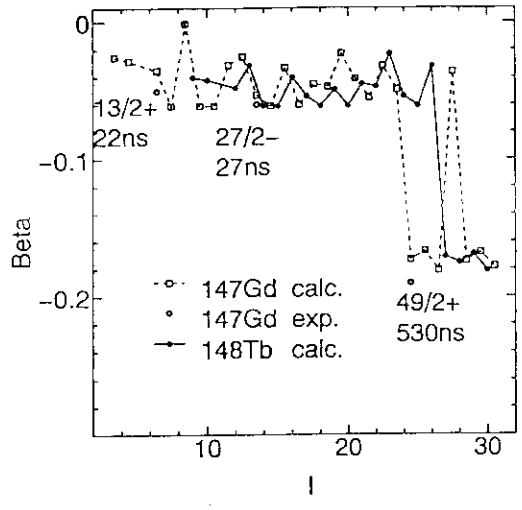

Fig.1 Deformation parameter β vs I for ^{147}Gd and ^{148}Tb resulted from DIPM.

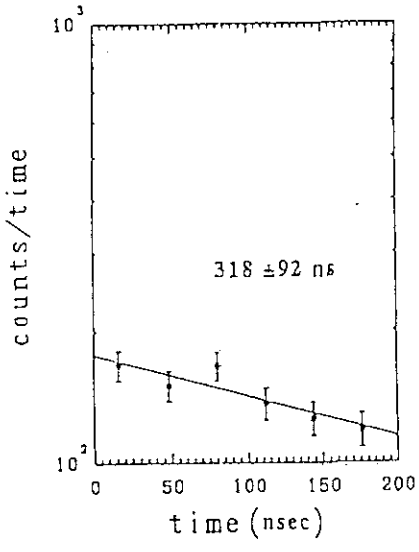

Fig.2 Time spectrum between RF and previously known γ-rays of ^{148}Tb

In order to study the mechanism to generate these isomers in detail, the decay scheme of ^{148}Tb was studied by in-beam γ-ray spectroscopic techniques. The high-spin states of ^{148}Tb were populated by the ^{141}Pr(^{13}C,6n)^{148}Tb reaction*. The ^{13}C beams of 95,98 and 100 MeV were provided by JAERI tandem accelerator. The target used was

1. Department of Physics, Kyushu University.
2. Radiation Laboratory, The Institute of Physical and Chemical Research(RIKEN)
3. Department of Physics, Tohoku University.
The enriched material ^{13}C was provided by KEK.

4.7mg/cm^2 self-supporting foil of ^{141}Pr. Six sets of HPGe and BGOACS of RIKEN were used for γγ-coincidence experiments. The detectors were placed at 6 different angles with respect to the beam, so that the DCO information could be obtained. A new isomeric state with half-life of ~300ns was found in addition to the previously reported[5] ~1.1 μs isomer. The decay curve is given in Fig.2.
A tentative level scheme so far constructed is given in Fig.3.
The data analysis is still in progress.

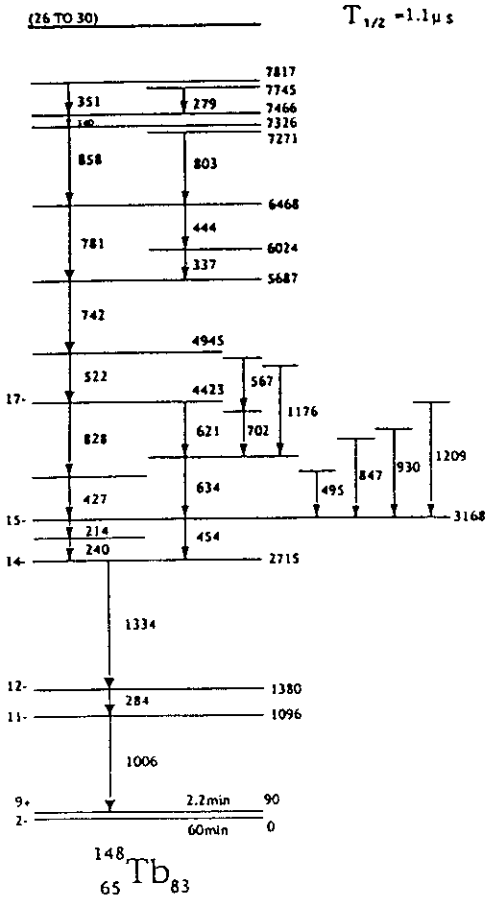

Fig.3 Level scheme of ^{148}Tb

References

[1] Y.Gono et al., Nucl.Phys. A557(1993)341c.
[2] For example, B.Haas et al., Nucl.Phys.A362(1981)254.
[3] For example, T.Dossing et al., Phys.Scr.24(1981)258.
[4] O.Hauser et al., Phys.Rev. Lett.42(1979)1451.
[5] J.Borgrgreen et al., Z.Phys.A294(1980)113.

2. 6 TWO-PHONON γ-VIBRATIONAL STATE IN ^{166}Er

H. Kusakari,[1] N. Kobayashi,[1] M. Taki,[1] M. Sugawara,[2] M. Oshima, T. Morikawa, Y. Hatsukawa, H. Iimura, and N. Shinohara

Surface vibration is a fundamental collective motion in atomic nucleus. Such vibrational mode is well established as one-phonon β- and γ-vibrational states at low excitation energy. However, multi-phonon vibrational excitations are not well known especially in deformed or transitional region. Their existence and collectivity is important for elucidating the collective excitation of nuclei. Since the B(E2) value from the two-phonon to the one-phonon state is a direct measure of collectivity, it is important to derive the B(E2) value for identifying the two-phonon state and for discussing the anharmonicity of collective vibration. Because of this we made a Coulomb-excitation experiment for the well deformed nucleus ^{166}Er.

The ^{166}Er nucleus was multiply Coulomb-excited with beams of 295-MeV ^{74}Ge and 235-MeV ^{58}Ni, which were obtained from the tandem accelerator. The target was a self-supporting metallic foil of 1.8 mg/cm^2. A detailed experimental method can be seen in Ref. [1]. We observed members of the g band up to 16^+ and of the γ band up to 10^+. The 1192-keV and 1315-keV transitions from the candidates of double-γ vibrational state at 2101.6 keV to the one-phonon γ-vibrational state are observed for the first time in Coulomb excitation. The Eλ matrix elements have been derived through the analysis based on Coulomb excitation code GOSIA [2]. The observed B(E2; $2_2 \rightarrow 4_3$) value for this state reveals relatively large collectivity. Thus this state is demonstrated to have a dominant two-phonon γ-vibrational character. The properties of this state will be detailed elsewhere [1].

References

1) M.Oshima et al., to be submitted to Proc. of Int. Conf. on Selected Topics in Nuclear Structure (July 5-9, 1994, Dubna).
2) D.Cline, Ann. Rev. Nucl. Part. Sci. 36, 681 (1986); and references therein.

[1]Faculty of Education, Chiba University
[2]Chiba Institute of Technology

2. 7 DEVELOPMENT OF A NEW-TYPE ELECTRON SPECTROMETER FOR SPECTROSCOPY OF HEAVY NUCLEI

M. Oshima, T. Morikawa, Y. Hatsukawa, M. Kidera, E. Ideguchi,[1] H. Kusakari,[2] and M. Sugawara[3]

A γ-ray transition is converted to an internal conversion electron with high probability when the transition energy is low and nuclear charge is high. Thus it is important to measure the conversion electrons in spectroscopic study of heavy nuclei. In in-beam environment, however, low-energy delta electrons arising from atomic collisions of beam particles with the target atoms have large cross sections as compared with nuclear processes. Also γ-rays of nuclear transitions cause large back ground in electron measurements.

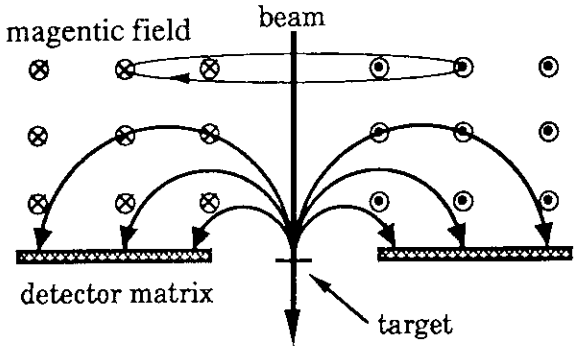

Fig. 1. Principle of a new-type spectrometer.

For this purpose we develop a new-type electron spectrometer. This consists of a magnetic filter made of NdFe permanent magnet, a lead shield, and a matrix of Si detectors as described in Fig. 1. Its principle is similar to the widely used mini-orange spectrometer[1]: a cylindrical magnetic field filters out low-energy electrons and lead shield prevents γ-rays from entering the detectors. By using a detector matrix, we intend to obtain angular distribution information, which enables us to correct Doppler shift. To know the performance of this spectrometer in in-beam environment, we made a test experiment by using Coulomb excitation of ^{232}Th by a 250-MeV ^{58}Ni beam. A surface barrier Si detector was placed on the detector plane shown in Fig. 1. A large-area (45x45mm) position sensitive detector was used to detect scattered beam particles at backward angles. Figures 2 and 3 show a time spectrum between the two detectors and an electron energy spectrum in

[1]Kyushu University
[2]Faculty of Education, Chiba University
[3]Chiba Institute of Technology

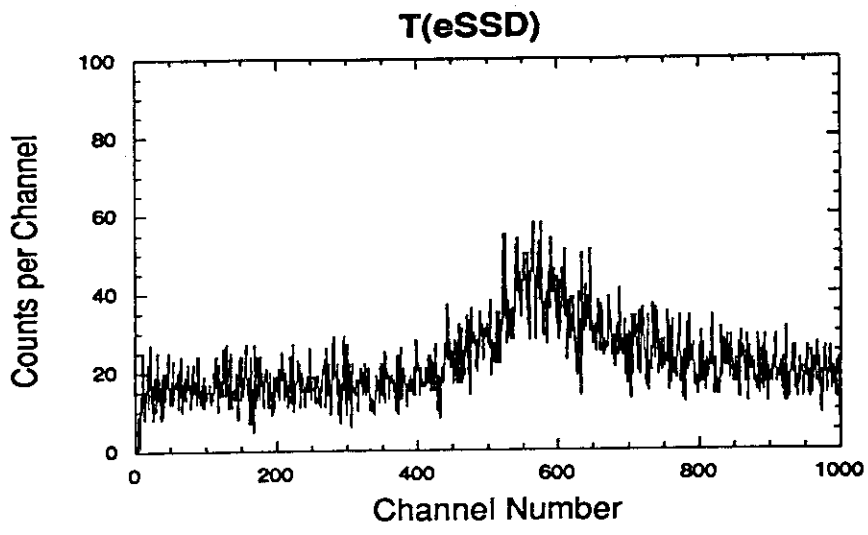

Fig. 2. A time spectrum between a Silicon detector and a PSD detector.

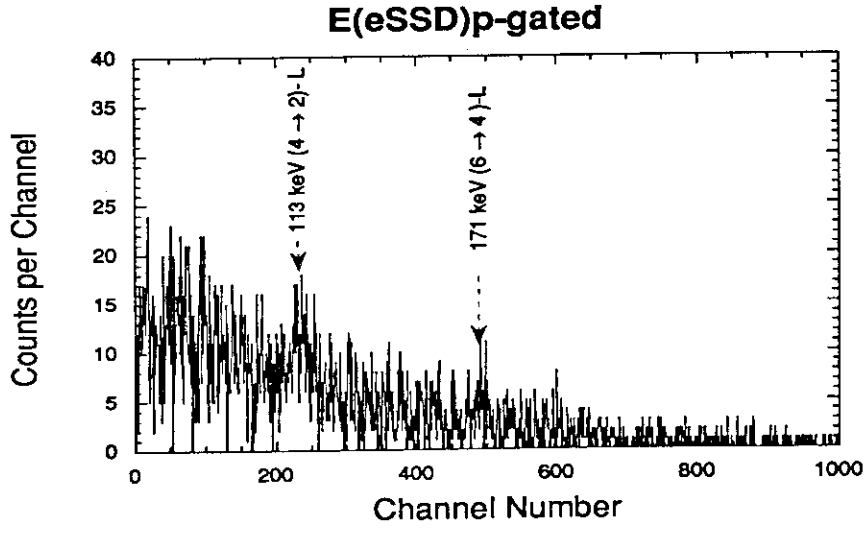

Fig. 3. An electron energy spectrum in coincidence with scattered particles.

coincidence with the scattered particles, respectively. We could observe prompt coincidence peak at the former and discrete lines in the latter (the energy calibration has not been complete so that peak energies are tentative). These clearly show conversion electrons can be detected in the in-beam condition by this new-type detector. The energy resolution was not sufficiently good but it will be improved by cooling the detectors in future experiment.

References

1) see, for example, J. Van Klinken et al., Nucl. Instrum. Meth. **130** (1975) 427.

2. 8 THE MULTIPLE-TARGET SYSTEM FOR A GAS-JET TYPE ISOL

M. ASAI[1], K. TSUKADA, S. ICHIKAWA, A. OSA, N. SHINOHARA,
H. YAMAMOTO[2] and K. KAWADE[2]

In our previous work[1], the gas-jet coupled ion source was installed at JAERI-ISOL to study short-lived neutron-rich nuclei around A=160 produced in charged-particle induced fission of actinides. In order to increase the ion yield of mass-separated fission products, the multiple-target system has been developed, and its collection efficiency for fission products was measured in off-line experiments.

The multiple-target system, shown in Fig. 1, consists of four target holders, one semi-separated reaction chamber and single capillary for a gas outlet. Fission products, escape from targets, are thermalized in Ar gas used as a carrier gas, then transported through the capillary with 1.6 mm inner diameter and 8 m length. To measure the collection and transport efficiency, ^{252}Cf fission source was set at one of the target positions, and transported activities were collected at the end of the capillary and measured with an HPGe detector.

As shown in Fig. 2, almost constant efficiency of 80% was obtained at the chamber pressure between 0.6 and 1.1 atm for light and heavy fission fragments. It indicates that the collection efficiency is not dependent of the range of fission products, if they stop in Ar gas. In addition, the efficiency was also constant whether the source position was at the end or the center of the chamber. As a result, it becomes possible to obtain the ion yield four times larger than before.

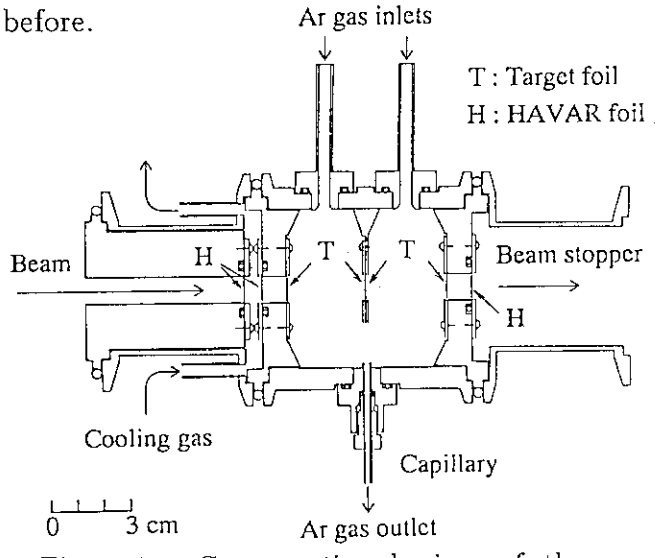

Fig. 1. Cross-sectional view of the multiple-target system used for charged-particle induced fission.

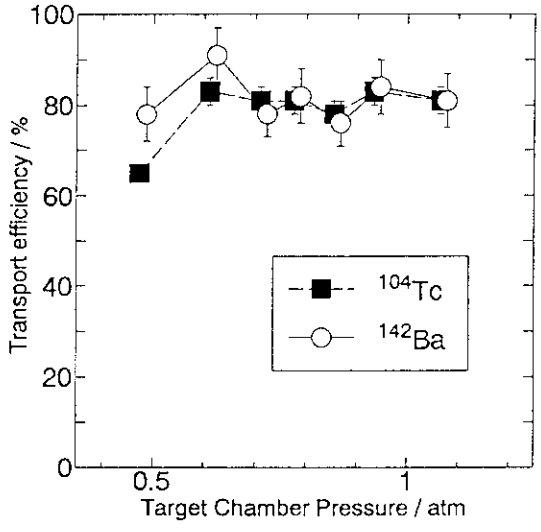

Fig. 2. Transport efficiencies for the fission products of ^{104}Tc and ^{142}Ba as a function of target chamber pressure.

Reference

1) S. Ichikawa, M. Asai, H. Iimura, N. Shinohara, K. Tsukada and A. Osa, JAERI-M93-174 (1993) p.77.

[1]Department of Nuclear Engineering, Nagoya University
[2]Department of Energy Engineering and Science, Nagoya University

3. Nuclear Reactions

3. 1 FESHBACH-KERMAN-KOONIN MODEL ANALYSIS OF PREEQUILIBRIUM (p,p') AND (p,n) REACTIONS AT LOW INCIDENT ENEGIES

Y. WATANABE[1], A. AOTO[1], H. KASHIMOTO[1], S. CHIBA, T. FUKAHORI, K. HASEGAWA, M. MIZUMOTO, S. MEIGO, M. SUGIMOTO, Y. YAMANOUTI, N. KOORI[2], M.B. CHADWICK[3], P.E. HODGSON[4]

We have so far measured double differential charged-particle emission cross sections of proton-induced reactions for ^{nat}C, ^{27}Al ,^{nat}Si, ^{98}Mo,^{106}Pd,^{159}Tb and ^{181}Ta at energies around 26 MeV using JAERI tandem accelarator[1]. The Feshbach-Kerman-Koonin (FKK) model[2] is applied to analyse preequilibrium (p,p') spectra for both ^{98}Mo and ^{106}Pd, as well as (p,n) spectra measured by Hamburg group [3] and (p,p') spectra at lower incident energies of 12 to 18 MeV[4]. The aims of the present analysis are to investigate the systematics of the strengh V_0 of the effective N-N interaction and the sensitivity of the other model parameters, and to test the applicability of the FKK model to proton-induced reactions at low incident energies. Some of the results are reported briefly below. The detail has been presented elsewhere[5].

In the present analysis, we use the FKK-GNASH code[6] to calculate the whole nucleon emission spectrum including Hauser-Feshbach equilibrium emission. The strengh V_0 of a Yukawa potential with 1 fm range is the only free parameter in the multistep direct (MSD) calculation based on the FKK model. The value can be extracted from a fit of the calculated MSD spectrum to the experimental data with the subtraction method[7] which isolates the MSD component alone by taking the forward and backward differences in the cross sections for complementary C.M. angle pairs. In the MSD calculation, only the one-step direct process is taken into account, because the MSD components involving more than two-step process were found to be negligibly small at low incident energies of our interest. The following default values are employed as the other input parameters: Walter and Guss's optical potential parameter[8], single particle level density parameterg g=A/13, spin cut-off parameter $\sigma^2 = 0.24\ nA^{2/3}$ [9], no pairing correction, and nonlocality correction [10] with the range $\beta = 0.85$ fm.

The extracted strength V_0s are plotted as a function of incident energy in Fig.1. The results for ^{93}Nb(n,n') are also illustrated. First, the V_0 values for (p,p') are approximately proportional to $E_{inc}^{-1/2}$, where E_{inc} is the incident energy, as was found in an earlier work for (n,n') at low energies[6] and a more recent work[11] for higher proton energies up to 200 MeV using the same code. In the present work, however, the V_0s for (n,n') show a little weaker dependence and smaller values than those for (p,p'). This might be related to the difference in the kinetic energies of incident nucleons near the surface region of nucleus where direct inelastic scattering occurs strongly, originating from the Coulomb effect and the asymmetry term of optical potentials. Next, it should be noted that the V_0 values extracted from the (p,n) reactions are about a half those from the (p,p') reactions for the same targets and incident energies. This is because a 1-component state density is used for both calculations. If a 2-component state density treating protons and neutrons separately is used, both values are expected to become closer because of the difference by a factor of about two in the number of 1p-1h residual states between (p,p') and (p,n) reactions as has been considered in refs.[11,12].

In Fig.2, the calculated double differential ^{98}Mo(p,xp) and (p,xn) cross sections including multistep compound (MSC) and equilibrium emission are compared with the experimental data at 25.6 MeV. Collective (p,p') excitation to the first 2^+ and 3^- states is also taken into account by a DWBA calculation using collective form factors with experimental deformation parameters. The measured (p,p') and (p,n) spectra are reproduced well by the calculation with the FKK-GNASH code. Similar good agreement is obtained for ^{106}Pd(p,p') and (p,n) at 26 MeV as well.

[1] Department of Energy Conversion Engineering, Kyushu University, Kasuga, Fukuoka 816
[2] Faculty of Integrated Arts and Sciences, The University of Tokushima, Tokushima 770.
[3] Lawrence Livermore National Laboratory, Livermore, California, U.S.A.
[4] Nuclear Physics Laboratory, Physics Department, University of Oxford, Oxford, UK

References

[1] A. Aoto et al, JAERI-M 92-027 (1992) p.330 ;Y. Watanabe et al., JAERI-M 93-043 (1993) p.297
[2] H. Feshbach, A. Kerman and S. Koonin, Ann. Phys. **125** (1980) 429.
[3] E. Mordhorst et al., Phys. Rev. **C 34** (1986) 103; S. Hölbling et al., Z. Phys. **A 338** (1991) 11.
[4] Y. Watanabe et al., Phys. Rev. **C 36** (1987) 1325; Y. Watanabe et al., Z. Phys. **A 336** (1990) 63.
[5] Y. Watanabe et al., Int. Conf. on Nuclear Data for Science and Technology , May 9-13, 1994, Gatlinburg, Tennessee, USA.
[6] M.B. Chadwick and P.G. Young, Phys. Rev. **C 47** (1993) 2255.
[7] P. Demetriou, P. Kanjanarat, and P.E. Hodgson, J. Phys. **G19** (1993) L193.
[8] R.L. Walter and P.P. Guss, Proc, Int. Conf. Nucl. Data for Basic and Applied Science, Santa Fe, 1985, p. 1075.
[9] H. Gruppelaar, IAEA Advisory Group Meeting on Basic and Applied Problems on Nuclear Level Densities (Brookhaven National Laboratory, 1983).
[10] F.G. Perey and B. Buck, Nucl. Phys. **32** (1962) 353.
[11] M.B. Chadwick et al., to be published in Phys. Rev. **C** (1994).
[12] Y. Watanabe et al., Oxford University Report, OUNP-93-30 (1993).

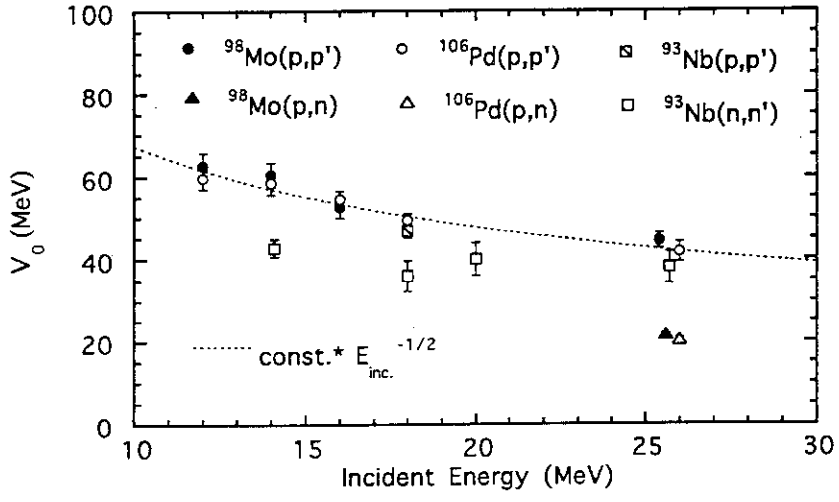

Fig.1 The extracted strength V_0 of effective N-N interaction as a function of incident energy.

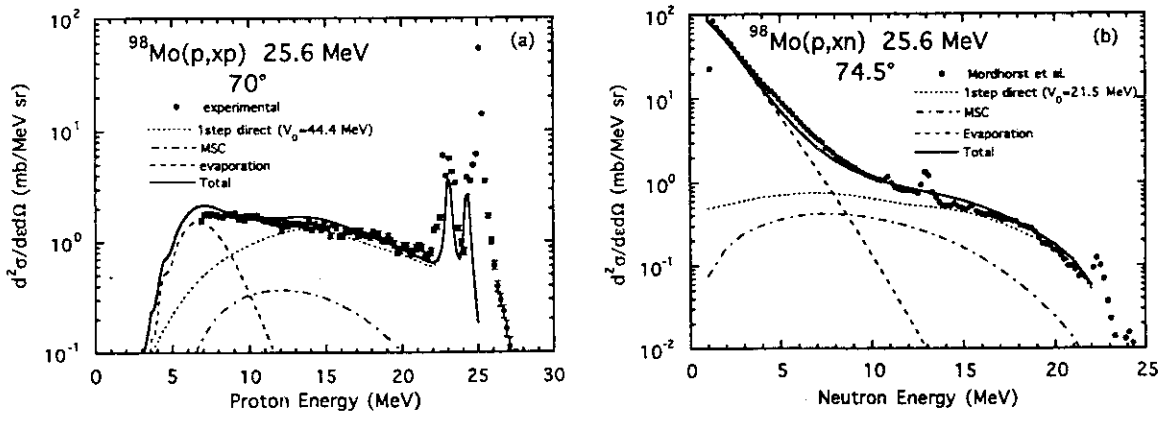

Fig.2 The experimental double differential ^{98}Mo(p,xp) and (p,xn) cross sections for 25.6 MeV and those calculated with the FKK-GNASH code.

3. 2 Measurements of Activation Cross Sections at 18-30 MeV by Using the ^{7}Li(p,n) Quasi-monoenergetic Neutron Source at JAERI-TANDEM

Y. UNO, S. MEIGO, S. CHIBA, T. FUKAHORI, Y. KASUGAI[1] and Y. IKEDA

The demands for the neutron cross section date above 20 MeV have been increased recently. The experiment of neutron activation cross section measurement by using the ^{7}Li(p,n) quasi-monoenergetic neutron source at 18-30 MeV was started at the TANDEM accelerator facility of JAERI.

The 20 and 25 MeV protons bombarded the thin ^{7}Li target. There is the cooling water layer separated by a 0.1-mm-thick aluminum plate and the protons passing through the ^{7}Li target are fully absorbed in this water. The neutron energy spectrum in the forward direction was measured by the TOF method by using an NE213 liquid scintillation detector. The measured neutron energy spectra are shown in Fig. 1. A quasi-monoenergetic peak produced by the ^{7}Li(p,n)^{7}Be[0.0, 0.429MeV] reaction is observed. There are low energy neutron tails corresponding to the breakup of higher excitation states of ^{7}Be, and to the interaction of protons with the cooling water and the structural materials of the target. The absolute flux of peak neutrons was measured by the proton recoil counter telescope. The characteristics of the p-Li neutron source are tabulated in the Table 1. The angular distributions of the peak neutron yield were also measured with the NE213 detector.

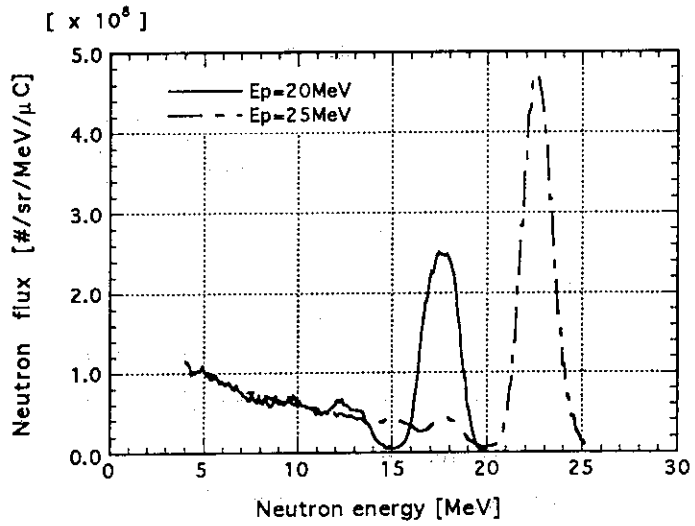

Fig. 1 Neutron spectra of 20 and 25 MeV proton

Table 1 The characteristics of the p-Li neutron source

Proton energy [MeV]	Thickness of Li [mm]	Effective energy of peak neutrons [MeV]	Peak neutron yield in the forward direction [#/Sr/μC]
20	1.8	17.6	6.05×10^{8}
25	1.45	22.7	9.49×10^{8}

[1]Department of engineering, Nagoya University

The samples of Co, Nb, Cu, Y, Tm, Ti, Ni, Fe, Zr, W, Au and Al were irradiated at the distance of 10 cm from the Li target. After the irradiation, the gamma-rays of each samples were measured by HP-Ge detectors and the reaction rates were derived from the measured induced activities. The obtained reaction rates include the contribution from the low energy neutrons. Therefore the correction for this low energy neutrons is necessary. The cross section for the effective peak energy, σ, is calculated as follows,

$$\sigma = R \cdot \frac{\int_{E_{min}}^{E_{max}} \sigma_0(E) \cdot \phi(E)\, dE}{\int_{E_{th}}^{E_{max}} \sigma_0(E) \cdot \phi(E)\, dE} \cdot \frac{1}{\phi_{peak}} , \qquad (1)$$

where R is the obtained reaction rate, $\sigma_0(E)$ is the cross section data cited from the literature, $\phi(E)$ is the neutron spectrum, E_{th} is the threshold energy of the reaction, E_{max} and E_{min} are the highest and the lowest energy of the peak neutrons respectively, and ϕ_{peak} is the absolute peak neutron yield. The measured cross sections of ^{197}Au(n,2n)^{196}Au reaction are shown in Fig. 2. The cross section data evaluated by M. Wagner et al.[1] were used as $\sigma_0(E)$ in the eq. (1). The presently derived cross sections are in good agreements with the evaluated data. This result demonstrated the adequacy of the method.

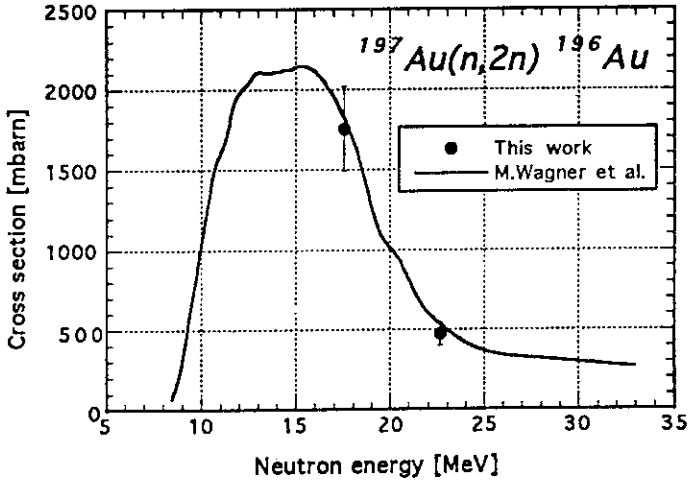

Fig. 2 Cross section of ^{197}Au(n,2n)^{196}Au

References

1) M. Wagner et al. : PHYSICS DATA No. 13-5 (1990)

3. 3 OBSERVATION OF NUCLER RAINBOW SCATTERING IN THE $^{16}O+^{16}O$ SYSTEM AT E_{lab}=124MeV AND 145MeV

Y.SUGIYAMA,Y.KONDO[1], Y.TOMITA,Y.YAMANOUCHI,H.IKEZOE,
K.IDENO,S.HAMADA,T.SUGIMITSU[2],M.HIJIYA[2] and H.FIJITA[3]

The 90° excitation functions for the elastic scattering of light heavy-ion systems like $^{12}C+^{12}C$ and $^{16}O+^{16}O$, in the laboratory energy range below 180MeV, exhibit complex structures of peaks and valleys whose nature has remained an unsolved mystery for more than 20 years. The data for the $^{12}C+^{12}C$ system have recently been analyzed by McVoy and Brandan[1]. They have interpreted that the prominent 102MeV minimum in the 90° excitation function is due to an Airy minimum crossing 90° at this energy. In spite of their interpretation, the angular distributions for the $^{12}C+^{12}C$ system do not show clear indication of the Airy structure.

On the other hand recent observation of nuclear rainbow scattering in the $^{16}O+^{16}O$ system at E_{lab}=350MeV[2] and 145MeV[3] has attracted considerable interest in this system, since the phenomena provide important information on the depth of the real nucleus-nucleus interaction. An analysis of the data at E_{lab}=145MeV shows that the observed dip at $\theta_{cm}\approx$54°and the modulated peak at $\theta_{cm}\approx$62° are an Airy minimum and an Airy maximum, respectively. We found several discrete sets of optical potentials which fit the data. One of them provides a real volume integral which agrees with the previously proposed energy dependence[4].

We measured the elastic scattering angular distributions for the $^{16}O+^{16}O$ system at E_{lab}=124MeV and 145MeV from θ_{cm}=10° to 94°. The results are shown in Fig.1. The angular distribution shows a prominent minimum at θ_{cm}=90° at E_{lab}=124MeV where a deep minimum has been observed in the 90° excitation function[5]. On the other hand the angular distribution at E_{lab}=145MeV shows a maximum at θ_{cm}=90°. Several discrete sets of the optical potential which are consistent with the previous ones are obtained from chi-square analyses for the present data. Some of angular distributions calculated with these potentials are shown in the figures. The solid line for E_{lab}=124MeV in Fig.1 is one of the results which reproduce not only the angular distribution but also the 90° excitation function around these energies. Therefore we can conclude that the prominent 124MeV minimum in the 90° excitation function for the $^{16}O+^{16}O$ system is due to an Airy minimum crossing 90° at this energy and thus supports the rainbow interpretation of the scattering phenomena.

---

[1]Department of Natural Sciences, Kyoto Women's University, Kyoto 605, Japan
[2]Department of Physics, Kyushu University, Fukuoka 812, Japan
[3]Daiichi College of Pharmaceutical Sciences, Fukuoka 815, Japan

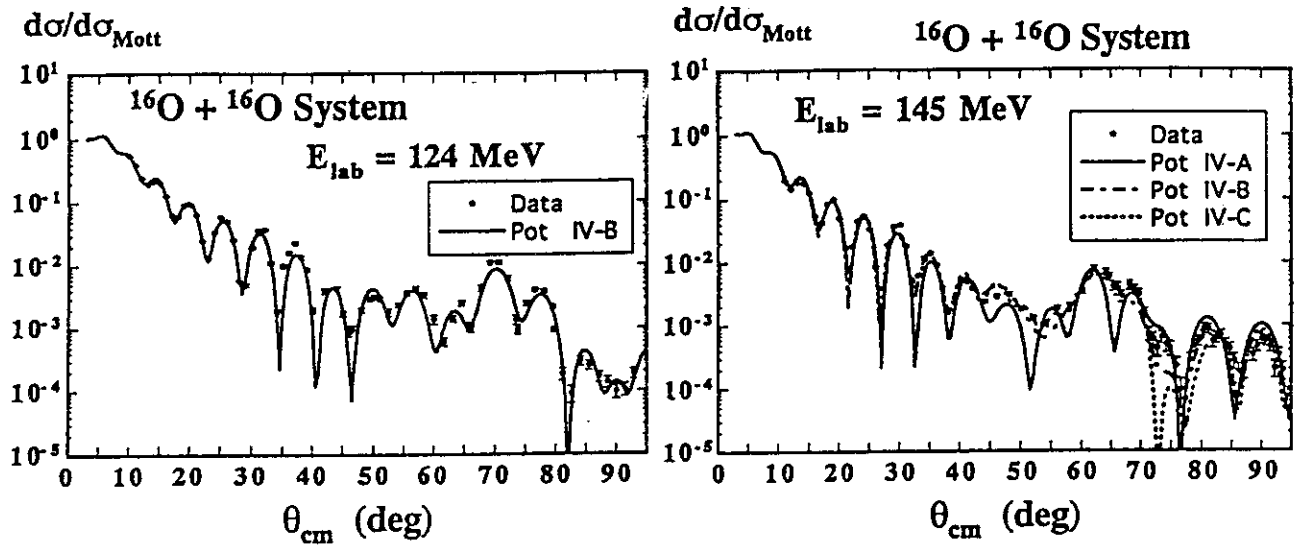

Fig.1 Elastic scattering angular distributions for $^{16}O+^{16}O$ measured at E_{lab}=124 and 145 MeV. Lines are typical examples of the optical model calculations.

References
1) K.W.McVoy and M.E.Brandan,Nucl.Phys.A542(1992)295.
2) E.Stiliaris et al.,Phys.Lett.B223(1989)291.
3) Y.Sugiyama et al.,Phys.Lett.B312(1993)35.
4) Y.Kondo et al.,Phys.Lett.B242(1990)340.
5) M.L.Halbert et al.,Phys.Lett.B51(1974)341.

3. 4 ELASTIC AND INELASTIC SCATTERING OF ^{58}Ni + ^{60}Ni NEAR THE COULOMB BARRIER

Y.SUGIYAMA,D.R.NAPOLI[1],Y.TOMITA,H.IKEZOE,Y.YAMANOUCHI, K.IDENO,T.SUGIMITSU[2],M.HIJIYA[2], Y.NAGASHIMA[3] and S.LANDOWNE[4]

A coupled-channels approach to heavy-ion collisions has provided a consistent framework for simultaneously calculating elastic and inelastic scattering, transfer reactions and the fusion cross section at energies around the Coulomb barrier. One of the successful results has been obtained for the ^{28}Si+^{58,64}Ni systems where the quasielastic-scattering cross sections[1] and the fusion cross section[2] have been measured at energies near the Coulomb barrier. The coupled-channels calculation including neutron transfer and inelastic excitation has explained well not only the energy dependence but also the isotope dependence of the quasi-elastic scattering and the fusion with a single energy- and isotope-independent bare potential.

In this paper we present the results of elastic and inelastic scattering measured in the ^{58}Ni + ^{60}Ni system at energies near the Coulomb barrier. This system is suitable for investigating the role of nucleon-pair transfer in the elastic channel, since neutron transfer can occur elastically between the ground states. The measurements were carried out at the JAERI tandem accelerator by using the heavy-ion magnetic spectrograph ENMA[3]. The spectrograph has the characteristic feature that the kinematic momentum shift k is well compensated , so that a high energy resolution is achieved over a wide range of k. Elastic and inelastic scattering angular distributions were measured at E_{lab}=204, 220, 236 and 250 MeV. We used targets of ^{60}Ni (50μg/cm^2 in thickness) on 10μg/cm^2 carbon backing. The enrichment of ^{60}Ni targets were 99.08%. The outgoing particles were momentum analyzed in the magnetic spectrograph ENMA and detected in the focal plane with a 40cm long hybrid focal plane detector.

In order to separate ^{58}Ni and ^{60}Ni, we measured a time-of-flight (TOF) of the product passing through the entrance position to the focal plane of the spectrograph whose flight path length was about 8 meters ,in addition to total energy E, energy loss δE and position Bρ . The start and stop signals were detected by a multi-channel plate detector placed in the scattering chamber and a plastic scintillation detector placed in the focal plane, respectively. The momentum spectrum of recoil ^{60}Ni obtained at θ_{lab}=25° at E_{lab}=204MeV after setting a proper window in the TOF spectrum is shown in Fig.1. An energy resolution of 600keV was enough to separate elastic and inelastic scattering in the ^{58}Ni+^{60}Ni system. The entrance slits of the spectrograph were opened 2.3° horizontally and 2° vertically which corresponded to a solid angle of 1.44 msr.

The angular distributions for elastic scattering at $E_{c.m.}$=103.7, 111.9, 120.0 and 127.1 MeV are shown in Fig 2. The data at backward angles larger than

---

[1]INFN-Laboratori Nazional di Legnaro, Legnaro, Italy
[2]Department of Physics, University of Kyushu, Fukuoka, Japan
[3]Tandem Accelerator Center, University of Tsukuba, Tsukuba, Japan
[4]Physics Division, Argonne National Laboratory,Argonne, USA

θ_{cm}=90° were obtained by measuring recoil ^{60}Ni. Charge state distributions of Ni were measured at several angles and analyzed by a semi-empirical formula based on Sayer's one[4]. The obtained parameters in the formula were used to estimate charge state distributions for the other angles.

We made the same type of the coupled-channels calculations[5] which explained well the results of other Ni+Ni systems. The calculations employ ingoing wave boundary conditions inside the Coulomb barrier to account for the fusion process, contain explicit couplings to inelastic excitations and transfer reaction channels, use an energy-independent real potential and have no phenomenological imaginary potentials. The dashed curves in Fig.2 allow for first- and second-order vibrational couplings to the one- and two-phonon states corresponding to the 2^+ and 3^- excitations of the projectile and target. The solid curves include, in addition, coupling to one- and two-neutron transfer channels. It is seen in Fig.2 that overall agreement between the full calculations and our elastic scattering data is quite good. The calculations also agree with the available fusion reaction data[6] and are consistent with precedent data for other Ni+Ni systems.

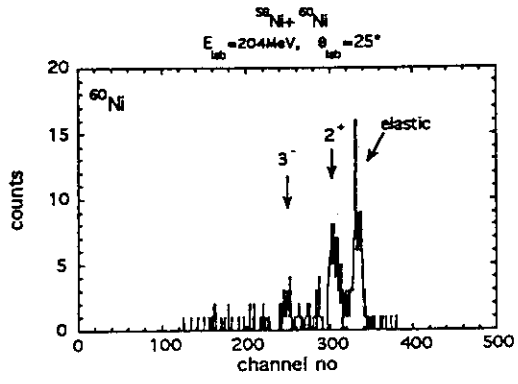

Fig.1.
A momentum spectrum of ^{60}Ni(recoil) obtained at θ_{lab}=25° from the ^{58}Ni+^{60}Ni reaction at E_{lab}=204MeV

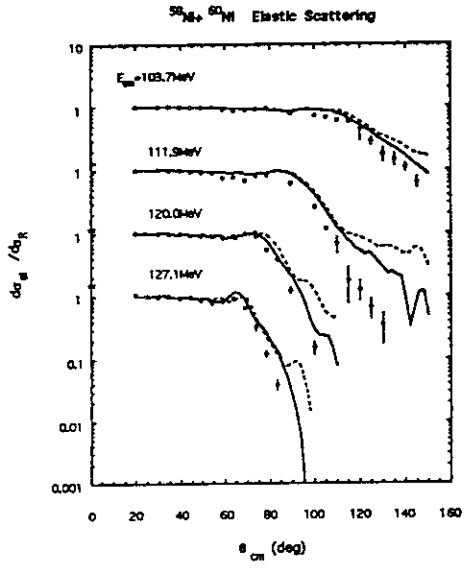

Fig.2. The angular distributions for elastic scattering. The dashed lines are the CC calculations including the first- and second-order vibrational couplings. The solid lines include, in addition, coupling to one- and two-neutron transfer channels.

References

1)Y.Sugiyama et al., Phys. Rev. Lett. **62**(1989)1727.
2)A.M.Stefanini et al., Phys. Rev. **C30**(1984)2088.
3)Y.Sugiyama et al., Nucl. Instr. and Meth. **A281**(1989)512.
4)R.O.Sayer,Revue de Phys.Appl.**12**(1977)1543.
5)H.Esbensen and S.Landowne, Nucl.Phys. **A492**(1989)473.
6) A.M.Stefanini et al., to be published.

3. 5 INVESTIGATION OF THE MULTI-NUCLEON TRANSFER REACTION (^{18}O,^{14}O) FOR NEUTRON-RICH NUCLEI

S. KUBONO[1], Y. FUCHI[1], T. NOMURA[1], M. H. TANAKA[1], S. KATO[2], Y. SUGIYAMA, S. HAMADA, K. IDENO, H. IKEZOE, Y. TOMITA, and Y. YAMANOUCHI

Multi-nucleon transfer, two-body reactions[1,2] are very useful especially in the light mass region for investigating the masses and the structures of them near the proton and neutron drip lines. The usefulness of the three-nucleon transfer reaction was demonstrated in a recent work on $^{24}Mg(^{3}H,^{6}He)^{21}Mg$[1]. The angular distributions measured for the reactions are well characterized by the transferred angular momentum, which enables a spin-parity assignment for the transition. The four-nucleon transfer reaction (^{18}O,^{14}O) seems to be also a useful tool for investigating the structure of neutron-rich nuclei of light mass region. This reaction was used before only for learning the masses of limited nuclei.

Test experiments were performed with a 100-MeV $^{18}O^{8+}$ beam from the JAERI Tandem accelerator. The reaction products ^{14}O from the $^{24}Mg(^{18}O,^{14}O)^{28}Mg$ reaction were analyzed by a heavy-ion magnetic spectrograph ENMA, and detected by a position-sensitive ionization chamber together with a plastic scintillator placed on the focal plane. They were identified by ΔE, E, and Time-of-Flight (TOF) signals which were determined by the flight time between the multi-channel plate (MCP) detector placed just after the target and the plastic scintillator. This focal-plane counter also provides two position-informations, enabling one to reduce background events of abnormal incidence to the focal plane. The average beam current used was about five hundred nanoamperes, and the target thickness of a self-supporting foil of enrich ^{24}Mg was about 680 $\mu g/cm^2$.

The ^{14}O particles from the reaction were identified and separated clearly from other oxygen isotopes at 20°. An ^{14}O spectrum accumulated for a day has some peaks which correspond well to the low-lying states in ^{28}Mg. The strongest transition is for the ground state, and has about one nb/sr. The data clearly indicates that the background level is far below the cross section of 1 nb/sr, confirming the usefulness of the present method for investigating the structure of light neutron rich nuclei. This success was achieved by the use of the TOF signals and also the good resolution of ΔE signals from the ionization chamber.

Some improvements should be made for extensive experimental programs. The energy resolution of the plastic scintillator may be improved, and also the solid angle will be enlarged by having a new MCP detector of a large area. These works are in progress.

References

1) S. Kubono, N. Ikeda, T. Nomura, Y. Fuchi, H. Kawashima, S. Kato, H. Miyatake, and H. Orihara, Phys. Rev. **C43** (1991) 1821.
2) S. Kato, S. Kubono, T. Nomura, Y. Fuchi, Y. Funatsu, S. Ohkawa, T. Miyachi, T. Suehiro, and Y. Yoshida, Phys. Rev. **C41** (1990) 2004.

1 Institute for Nuclear Study, University of Tokyo, Tanashi, Tokyo, 188 Japan
2 Physics Department, Yamagata University, Yamagata, 990 Japan

3. 6 SPIN ASSIGNMENTS OF INTERMEDIATE STRUCTURES IN $^{12}C(^{16}O,^{12}C(2_1^+))^{16}O$ USING THE γ-RAY RECOIL METHOD

H. FUJITA[1], M. HIJIYA[2], T. MUKAE[2], K. NAKAMOTO[2], T. OKAMOTO[2], S. KOJIMA[2], T. SUGIMITSU[2], N. IKEDA[2], S. MORINOBU[2], Y. SUGIYAMA, Y. TOMITA, H. IKEZOE, K. IDENO, Y. YAMANOUCHI and S. HAMADA

Some resonance-like structures in $^{12}C+^{16}O$ inelastic scattering for the single $^{12}C(2^+)$ and the mutual $^{12}C(2^+)$ + $^{16}O(3^-,0_2^+)$ channels have been investigated by measuring magnetic substate population for the 2^+ state at 4.44 MeV in ^{12}C by the γ-ray recoil method [1]. The magnetic substate population was determined in the coordinate frame where a quantization axis is taken along the center of mass scattering angle of a reaction product.

The experiment was performed by using the JAERI tandem accelerator. We used the advantages of the reversed kinematics for the backward-angle measurement by bombarding a ^{12}C target (50 $\mu g/cm^2$ in thickness) with an ^{16}O beam. Momentum spectra of ^{12}C ejected were measured with a high resolution by the heavy ion magnetic spectrograph "ENMA". The magnetic substate population has been obtained by unfolding the line shape broadened by γ decay in flight.

As mentioned in the previous reports [2,3], resonance-like structures were observed at $E_{c.m.}$ = 22.4, 29.8 and 31.8 MeV for the single excitation channel and at $E_{c.m.}$ = 30.1 and 31.8 MeV for the mutual one. The angular distributions for the individual magnetic substates were measured in the laboratory angle range from 4° to 17° in steps of 1° at $E_{c.m.}$ = 22.4, 29.8 and 31.8 MeV on-resonances and 33.0 MeV off-resonance for the single excitation channel and at $E_{c.m.}$ = 30.1 and 31.8 MeV on-resonances and 33.0 MeV off-resonance for the mutual one.

In the present work, the magnetic substate population has been extracted from a line shape of excited reaction products which are broadened by γ decay in flight. The broadened line shape is described only by the diagonal matrix elements of the nuclear density matrix by taking a z-axis along the center of mass scattering angle of the products, so that the magnetic substate population can be extracted properly from the line shape [1]. In this coordinate frame, the scattering amplitude for single excitation is given as

$$A_M(\theta) = (\sqrt{\pi}/ik)\sum_L \sqrt{2L+1}\exp(i\sigma_L)\sum_{L'} \langle LI-MM|L'0\rangle \exp(i\sigma'_{L'})S_{L'L}(-1)^{I-M}Y_{L'}^{-M}(\theta,0) \quad (1)$$

where L and L′ denote the initial and final orbital angular momentum, respectively, and I and M the spin and the magnetic substate, respectively, of the ejectile. The cross section is given as $(d\sigma/d\Omega)_M = |A_M(\theta)|^2$. If only one partial wave contributes, we can estimate directly the total spin J (= L) of the system by comparing the angular distribution with $|Y_L^M(\theta)|^2$. Furthermore, we can obtain the decay L′ value from the relative intensity between the cross sections for the individual magnetic substates.

For the single excitation channel, we tried to extract the S matrix elements $S_{L'L}$ by fitting the angular distributions for the individual magnetic substates with Eq. (1). We assumed that the resonances were dominated by a single value of J and the S matrix element of L′ = J + 2 for the anti-aligned configuration was negligible. We subjected the angular distributions of all substates to a fitting procedure. Results of the calculations are shown partly in Fig. 1. We suggest spin assignments of J = 16 or 17 for the resonance-like

[1]Daiichi College of Pharmaceutical Sciences
[2]Department of Physics, Kyushu University

structures at 29.8 and 31.8 MeV. Table 1 shows the magnitude of the S matrix element of L´ = J - 2 for the aligned configuration and the ratio of the magnitude for the non-aligned configuration to the aligned one along with the spin assignments for the structures at 29.8 and 31.8 MeV. Table 1 implies that

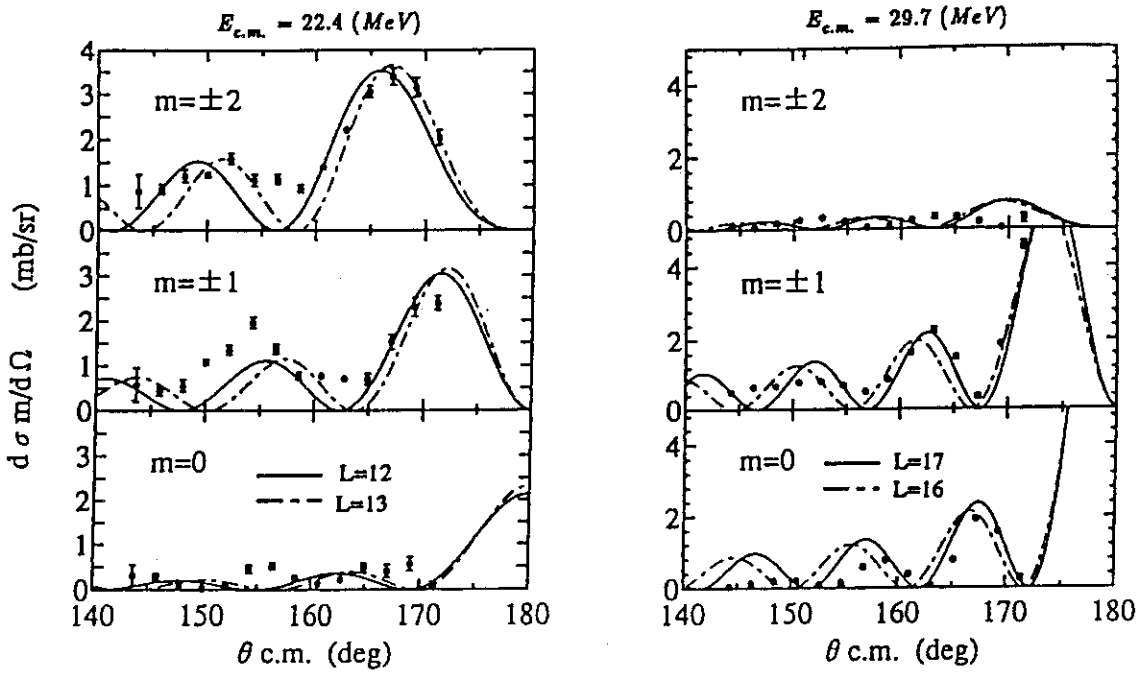

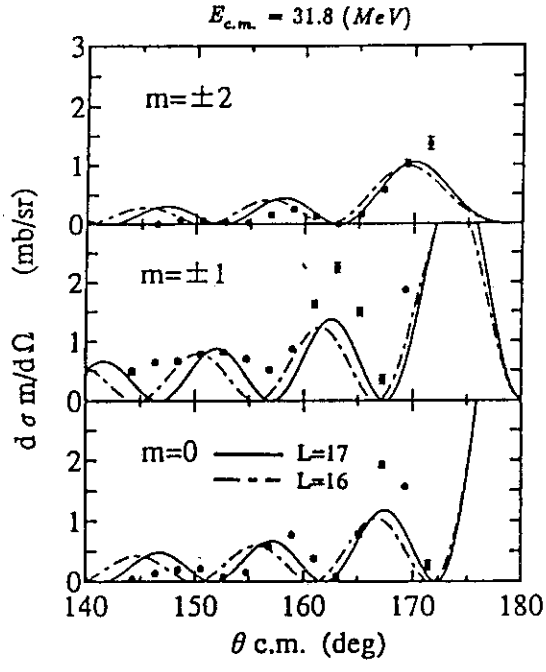

Fig. 1

Table 1

$E_{c.m.}$	J^{π}	|S(J-2)|	|S(J)/S(J-2)|
29.8	17^-	0.36	0.094
31.8	16^+	0.28	0.073
	17^-	0.28	0.064

the decay of the structures at 29.8 and 31.8 MeV proceeds dominantly through the L´ value of the aligned configuration. For the structure at 22.4 MeV, the χ^2-value of fitting is minimized at J = 12 and it is suggested that the non-aligned configuration is important. However, the angular distribution of m = 0 is not reproduced as shown in Fig. 1. This problem is now open. For the mutual excitation channel, similar analysis was performed and the importance of the partially aligned configuration is suggested. A part of the present results has been published in Ref. [4].

References

[1] Y. Sugiyama, Y. Tomita, H. Ikezoe and N. Shikazono, Z. Phys. A - Atoms and Nuclei **322** (1985) 579
[2] T. Mukae et al., JAERI TANDEM, LINAC & V.D.G. Annual Report 1991, p.154
[3] H. Fujita et al., JAERI TANDEM, LINAC & V.D.G. Annual Report 1992, p.129
[4] Y. Sugiyama et al., Phys. Rev. C **49** (1994) 3305

3. 7 3-α COINCIDENCE MEASUREMENTS FROM THE $^{16}O + ^{12}C$ REACTION AT 90 MEV

K. IDENO, Y. SUGIYAMA, H. IKEZOE, Y. YAMANOUTI,
S. HAMADA, Y. TOMITA, and S. HANASHIMA

High spin states of the ^{12}C nucleus are predicted[1-3] at ~10 to 35 MeV, but most of them are not experimentally confirmed. Caussyn et al.[4] searched for high spin states for the $^{12}C + ^{12}C$ system through the decaying mode of $^{12}C^* \rightarrow \alpha + {}^{8}Be_{g.s.}$. For the system of $^{16}O + ^{12}C$, we made a similar search for highly excited ^{12}C levels. A detection system was chosen to include the 7.65 MeV excitation of the ^{12}C nucleus. An ^{16}O beam of 90 MeV was generated by the JAERI tandem accelerator.

An experimental arrangement is shown schematically in Fig. 1. Detectors I and II, which were used for $^{8}Be_{g.s.}$ detection, consisted of a drift chamber and SSD's. Detectors I and II were placed in a drift chamber, and each of SSD's was made position-sensitive in a x-direction[5] and particle-identification was made. A detector III consisted of SSD's, where ΔE counter was position-sensitive.

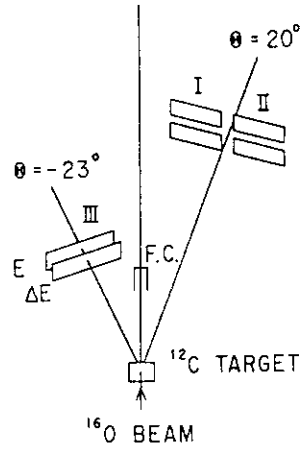

Fig. 1. Experimental arrangement.

By measuring the positions and energies of coincident three alpha-particles, we can kinematically reconstruct a Q-spectrum of an uncounted residual nucleus of ^{16}O. Particles of ^{8}Be in a ground state were selected from the relative energies between two alpha-particles detected in detector I or II.

1) The ^{12}C spectrum is shown in Fig. 2. It was obtained from the relative energies of $E_{rel}({}^{8}Be_{g.s.}, \alpha)$ for detectors I and II, gated by Q-spectra including $^{16}O_{g.s.}$, and its first excited states of doublets. Limited covering angle of the detectors I and II restricted the observation of high excitations of the ^{12}C levels. Below 12 MeV no unknown levels were observed. To observe higher excitations of the ^{12}C levels, it is necessary to extend a horizontal opening angle of the detectors I and II.

2) When $^{8}Be_{g.s.}$ and an alpha-particle are emitted each into the opposite side of the beam as in the case of I-III (Fig. 1), there is a possibility that they decayed from a highly excited nucleus of ^{12}C. However, there are many possible reaction channels which contribute to the production of $^{8}Be_{g.s.}$ and alpha-

particles[6]. It was difficult to separate the ^{12}C levels from α-backgrounds; there were dominant sequential components of $^{20}Ne^* \rightarrow {}^{16}O_{g.s.} + \alpha$ and $^{24}Mg^* \rightarrow {}^{16}O_{g.s.} + \alpha\alpha$, where these decays were mainly processed through the ^{24}Mg resonances in the energy range of 25 to 35 MeV.

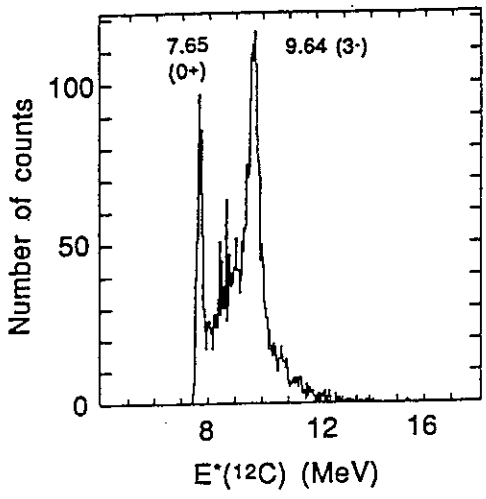

Fig. 2. Excitation spectra of ^{12}C nucleus generated by $E_{rel}(^8Be_{g.s.}, \alpha)$.

References

1) H. Morinaga, Phys. Lett. 21 (1966) 98.
2) D. Robson, Nucl. Phys. **A308** (1978) 381.
3) L. Ragnasson et al., Nucl. Phys. **A361** (1981) 1.
4) D. D. Caussyn et al., Phys. Rev. **43** (1991) 205.
5) K. Ideno et al., Nucl. Instr. and Meth. in Phys. Research, **A302** (1991) 385.
6) W. M. Rae et al., Phys. Rev. **C30** (1984) 158.

3. 8 MEASUREMENTS OF CAPTURE CROSS SECTIONS BETWEEN HEAVY IONS

H. IKEZOE, Y. NAGAME, T. OHTSUKI[1], S. HAMADA, R. SASAKI[1], Y. AOKI[1], I. NISHINAKA, Y. SUGIYAMA, Y. TOMITA and K. IDENO

The nuclear interaction acting between two colliding nuclei shows characteristic features that fusion probabilities at bombarding energies below fusion barrier are considerably enhanced compared to one–dimensional barrier penetration calculations and hindered at energies above fusion barrier especially for heavy target and projectile ($Z_1 \times Z_2 > 1600$, where Z_1 and Z_2 are the atomic numbers of target and projectile, respectively). So called sub–barrier enhancement of the fusion probability has been extensively studied[1] and the inelastic coupling to the fusion process in the approaching stage of two colliding nuclei becomes evident[2]. On the other hand, the nuclear dissipation and the Coulomb repulsion in the amalgamation process of two heavy nuclei act against the formation of compound nucleus[3]. These two mechanisms coexist in reactions using lead or uranium targets bombarded by heavy ions, which are generally used to synthesize new heavy elements.

We report the measurements of the capture cross sections in ^{209}Bi + ^{37}Cl, ^{45}Sc, ^{56}Fe and ^{59}Co reactions at bombarding energies near fusion barriers. Fusion events were identified by detecting symmetric fission fragments. In the present heavy reaction systems, the cross sections of fusion–evaporation products were assumed to be negligible. Two fission fragments were detected in kinematical coincidence by using two position sensitive parallel plate avalanche detectors (20 cm length × 12 cm high). The mass and the total kinetic energies of two detected fragments were obtained by analyzing the detected inplane and out–of–plane angles and arrival time differences between two detectors.

Figure 1 shows the two dimensional spectra of mass versus total kinetic energy obtained for the present reactions. In order to obtain the capture cross sections, the yields of symmetric mass division products were integrated assuming their angular distributions of $1/\sin(\theta_{cm})$. The measured capture cross sections were always enhanced at bombarding energies below fusion barriers and also especially in the ^{209}Bi + ^{56}Fe reaction, a large hindrance of the capture cross section was observed compared to an one–dimensional barrier penetration calculation. This hindrance was consistent with the Swiatecki extra–push model[3] using the parameters $X_{th} = 0.7$, $a = 7$ and $f = 0.5 - 0.75$, where X_{th} is the effective fissility defined by Toke et al.[4], a the slope coefficient and f the angular momentum fraction. Asymptotic energy shifts D_0 were obtained by comparing the measured capture cross sections to the one–dimensional barrier penetration calculations including the extra–push energies. The asymptotic energy shifts ($D_0 = 10 - 20$ MeV) increase as the effective fissility and the halves of the observed D_0 can be explained due to the inelastic coupling (2^+ and 3^-) of target and projectile. The detailed data analysis is in progress.

References

1)M. Beckerman, Rep. Prog. Phys. **51** (1988) 1047 and see references therein.
2)C. H. Dasso and S. Landowne, Nucl. Phys. **A407** (1983) 221.
3)W. J. Swiatecki, Nucl. Phys. **A376** (1982) 275.
4)J. Toke et al., Nucl. Phys. **A440** (1985) 327.

[1]Laboratoty of Nuclear Physics, Tohoku University, Sendai–shi, Miyagi–ken 982, Japan.

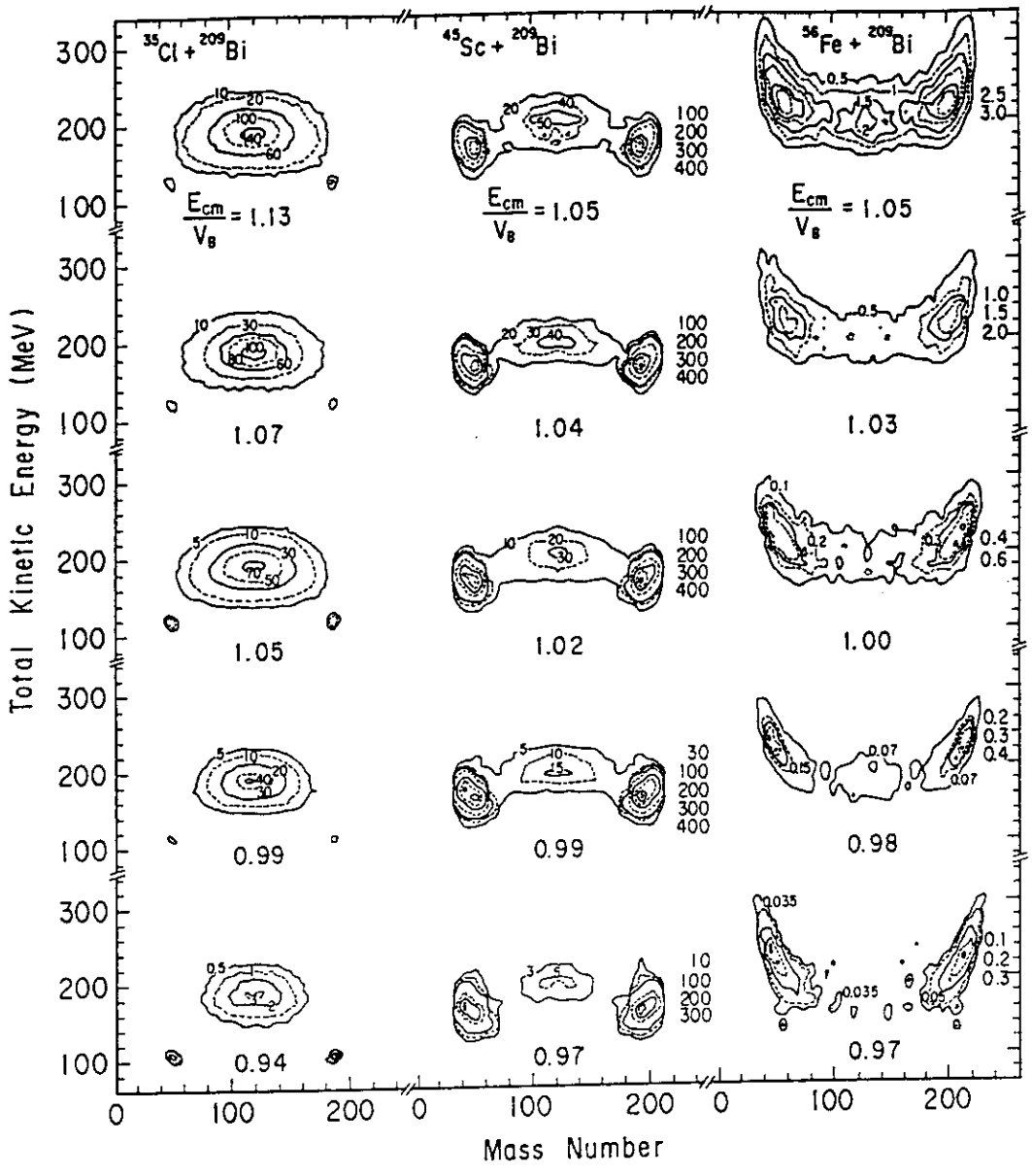

Fig.1 Two dimensional spectra of mass versus total kinetic energy for various reactions(μb/MeV.A). The ratios of center–of–mass energy E_{cm} to fusion barrier V_b are shown in each figure. The yields of projectile–like and target–like components are reduced by setting gates on fission fragments.

3. 9 TRANSITION OF THE FISSION MECHANISM IN THE PROTON-INDUCED FISSION OF ^{238}U AROUND E_x = 14 MeV

R. KASUGA[1], T. YAMAGUCHI[1], D. YANO[1], N. TAKAHASHI[1], A. YOKOYAMA[1], H. BABA[1] and S. SHINOHARA

Spontaneous and thermal-neutron-induced fissions of actinide nuclei reveal different features from those at high excitation energies. In the proton-induced fission of ^{238}U the systematics varies at the region near E_x = 14 MeV[1]. It suggests that the transition of the fission mechanism is expected to occur around this energy. We carried out further investigation and found the change of the fission characteristics in the range 16-18 MeV. The purpose of this work is to investigate the mass distribution in detail near this region.

In the present work, uranium was electrodeposited onto a aluminum foil in the thickness of about 2 mg/cm^2. The proton energies of the tandem Van de Graaf accelerater at JAERI were chosen to be 12.1 MeV and 13.5 MeV; the excitation energies were 17.2 MeV and 18.6 MeV, respectively. After the irradiation γ-rays were measured by means of Ge detectors. Measured γ-ray spectra were analyzed by use of the BOB code[2].

The most probable charge can be expressed in the form

$$Z_p = \frac{Z_c}{A_c - \nu_{pre}}(A + \nu_{post} \pm \Delta), \tag{1}$$

where subscripts c refer to compound nuclei, ν_{pre} is the number of pre-scission neutrons and expressed as

$$\nu_{pre} = \frac{E_x}{7.5} + \frac{Z_c^2}{2A_c} - 18.5. \tag{2}$$

In this equation ν_{post} is the number of the post-scission neutrons and Δ is the charge polalization(the plus sign stands for light fragments wheareas the minus sign is for heavy fragments). We found that Δ could be constant (1.5) at all excitation energies and therefore only the value of ν_{post} is an adjustable parameter to obtain the best mass yield distribution. The mass distributions are shown in Fig. 1 and Fig. 2.

The figure of merit χ for the fit to a Gaussian curve was calculated by the formula;

$$\chi = \frac{\sqrt{\sum(\log \frac{\sigma_{obs}}{\sigma_{cal}})^2}}{N}, \tag{3}$$

where σ_{obs} and σ_{cal} are the observed and calculated (by the Gaussian distribution) cross sections, respectively, and N is the number of data. We obtained χ = 0.58 for ν_{post} = 1.5 as the best fit in the case of the E_x = 17.2 MeV. Wheareas we obtained χ = 1.07 for ν_{post} = 1.0 as the best fit in the case of the E_x = 18.6 MeV. This implies that the scission takes place with a somewhat more compact shape in the case of the higher energy fission. In Fig. 1 the best mass yield distribution is exemplified for the case of E_x = 17.2 MeV with ν_{post} = 1.5.

[1]Department of Chemistry, Faculty of Science, Osaka University

The width parameter of charge dispersion σ has previously been obtained as 1.05 from the results around this energy region[3], which is characteristic of the high energy fission. Therefore, we should admit that we have not yet reached any definite conclusion on this problem.

References

1) S. Baba, H. Umezawa and H. Baba, Nucl. Phys., **A175**(1971)177.
2) H. Baba, T. Sekine, S. Baba and H. Okashita, JAERI Rept, No.1227(1972).
3) R. Kasuga, N. Nitani, T. Yamaguchi, D. Yano, N. Takahashi, H. Baba and N. Shinohara, OULNS Ann. Rept. **1992**(1993)120.

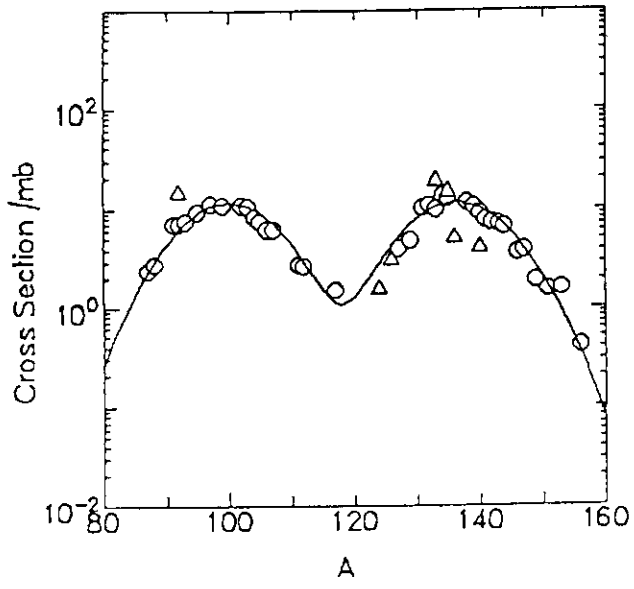

Fig. 1. Mass distribution at E_x = 17.2 MeV obtained using ν_{post} = 1.5. Open cercles and triangles indicate cumulative yields and independent yields, respectively.

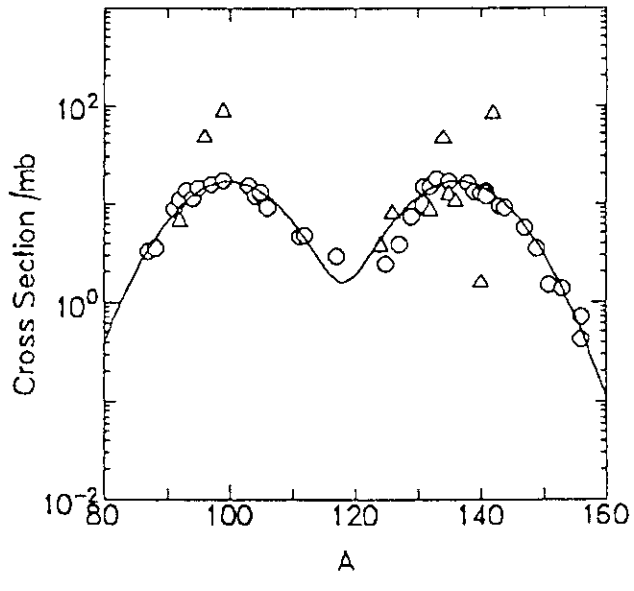

Fig. 2. Mass distribution at E_x = 18.6 MeV obtained using ν_{post} = 1.0. Open cercles and triangles are same as in Fig. 1.

3.10 STUDY OF THE U + Li REACTION FOR THE SYNTHESIS OF AMERICIUM ISOTOPES.

Y. HATSUKAWA, K. TSUKADA,
N. SHINOHARA, Y. NAGAME and M. OSHIMA

Recently, characteristics of the delayed-fission decay mode in light americium nuclei(^{232,234}Am) have been investigated.[1] The ^{236}Am, unknown nucleus, is also expected to be observed in EC-delayed fission activity. Production of ^{236}Am was attempted by U + Li reaction. To obtain the synthesis conditions of Am isotopes, excitation functions were measured. Depleted uranium target (1.0 to 1.2 mg/cm^2 in thickness, 99.98 % ^{238}U) were prepared by the electro-deposition using isopropyl alcohol onto aluminum backing foils(7 μm in thickness).[2] The uranium targets were irradiated with ^{7}Li ions (44 MeV) for 15 hours with JAERI Tandem accelerator. After the irradiation both the uranium target and the aluminum catcher foil were dissolved in concentrated HCl solution, where ^{243}Am tracer as a chemical yield monitor was added to the solution. The ion-exchange separation using HCl-CH_3OH mixed media was carried out on the dissolved sample to isolate the americium fraction.[3] The radiometric source was prepared by evaporating the solution of the americium fraction on tantalum disk. Alpha and γ-rays were measured with a Si-surface barrier detector and Ge detector,respectively. The measured excitation functions of the ^{238}U + ^{7}Li are shown in Fig.1. Excitation functions of the ^{235}U + ^{7}Li and the ^{238}U + ^{6}Li are also given in similar method. Based on these data, the new isotope, ^{236}Am, will be searched for investigation.

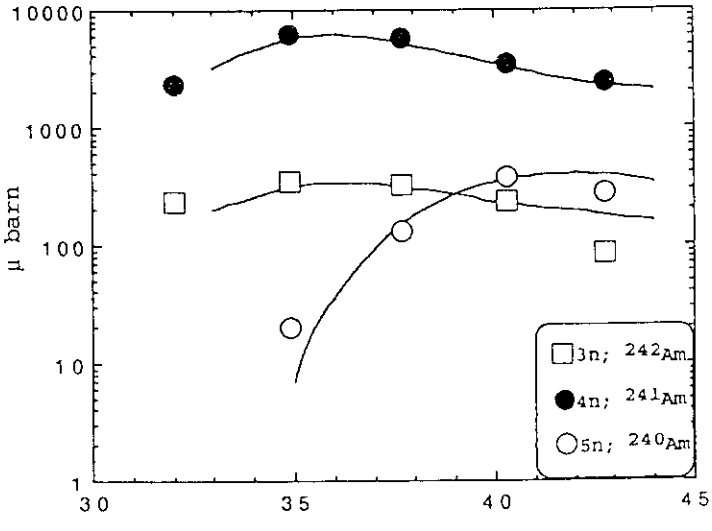

Fig.1 Excitation functions for Am isotopes produced in bombardment of ^{238}U with ^{7}Li ions. Solid lines show the calculated results of the Alice code. The calculations are normalixed to the maximium points of the experimental data.

References

1)H.L. Hall, et al., Phys. Rev. Lett. 63(1989) 2548
2)N. Shinohara and N. Kohno, Appl. Radiat. Isot. 40(1989) 41
3)S. Usuda, J. Radioanal. Nucl. Chem. 111(2) (1987) 477

3.11 ENTRANCE-CHANNEL DEPENDENCE OF SUB-BARRIER FUSION CROSS SECTIONS IN FERMIUM (Z=100) REGION

Y. NAGAME, H. IKEZOE, K. TSUKADA, I. NISHINAKA, Y. HATSUKAWA, S. HAMADA, T. OHTSUKI [1], R. SASAKI [1] and Y. AOKI [1]

Heavy-ion induced fusion reaction at near barrier or even at sub-barrier energy region are an excellent tool for the synthesis of exotic heavy nuclei with $Z \geq 100$. However, in very heavy systems it is well known that the fusion process is increasingly hindered with mass symmetry of entrance channels, although enhancement of sub-barrier fusion cross section has been observed in light and medium-heavy mass systems.

In the present work, the enhanced sub-barrier fusion and the dynamical hindrance of fusion processes are examined by studying the production of Fm compound nuclei in complete fusion reactions with different target-projectile combinations at close to barrier and sub-barrier energies. The used reaction systems are following: $^{35,37}Cl + ^{209}Bi$ and $^{45}Sc + ^{197}Au$.

The experiments were carried out at the JAERI tandem accelerator using the $^{35,37}Cl$ and ^{45}Sc beams to bombard ^{209}Bi and ^{197}Au targets, respectively. Since the evaporation residue cross section is negligible fraction of the fusion cross section in these mass region, we have measured fusion-fission cross sections which are nearly equal to fusion cross sections. Complete fusion-fission products were detected with two x- and y- position sensitve parallel plate avalanche counters (PPAC), each with an active area of 20 x 12 cm^2, placed at either side of the beam.

In Fig. 1, the fission cross sections are plotted as a function of the difference between center-of-mass (c.m.) bombarding energies and Coulomb barriers, together with the data of the $^{40}Ar + ^{208}Pb$ [1] and $^{16}O + ^{238}U$ [2] systems. The ordinate is the dimensionless fission cross sections $\sigma_{fiss}/\pi\lambda^2$. As shown in Fig. 1, the large enhanced sub-barrier fusion cross sections are observed in the $^{35,37}Cl + ^{209}Bi$, $^{45}Sc + ^{197}Au$ and $^{40}Ar + ^{208}Pb$ systems, while in the most asymmetric reactions system $^{16}O + ^{238}U$ [2], a slight sub-barrier enhancement is seen. The dynamical hindrance of the fusion is not clear in the present systems studied. We are planning to perform the experiment in the more symmetric system $^{59}Co + ^{181}Ta$ to further study on the sub-barrier fusion process.

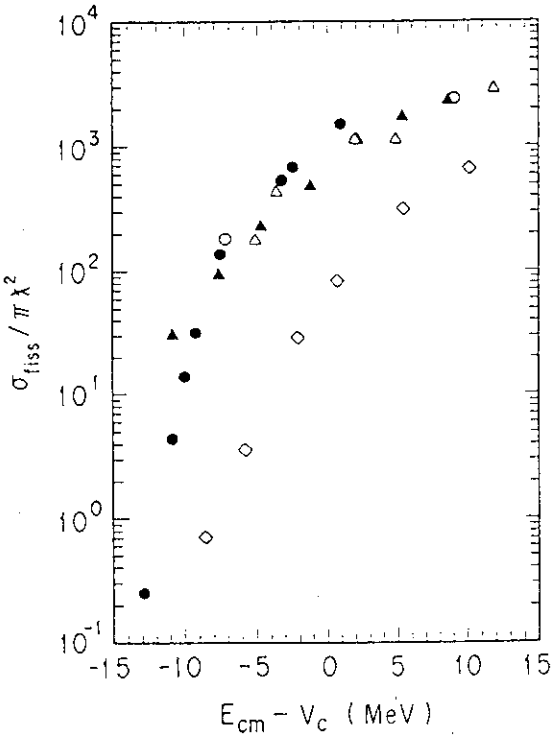

Fig. 1. Dimensionless cross sections $\sigma_{fiss}/\pi\lambda^2$ as a function of the difference between c.m. bombarding energies and Coulomb barriers for the reactions ○ $^{35}Cl + ^{209}Bi$, ● $^{37}Cl + ^{209}Bi$, △ $^{45}Sc + ^{197}Au$, △ $^{40}Ar + ^{208}Pb$, and ◇ $^{16}O + ^{238}U$.

References
1) H.-G. Clerc *et al.*, Nucl. Phys. A419 (1984) 571.
2) H. Zhang *et al.*, Phys. Rev. C 49 (1994) 926.

[1]Laboratory of Nuclear Science, Tohoku University

3.12 FRAGMENT MASS AND KINETIC ENERGY DISTRIBUTIONS IN FISSION OF Z_{CN}=100

T. OHTSUKI[1], R. SASAKI[1], Y. AOKI[1], J. KASAGI[1], H. IKEZOE,
S. HAMADA, Y. NAGAME, K. TSUKADA, I. NISHINAKA

Using the JAERI tandem accelerator, we are studying fission in the region of heavy actinides[1,2,3]. Especially, The correlation between fragment mass and total kinetic energy has been studied for heavy ion induced fission of fermium isotopes with TOF method. The reaction systems used were for the $^{35}Cl+^{209}Bi$, $^{37}Cl+^{209}Bi$, $^{45}Sc+^{197}Au$ and $^{59}Co+^{181}Ta$. They make different compound nucleus from neutron number 140 to 146 of fermium (Z=100). The structure of mass and kinetic energy distrubutions for different neutron number of fermium isotopes would be estimated as a function of excitation energy. The targets were bombarded from just on Coulomb barrier to sub-barrier region as far as possible. The start and stop detectors of the TOF system were delivered with large area parallel-plate avalanche counters (PPACs).

The primary mass and kinetic energy of fission fragments were obtained from the ratio of the velocities of the pair fragments as a first assumptions of the compound nucleus for each system. Analysis is in progress and some results are presented. FWHMs of the mass distributions(MASS) and total kinetic energy distributions(TKE) for the $^{37}Cl+^{209}Bi$ are shown in Fig. 1 as a function of excitation energy. Each slope for the FWHMs of MASS and TEK is roughly in agreement with a theoretical prediction[4] of the liquid drop model using nuclear temperature T.

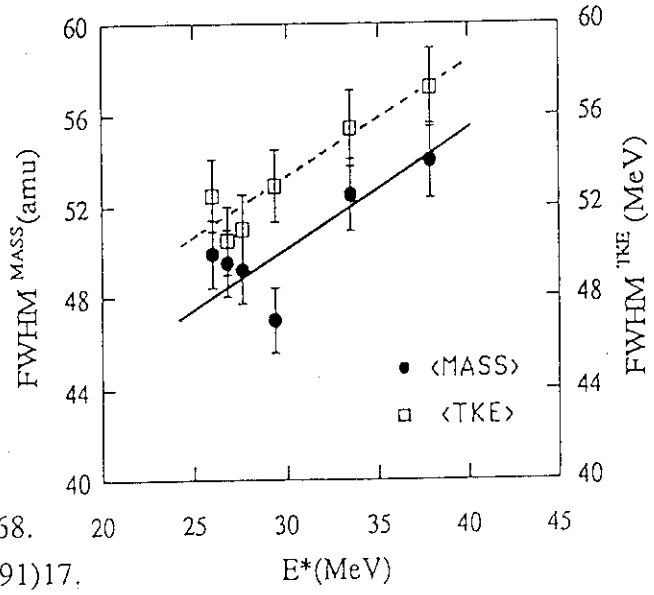

Fig.1 Full width at half maximum height (FWHM) of the mass and total kinetic energy distributions for the $^{37}Cl+^{209}Bi$ system as a function of the excitation energy. Solid line and dotted line indicate the slopes estimated by the liquid drop model including nuclear remperature T for the FWHM values experimentally obtained of MASS and TKE, respectively.

[1] H. Ikezoe et al., Phys. Rev. C49, (1994)968.
[2] T. Ohtsuki et al., Phys. Rev. Lett., 66, (1991)17.
[3] Y. Nagame et al., Nucl. Instr. Meth., B56/57, (1991)511.
[4] J.R. Nix, Nucl. Phys. A130, (1969)241.

[1] Laboratory of Nuclear Science, Faculty of Science, Tohoku University.

3.13 Heavy ion induced D-D fusion in deuteride solid

M. Teshigawara[1],K. Konashi[1],T. Yamamoto[1],H. Kayano[1]
Y. Aratono,K. Furukawa and E. Tachikawa

Introduction

Experimental data of D-D fusion at low energy are important for understanding of cold fusion phenomena. In particular,we are interested in D-D fusion in solid. It is well known that an energetic heavy ion particle generates collision cascade in solid, which includes a large number of low energy deuterons. We measured the D-D fusion caused by low energy deuteron in solid.

Experiment

The titanium deuteride, TiD_x ,was bombarded by Iodine(I^{7+}), which was accelerated by JAERI Tandem accelerator with the beam energy of 90 MeV.The experimental equipment was set at the R2 beam line. Target samples TiD_x(x =0.14,0.82,1.61, and 1.93) were prepared by deuterium absorption method. Neutrons were detected by BC-501 liquid scintillation counter (14.1 cm in diameter and 13.7 cm thickness) which includes ^{6}Li glass scintillator counter. The center of neutron detector at 90^0 to the beam axis was placed at 35 cm from target.

Results and discussion

Experimental results show almost constant neutron yield during irradiation time of 1 h. Figure 1 shows an example of 3-dimensional spectrum of $D(d,n)^3He$ in TiD_x bombarded by Iodine(I^{7+}). The signal for γ ray is presented by ridge peak at about 0.66 μ s fall time. The neutron appears as a ridge peak at 0.74 μ s fall time and sharp peak at 0.8~0.96 μ s fall time. The ridge peak at 0.74 μ s fall time is made from signal by BC501 liquid scintillator. The sharp peak is made from signal by ^{6}Li glass scintillator. We detected the neutron of $D(d,n)^3He$ reaction between lattice D atom and recoiled D atom under irradiation of heavy ion with very low background. After the irradiation, the TiD_x samples were analyzed by X ray diffraction method. Two phases in the samples were found. One is Ti phase and the other is $TiD_{1.97}$ -phase.

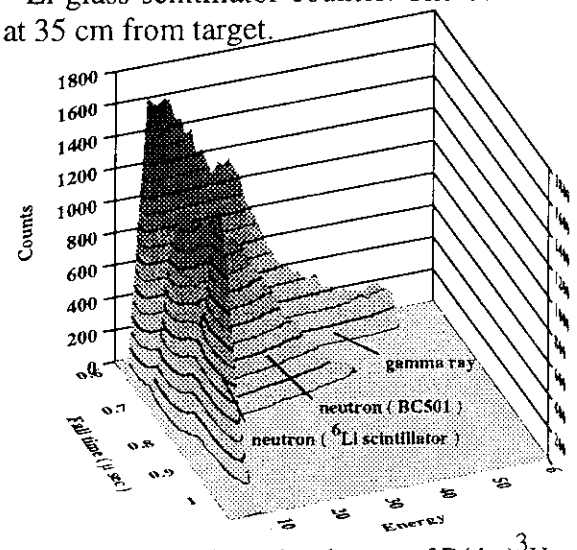

Fig.1. 3 dimensional curve of $D(d,n)^3He$ in $TiD_{1.61}$ bombarded by Iodine (I^{7+})

The simulation of the D-D fusion process was also performed by computer code. The D-D fusion rate has been calculated for the following process;

(1) Heavy ions are irradiated in TiD_x.

(2) Lattice D atoms are recoiled by heavy ion.

(3) D-D fusion occurs between lattice D atom and recoiled atom.The D-D fusion rate per incident ion is written by

$$T(E^0_{ion}, n_D) = \int_{E_D^{min}}^{E_D^{max}} Y(E^0_{ion}, E^0_D)\, P(E^0_D)\, dE^0_D$$

where

$T(E^0_{ion}, n_D)$ = D-D fusion rate per ion,

$Y(E^0_{ion}, E^0_D)$ = Probability of primary knock on D atom with energy of E^0_D,

$P(E^0_d)$ = D-D fusion probabity for primary knock on D atom with initial energy of E^0_d.

Figure 2 shows the comparison of experimental results of rate of the D-D fusion with theoretical predictions. Experimental values of D-D fusion values are ten times larger than those of theoretical predictions. We are investigating the cause of the difference between experimental data and theoretical predictions.

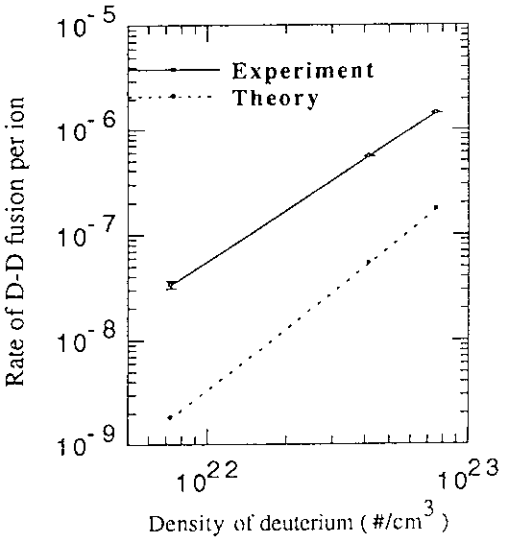

Fig.2. Rate of d-d fusion in Ti Dx for ion beam of Iodine with energy of 90 MeV

1 Oarai Branch,Institute For Materials Research,Tohoku University

4. Nuclear Theory

4. 1 APPLICATIONS OF IBM-3 TO THE $Z \sim N \sim 40$ NUCLEI

M. SUGITA

Using a complete diagonalization program of IBM-3 hamiltonians, the shape transitions from $A = 80$ to 90 are investigated. The nuclei at $A \sim 80$ are characterized by huge deformation ($\beta_2 \sim 0.4$) but rather low values of the ratio $\mathrm{Ex}(4_1^+)/\mathrm{Ex}(2_1^+) \sim 2.5$. Indeed, for the $^{80}_{32}$Sr nucleus, the energy spectrum and the $\mathrm{B(E2};I \to I-2)$ values within the ground band ($I = 2, \ldots, 10$) can be fitted almost completely using the O(6) limit of IBM. We use the following IBM-3 hamiltonian:

$$H = e_d n_d - \sum_{t=0,1,2} \kappa(t) Q(t) : Q(t) + \alpha T(T+1), \tag{1}$$

where the symbol (:) means the scalar products with respect to both the angular momentum and the isospin, and Q is an O(6)-type quadrupole operator; $Q(t) = [s^\dagger \tilde{d} + d^\dagger \tilde{s}]^{(l=2,t)}$. This hamiltonian is O(5) invariant. The IBM-3 wavefunctions can be classified by the permutation symmetry of charge and orbital wavefunctions $[f] = [f_1 f_2 f_3]$ as $|[N]; [f] T T_z; [f] \beta L M >$; both the charge and orbital permutation symmetries should be the same because of boson symmetry. The hamiltonian Eq.(1) contains the isovector and isotensor Q forces and thus does not conserve [f]. We assume that there is no quadrupole force between identical particles, which leads to $2\kappa(0) + 3\kappa(1) + \kappa(2) = 0$. Then the quadrupole force can be rewritten as $-x\{[s^\dagger d^\dagger]^{(t=0)} : [\tilde{d}\tilde{s}]^{(t=0)} + \sqrt{5/2}([s^\dagger s^\dagger]^{(t=0)} : [\tilde{d}\tilde{d}]^{(t=0)} + \mathrm{h.c})\} + \xi_2 [s^\dagger d^\dagger]^{(t=1)} : [\tilde{d}\tilde{s}]^{(t=1)}$, where $x = 2(\kappa(0) + 2\kappa(2)) = 3(\kappa(2) - \kappa(1))$ and $\xi_2 = 2/3(x - 6\kappa(2))$. The second term is one of the so-called Majorana interactions and gives the energy splitting between $[f] = [N]$ and $[N-1, 1]$ states. The values for α in Eq.(1) and ξ_2 are determined so as to reproduce the excitation energies (7 Mev, 9 Mev) of the $T = 1, 2$ states of the lighter $Z = N$ nuclei such as ^{44}Ti, ^{48}Cr and ^{52}Fe. The x value is determined by ^{80}Sr. The values for κ are decreased linearly from the values obtained at $A = 80$ to 0 at $A = 90$. The d-boson energy e_d is determined so as to reproduce $\mathrm{Ex}(2_1^+)$ for each nucleus. We got resonably good reproduction of the systematics of the energy levels of the ground bands and $\mathrm{B(E2:}0_1^+ \to 2_1^+)$. In the figures, we show an example of the results of the present study, where the excitation energies of the *scissors* states with $J^\pi = 1^+$ and the $\mathrm{B(M1:}0_1^+ \to 1^+)$ values to them from the ground states are plotted for the $_{40}$Zr isotopes. We use the the following M1 operator: $T(\mathrm{M1}) = \sqrt{3/4\pi}(g_\pi L_\pi + g_\nu L_\nu + g_{\pi\nu} L_{\pi\nu})$ with $g_\pi = 1, g_\nu = 0, g_{\pi\nu} = 1/2(\mu_N)$. In the $N = Z$ nucleus ^{80}Zr, the *scissors* mode is concentrated to a single state with $T = 1$ at the relatively high excitation energy ~7 MeV. However, in the $N \neq Z$ nuclei, they split into T and $T+1$ states and the B(M1) values to $T_f = T$ is much bigger than the values to $T_f = T+1$, where T is the isospin of the ground state. It would be interesting to search experimentally for the rather low-lying (~3 MeV) *scissors* states in the current region of nuclei.

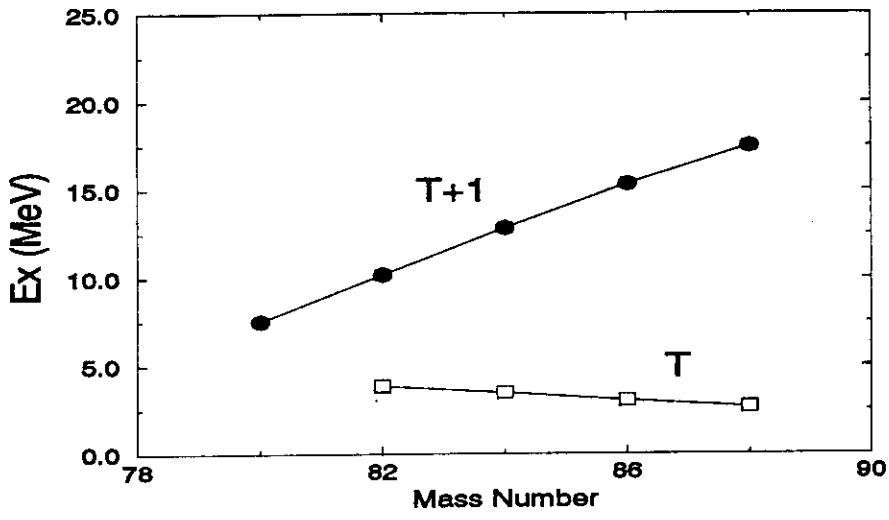

Figure 1: Excitation energies of the Scissors modes for the Zr isotopes.

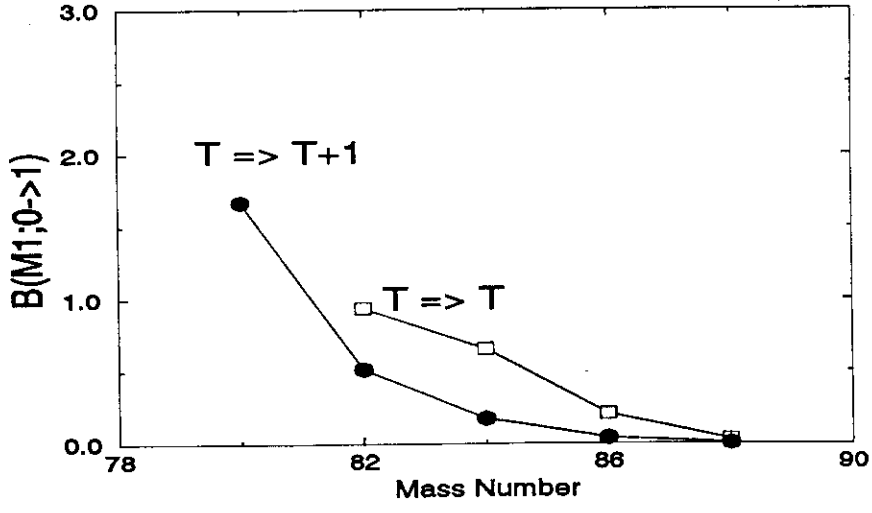

Figure 2: B(M1) values to the Scissors states for the Zr isotopes.

4. 2 QUANTUM MOLECULAR DYNAMICS CALCULATION OF NUCLEON-NUCLEUS REACTIONS

S. CHIBA, H. TAKADA, T. HUKAHORI, K. NIITA[1],
T. MARUYAMA and A. IWAMOTO

Nuclear reactions reveal various aspects as a function of projectile/target mass, projectile energy and impact parameter. In nucleon induced reactions, the compound nuclear process is dominant in MeV region, while the pre-equilibrium and spallation processes become more likely as projectile energy increases. In heavy-ion (HI) nuclear physics, the reactions are also interpreted with different concepts applicable to each specific process.

Recently, the method of microscopic simulation has been developed quite rapidly in heavy ion physics. Quantum Molecular Dynamics [1] is one of those simulation methods. The basic ingredients of this model are the self-consistent nuclear mean field and the stochastic N-N collision term taking account of the Pauli blocking. The mean field plays an important role in low energy domain (e.g. success of TDHF theory) since Pauli blocking prohibits the N-N collision. On the other hand, nuclear reactions are well described by the collision term alone in a very high energy region as the cascade model indicates. Because of these two ingredients, QMD has been able to give a unified description for the various reaction mechanism of the HI-HI reactions over the projectile energy of several MeV to GeV/nucleon. The same prosperity is expected for nucleon-nucleus (N-A) reactions, because the mean field and two-nucleon collision correspond to the real and imaginary parts of the optical potential respectively, which are the most important quantities in understanding the N-A reactions.

In spite of its success in the heavy ion physics, the validity of QMD in nucleon-induced reactions is still uncertain, because QMD has not been applied intensively to the latter field except for an analysis of (p,xn) reaction carried out by Peilert et al. [2]. In their analysis, however, contribution of the statistical decay from the residues produced in the QMD calculation was not considered. Therefore, we propose here an unified model of QMD incorporated with the statistical decay model, and apply it to nucleon-induced reactions.

The QMD with statistical decay model calculations have been carried out for C, Al and Fe in the energy region of 25 MeV to 3 GeV. In Figure 1 and 2 shown are the typical results of (p,xn) reactions for Fe with experimental data [3] and predictions of cascade+evaporation code (NUCLEUS[4]). At 113 MeV, the cascade model gives lower values compared with the experimental data at the most backward angle, which fact has been interpreted as an evidence of the pre-equilibrium contribution to be added to the cascade model calculations. The present results, on the contrary, reproduce the measured data satisfactorily over the whole angular region. Moreover, the agreement of the present calculation with the low energy neutron data confirms that the QMD gives a proper excitation spectra of residues

[1]Nuclear Energy Data Center

from which the statistical neutron emission takes place. Therefore, it is clear that the present calculation based on QMD + statistical decay includes the major three reaction mechanisms of nucleon induced reaction, i.e., the cascade (spallation), pre-equilibrium and statistical decay of compound system, in a unified framework. At 800 MeV, the agreement of the present calculation with the measured data is also remarkable.

The QMD + statistical decay model has been applied to analyze the nucleon-induced nucleon emission cross sections from several tens MeV to several GeV. It was proved that the present calculation could reproduce the measured data quite satisfactorily without assuming any additional reaction mechanism and without any adjusting parameters. The QMD gives a unified framework of the major three reaction mechanisms of nucleon-induced nuclear reactions; the spallation, pre-equilibrium and compound processes.

References

1) J. Aichelin, Phys. Rep. **202** 233 (1991); and references therein.
2) G. Peilert, J. Konopka, H.Stöcker, W. Greiner M. Blann and M. G. Mustafa, Phys. Rev. C**46** 1457 (1992)
3) M. Meier, private communication, LA-11518-MS, LANL(1989)
4) T. Nishida et al., JAERI-M 86-116 (1986)

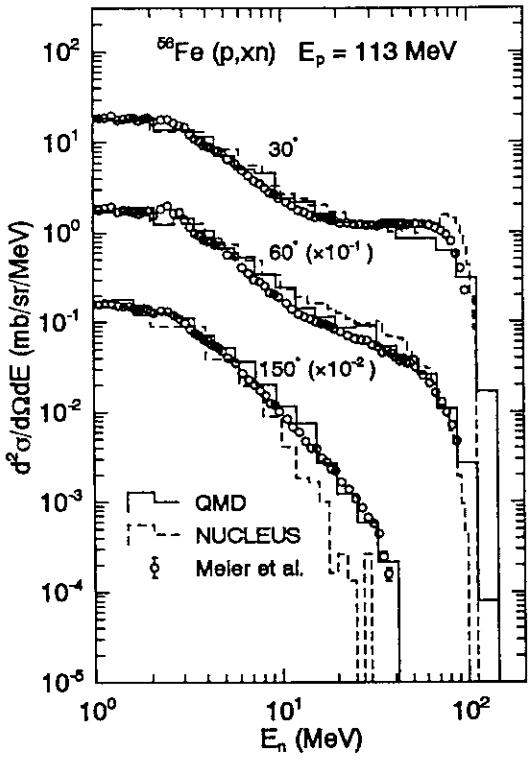

Fig.1 ^{56}Fe (p,xn) at 113 MeV

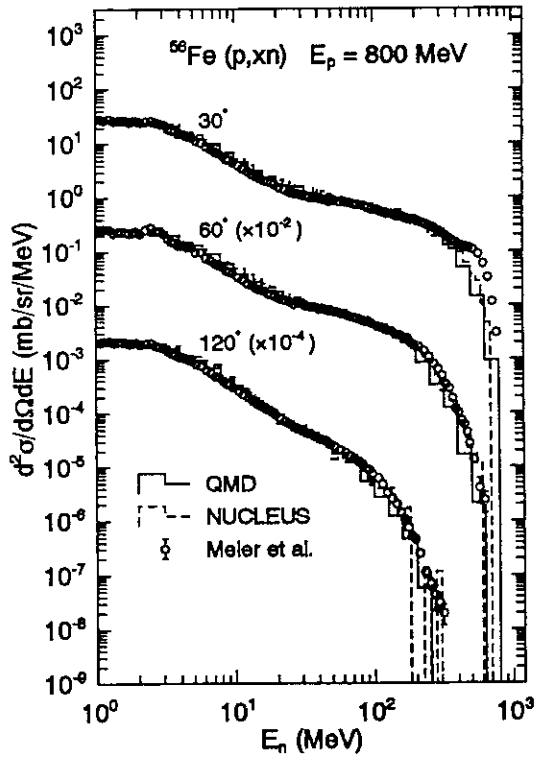

Fig.2 ^{56}Fe (p,xn) at 800 MeV

4. 3 Improvement of Quantum Molecular Dynamics

T. MARUYAMA, K. NIITA[1] and A. IWAMOTO

A microscopic simulation method of QMD (Quantum Molecular Dynamics)[1] is now widely used for analyses of heavy-ion reactions, since it is very practical and natural in describing fragments formation. However, it has classical nature, and can not well describe the ground state properties of initial nuclei. AMD (Antisymmetrized MD)[2] and FMD (Fermionic MD)[3] have been proposed in order to retain the quantum features by employing the Slater determinant for the total wave function of the system. The ground states obtained by AMD and FMD have appropriate values of binding energies, density distributions, and so on. Furthermore, shell effects are observed in the ground states and reaction dynamics. However, it consumes huge amount of CPU time especially for heavy systems. The mass-number dependence of the CPU time of AMD and FMD is its fourth power, while the CPU time of QMD calculation is proportional to the second power of the mass number. In this respect, some extensions of QMD is desirable.

One of possible improvements is to include the Pauli potential[4 – 6] into effective interaction. We propose a simple form of the Pauli potential defined as a function of overlap of the single-particle wave functions, which prevents the breaking of the Pauli principle. Another possibility is to treat widths of wave packets as physical variables according to time-dependent variational principle[7]. This makes the energy from the variance of momentum of each wave packet to transform to other degrees of freedom. With these two extensions, we can define clearly the ground state nuclei as an energy-minimum states, which is not always satisfied in the standard QMD. The initial ground nucleus obtained from this framework is completely stable, since all the variables stop their motion in the energy-minimum state.

We show in Fig. 1 the radial density distribution (a) and the density contour (b) of ground state of ^{12}C. This ground state has the binding energy of 93 MeV and root mean square radius (r.m.s.r.) of 2.64 fm, which agrees well with the experimental data ($E_{\rm bind}$ = 92 MeV, r.m.s.r. = 2.4 fm). It should be noted that the ^{12}C nucleus obtained here shows a kind of shell effect, i.e. three-α cluster structure (see Fig. 1 (b)) due to the effect of the Pauli potential. Similar structure is observed in the AMD calculation, but not in the standard QMD calculation. In Fig. 2, we show the width distribution (upper) and the radial density distribution (lower) of ^{48}Ca (a) and ^{100}Mo (b), respectively. Though we adjust slightly the parameters of Pauli potential, the binding energies of ^{48}Ca and ^{100}Mo nuclei show quite good agreement with experimental values. The upper part of Fig. 2 shows the distribution of the width of each wave packet as a function of its position from the center of the system. It is indicated that the width is wider near the center and narrower on the surface. This feature makes an important role to obtain a good shape of the density distribution, particularly on the surface. Though there are some fluctuations

⋆ 1 Nuclear Energy Data Center

of proton and neutron densities in the inner region, the overall density profiles are fairly good for ^{48}Ca and ^{100}Mo.

We should note that these extensions of QMD framework seem to be much promising since calculations of heavy system in the low energy region need enough stability of initial ground nuclei and reasonably small amount of CPU time.

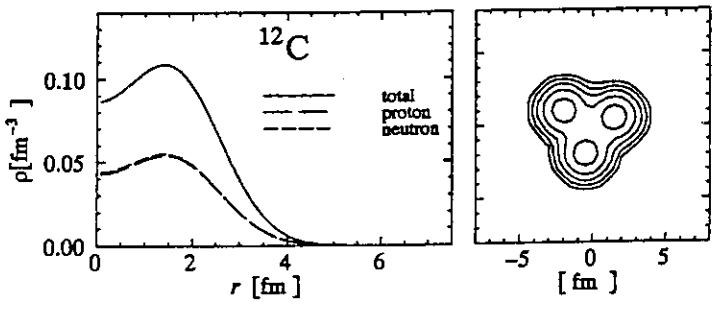

Fig. 1. Contour plot (left) and the radial distribution (right) of density in ^{12}C ground state.

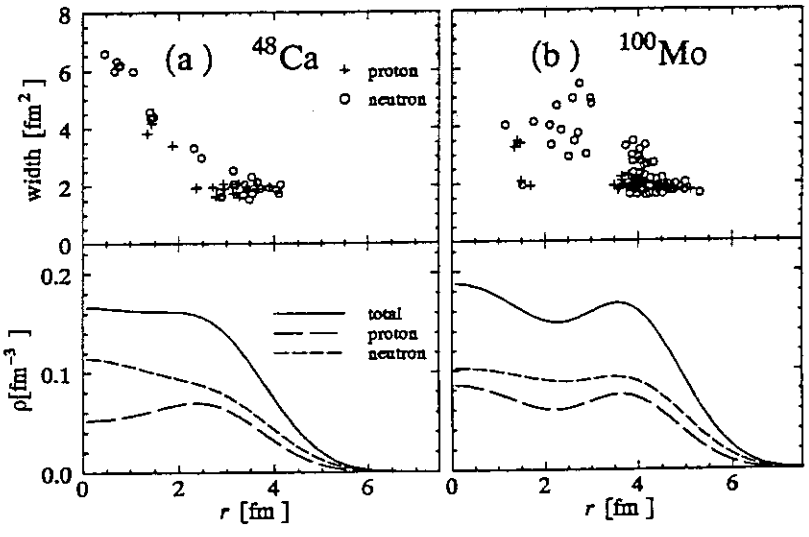

Fig. 2. Gaussian width (upper) and the density (lower) distribution of ^{48}Ca ground state.

References

1) J. Aichelin, Phys. Rep. **202** (1991), 233; and references therein.
2) A. Ono, H. Horiuchi, T. Maruyama and A. Ohnishi, Prog. Theor. Phys. **87** (1992), 1185.
3) H. Feldmeier, Nucl. Phys. **A515** (1990), 147.
4) G. Peilert, J. Konopka, H. Stöcker, W. Greiner, M. Blann and M. G. Mustafa, Phys. Rev. **C46** (1992), 1457.
5) C. Dorso and J. Randrup, Phys. Lett. **B301** (1993), 328.
6) A. Ohnishi, T. Maruyama and H. Horiuchi, Prog. Theor. Phys. **87** (1992), 417.
7) P. Valta, J. Konopka, A. Bohnet, J. Jaenicke, S. Huber, C. Hartnack, G. Peilert, L. W. Neise, J. Aichelin, H. Stöcker and W. Greiner, Nucl. Phys. **A538** (1992), 417c.

4. 4 GENERALIZATION OF NUCLEUS-NUCLEUS POTENTIAL

Akira IWAMOTO and Peter MÖLLER[1]

The potential energy between two colliding heavy ions is usually given as a sum of a Coulomb-energy term and a finite-range surface-energy term [1]. To allow a systematic evaluation of the potential energy for arbitrarily oriented, deformed heavy ions we develop the integrals that occur in macroscopic expressions for the nuclear and Coulomb interaction energies to a set of expressions that are suitable for numerical evaluation.

We start from the finite-range surface energy, or as it is also called *nuclear* energy

$$E_{\rm n} = -\frac{c_{\rm s}}{8\pi^2 r_0{}^2 a^3}\int\!\!\int \left(\frac{\sigma}{a} - 2\right)\frac{e^{-\sigma/a}}{\sigma}\, d^3r\, d^3r' \tag{1}$$

and for the direct sharp-surface Coulomb energy

$$E_{\rm C} = \frac{1}{2}\int\!\!\int \frac{1}{\sigma}\rho(\vec{r})\rho(\vec{r}')\, d^3r\, d^3r' \tag{2}$$

where

$$\vec{\sigma} = \vec{r} - \vec{r}' \tag{3}$$

and where the charge density at point $\vec{r}$ is given by $\rho(\vec{r})$.

The six-dimensional volume integrals that define these energy terms may be reduced to four-dimensional surface integrals by a two-fold application of Gauss theorem [1]. One obtains for the nuclear energy

$$E_{\rm n} = -\frac{c_{\rm s}}{8\pi^2 r_{01} r_{02}}\oint\!\!\oint \left\{2 - \left[\left(\frac{\sigma}{a}\right)^2 + 2\left(\frac{\sigma}{a}\right) + 2\right] e^{-\sigma/a}\right\}\frac{\left(\vec{\sigma}\cdot d\vec{S}\right)\left(\vec{\sigma}\cdot d\vec{S}'\right)}{\sigma^4} \tag{4}$$

The sharp-surface Coulomb energy is given by

$$E_{\rm C} = -\frac{\rho_{01}\rho_{02}}{12}\oint\!\!\oint \frac{\left(\vec{\sigma}\cdot d\vec{S}\right)\left(\vec{\sigma}\cdot d\vec{S}'\right)}{\sigma} \tag{5}$$

Up to now, the computer coding of equations (4) and (5) was performed for a limited class of shapes, mostly assuming a rotational symmetry for the whole system. We developed a computer code which enables us to calculate the interaction energy between arbitrary oriented deformed nuclei. The detail of the formalism is given in ref. [2] . This general treatment is required in phenomena like sub-barrier and above-barrier fusion of deformed nuclei, molecular resonance reaction of deformed nuclei and charged particle emission form the deformed nuclei. We will give some calculations of the fusion barrier for the super-heavy-element production.

We will give calculations of the fusion barrier for super-heavy element production via ^{248}Cm+^{48}Ca reaction. In fig. 1 we display the potential-energy surface for this reaction. The 15 MeV difference between the barrier in the equatorial and polar regions stands out clearly. At first sight

[1] Permanent address, *P. Moller Scientific Computing and Graphics, Inc*

collisions in the polar regions may seem preferable since such reactions are possible at energies leading to lower excitation energies of the compound system. However, this reaction would also lead to the most elongated of all the possible initial configurations. A collision in the equatorial region would have to take place at a 15 MeV higher energy, but would represent a more compact initial touching configuration. Thus, the amount of extra push required to bring the system to a sufficiently compact shape for complete fusion, that is to inside the fission saddle point, may be so much less than in the polar regions that it more than compensates for the higher Coulomb barrier in the equatorial region.

We have shown that deformation of the nuclei affects the barrier height for fusion reaction considerably. The same is true for the emission barrier for charged particles when the parent nucleus is highly deformed [3]. The model presented here allows the calculation of the potential energy for the particle emission from completely general shape of the compound nucleus [2].

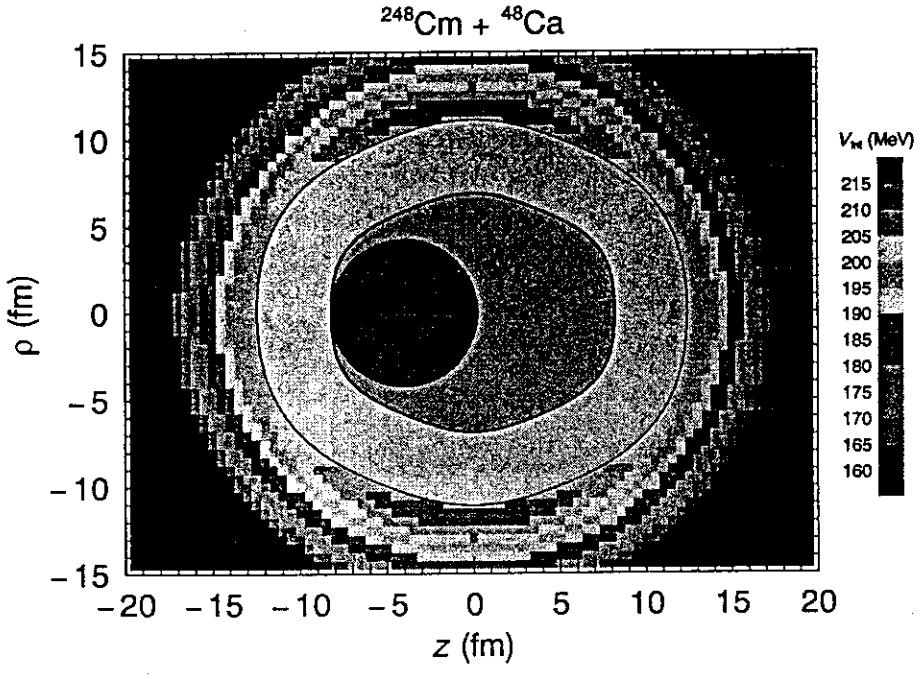

Fig.1. Potential-energy surface for the reaction ^{248}Cm+^{48}Ca. The Coulomb barrier in the equatorial region is about 15 MeV higher than in the polar regions.

References

1) H. J. Krappe and J. R. Nix, Proc. Third IAEA Symp. on the physics and chemistry of fission, Rochester, 1973, vol. I (IAEA, Vienna, 1974) p. 159.

2) P. Möller and A. Iwamoto, Nucl. Phys. **A575** (1994) 381.

3) A. Iwamoto and R. Herrmann, Z. Physik A - Atoms and Nuclei, **338** (1991) 303.

5. Atomic Physics

5. 1 PROJECTILE CHARGE STATE DEPENDENCE OF BINARY ELECTRON PRODUCTION FOR 1 MeV/u Au^{q+} (q=12–37) ION IMPACT ON He

M. SATAKA, M. IMAI, K.KOMAKI[1], Y.YAMAZAKI[1], K. KAWATSURA[2], Y. KANAI[3], H. TAWARA[4], D. R. SCHULTZ[5] and C. O. REINHOLD[6]

The absolute cross section for the production of binary encounter electrons has been studied at zero degrees for highly charged, clothed ions. Experimental and theoretical results for 1 MeV/u Au^{q+}(q=12–37) colliding with helium are presented.

Binary encounter electron production is well known process originating from a binary collision between a fast particle and a target electron. Recently, a number of departure from this simple behavior have been observed in collisions between multi-charged ion and atom.[1] Our purpose is make a systematic study of a collision system, from both an experimental and theoretical point of view, which could potentially be sensitive to the "anormalus" effect.

The experimental apparatus used and procedures has been reported earlier[2]. The electron spectra were obtained by a tandem type electron spectrometer with two parallel-plate electrostatic analyzer. A post stripper facility provided the ions with charge states 12–37, which are magnetically separated and directed through a collision chamber. To get absolute cross sections, an electron spectrum for 2 MeV/u F^{9+} ion on He measured with the same detection system, was compared with absolute data by Lee et al.[3]

Experimental and theoretical calculations are presented in Fig. 1.
It is found experimentally that as the charge state of the incident ion is increased
(1) the binary peak magnitude increases,
(2) the electron energy at which the peak occurs decreases, and
(3) the peak broadens.

Classical Trajectory Monte Carlo (CTMC) calculations are found to give good account for the magnitude and the shift to lower electron energy of the peak. The Continuum Distorted Wave-Eikonal Initial State (CDW-EIS) approximation is shown to yield cross sections which are much smaller in magnitude than the experiments, but reproduce well the relative magnitudes and shapes of the peaks for these ions.

It is noted that the increase in the binary peak magnitude with increasing ionic charge state is in distinction to previous measurements which showed enhancement of the binary peak with decreasing charge state for clothed ions.[4]
The next logical step towards the understanding the process would be develop a quantum mechanical two center theory which incorporates the short distance screening through a model potential. Experimentally, studies exploring more comprehensively the impact energy dependence of these effects, and for ionic charge states bridging the region between the normal "q-dependence" and enhancement apparent for lower charge states, would seem in order.

[1]Institute of Physics, College of Arts and Sciences, University of Tokyo
[2]Department of Chemistry, Faculty of Engineering and Design, Kyoto Institute of Technology
[3]Institute of Physical and Chemical Research (RIKEN)
[4]National Institute for Fusion Science
[5]Physics Division, Oak Ridge National Laboratory
[6]Physics Division, Oak Ridge National Laboratory and Department of Physics and Astronomy, University of Tennessee

References
1) for example, P. Richard, D. H. Lee, T. J. M. Zouros, J. M. Sanders and J. L. Shinpaugh, J. Phys. B23 (1990) L213.
2) K. Kawatsura, M. Sataka, H. Naramoto, M. Imai, K. Komaki, Y. Yamazaki, K. Kuroki, Y. Kanai, T. Kambara, Y. Awaya, I. Kadar and N. Stolterfoht, Nucl. Inst. Meth. B53 (1991) 421.
3) D. H. Lee, P. Richard, T. J. M. Zouros, J. M. Sanders, J. L. Shinpaugh and H. Hidmi, Phys. Rev. A41 (1990) 4816.
4) M. Sataka, M. Imai, K. Komaki, Y. Yamazaki, K. Kawatsura, Y. Kanai, H. Tawara, D. R. Schultz and C. O. Reinhold, J. Phys. B27 (1994) L124.

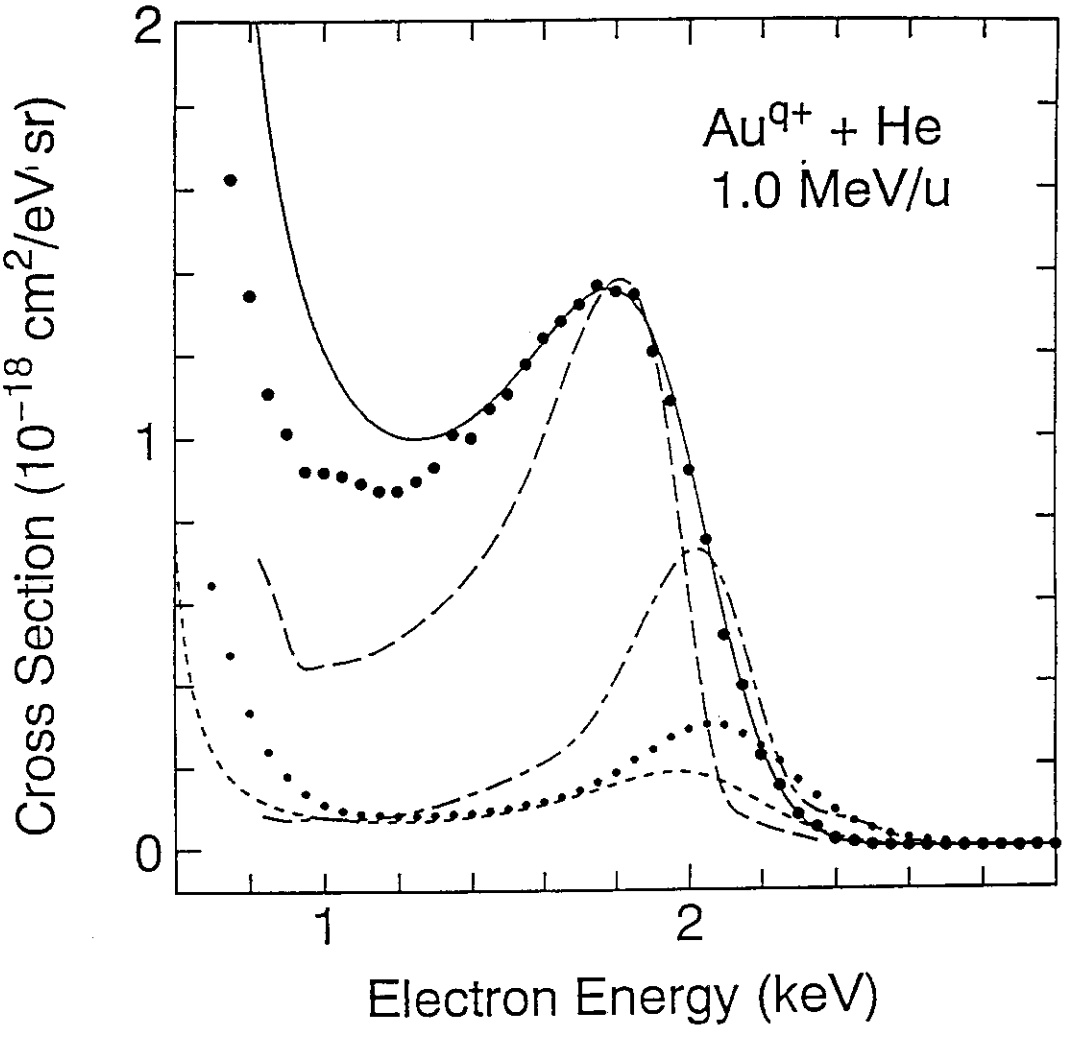

Fig. 1. Double differential cross sections at 0° as a function of electron energy for 1 MeV/u Au^{q+} impact of He. Experiment: ·, 12+ ion impact; ●, 37+ ion impact. CDW-EIS calculations: solid curve, 37+; dotted curve, 12+. CTMC calculations: dashed curve, 37+; dash dotted curve, 12+. The CDW-EIS cross sections are multiplied by 20.

5. 2

CHARGE STATE DISTRIBUTION OF NEON RECOIL ION BY CARBON ION IMPACT IN COINCIDENCE WITH PROJECTILE FINAL CHARGE STATES

M.IMAI and M.SATAKA

We have measured charge states of recoil ions produced in 100keV/amu C^{q+} + Ne (q=1-5) collisions in coincidence with projectile final charge states utilizing the experimental apparatus, reported in the earlier annual report[1]. Measured yields were converted to absolute cross sections σ^i_{qf}, where i,q and f denote recoil ion, projectile initial and final charge states respectively, using the absolute charge exchange cross sections[2]. Cross sections for the following processes were derived;

(i) $C^{q+} + Ne \rightarrow C^{(q-2)+} + Ne^{i+} + (i-2)e^-$ ($\sigma^i_{q\ q-2}$ for q=2-5),
(ii) $C^{q+} + Ne \rightarrow C^{(q-1)+} + Ne^{i+} + (i-1)e^-$ ($\sigma^i_{q\ q-1}$ for q=1-5),
(iii) $C^{q+} + Ne \rightarrow C^{q+} + Ne^{i+} + ie^-$ ($\sigma^i_{q\ q}$ for q=1-5),
(iv) $C^{q+} + Ne \rightarrow C^{(q+1)+} + Ne^{i+} + (i+1)e^-$ ($\sigma^i_{q\ q+1}$ for q=1-4),
(v) $C^{q+} + Ne \rightarrow C^{(q+2)+} + Ne^{i+} + (i+2)e^-$ ($\sigma^i_{q\ q+2}$ for q=1,2).

The present experiment has been performed at the "splendid" 2MV VdG accelerator facility at JAERI, Tokai. Figure 1 gives a typical two-dimensional linear plot of the number of coincident events against projectile final charge state and recoil ion flight time. For details about the experiments, please consult our earlier reports[1,3].

As the space allowed us is limited, only brief results for the pure ionization channel, which corresponds to the process (iii), will be given here. The pure ionization cross sections for producing i+ recoil ions are plotted in figure 2 against initial charge states q (q=1-5). Different dependences on initial charge state can be seen in the figure. The cross section for producing Ne^+ recoil ion increases as initial charge state increases, which is a genuine result of classical potential scattering theory. The cross sections for producing multiply ionized recoil ions, however, show maximum at q=2 and decrease when initial charge state gets larger, except for Ne^{5+} producing case, which shows maximum at q=3. Comparing these results with the cross sections for process (ii) – ionization with single capture –, enhancements of the process (ii) cross sections can be seen at the region where the process (iii) cross sections decrease, as if they compensate each other. Simply, these results may be explained through an equilibrium charge state of C ion. As we reported in the previous annual report[2], the equilibrium mean charge of C for this collision system and energy is 1.98, and the higher the initial charge state get over 1.98, the more cross section is expected for ionization with electron capture channel (ii) and the less for pure ionization channel (iii). This simple explanation, however, fails to express the reverse dependence on initial charge state between Ne^+ and Ne^{i+} (i=2-5) for $q \geq 2$. Another picture we are contriving for these phenomena is that to regard the main channel of process (iii) with producing multiply charged recoil ions as to be transfer and excitation followed by autoionization; the target electron(s) is ionized, the projectile is excited and another target electron is captured into projectile excited state simultaneously, forming an autoionizing state. Excited projectiles formed in this manner, autoionizes through either Auger electron emission, which makes the projectile final charge state unchanged and observed as process (iii) or X-ray emission, which makes the collision observed as process (ii). Because the Auger emission rate is expected to decrease when the initial charge state q gets higher, the number of collisions observed as pure ionization decreases and the one observed as ionization with single capture increases. This picture indicates that "indirect" ionization process exerts important influences to "pure" ionization process with multiply charged ion.

References

1) M.Imai and M.Sataka, JAERI-M 92-124 (1992) pp.19-21.
2) M.Imai and M.Sataka, JAERI-M 93-174 (1993) pp.15-18.
3) M.Imai and M.Sataka, Abstracts of the XVIII International Conference on the Physics of Electronic and Atomic Collisions, Aarhus 1993 p.474.

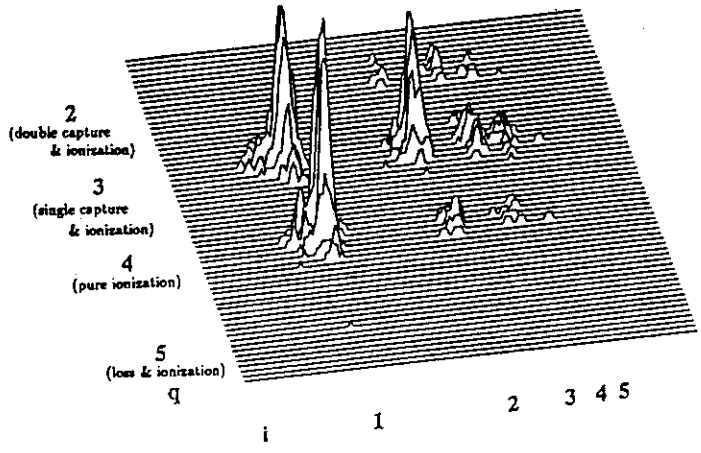

$$C^{4+} + Ne \rightarrow C^{q+} + Ne^{i+} + (q+i-4)e^{-}$$

Figure 1 Typical two-dimensional linear plot of the number of coincident events against projectile final charge state and recoil ion charge state.

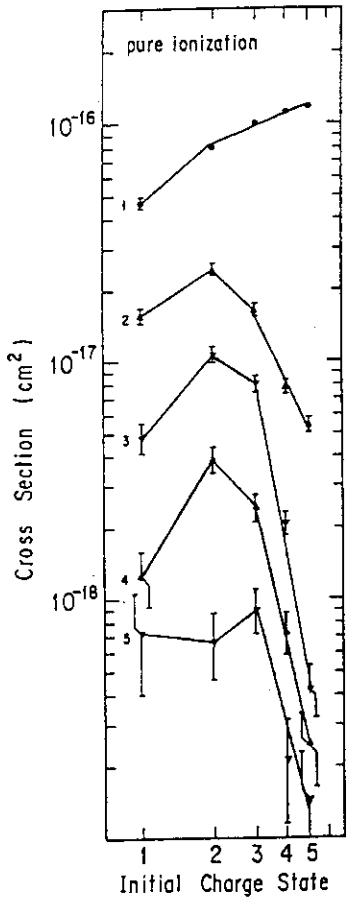

Figure 2 Cross sections σ^{i}_{qq}, where i and q denote recoil ion and projectile initial/final charge states respectively. Letters beside the plots indicate i.

6. Solid State Physics and Radiation Effects of Materials

6.1 X-RAY STUDY OF IRRADIATION DEFECTS CAUSED BY MeV ION IMPLANTATION INTO SI PERFECT CRYSTALS II

M.KURIBAYASHI[1)], T.KANAMARU[1)], E.TSUJI[1)], H.KATOH[1)], K.ISHIDA[1)], K.AIZAWA, S.OKAYASU, H.TOMIMITU and Y.KAZUMATA

Introduction

Ion implantation in an energy range of several 10-100 KeV is a well established technique for fabrication of semiconductor or integrated circuit device. Recently, high energy, over MeV, ion implantation becomes a new interesting technique for buried layer formation of dopants[1]. The defect distribution caused by MeV ion implantation is rather different from that by KeV implantation[2]. There is relatively a non-damaged region and then, a damaged region with finite width appears. On the other hand , in KeV ion implantation , there is a damaged region continued just under the irradiated surface.The main subjects of the present work are as follows.

(1) Determination of the strain distribution due to defects in MeV ion implanted Si(111) wafers by X-ray diffraction method with dynamical theory in a distorted crystal.

(2) Investigation of the mechanism to form the defects by comparing the experimentally obtained strain distribution with theoretically calculated energy loss and stopping atoms curves.

(3) Investigation of the annealing effect by the successive study of strain distribution change after annealing the sample.

Experimental

Cu, Ni and Au ions were implanted into Si(111) wafers using the tandem Van de Graff accelerator in JAERI at Tokai with accelerating voltages of 160MeV and 80 MeV. X-ray rocking curves of the irradiated samples were obtained with multi-crystal diffractmeter at BL-14B in Photon Factory at KEK in Tukuba. Our system used in the experiment was as follows; Vertically polarized synchrotron radiations were initially monochromatized by a pair reflection of Si(111) crystals with (+,-) setting and then more precisely by a Si(220) grooved crystal which was set to the first monochromator as (-,-), i.e. the monochromator reflection system was (+,-,-,+) setting.With the system, energy resolution ΔE=0.55eV, and angular resolution $\Delta\theta$=1.9sec were achieved.

Concluding remarks

In the last report[3],we had compared the obtained diffraction profiles with the calculated energy loss and stopping ion distribution curves and concluded that the strain distribution caused by MeV ion implantation was nearly equal to that of stopping ions.However,it was found that there was a thin surface layer, where the magnitude of strain,$\Delta d/d$,was smaller than that in the other region.In this report, we present an interesting relation between the ion dose and the angular deviation of the subsidiary maximum from the main peak in the diffraction pattern.

Fig.1 shows the Si(333) diffraction patterns of Si(111) implanted wafers 80MeV Cu ion with dose rate of $2.0\times10^{14}/cm^2$ (a) and $5.0\times10^{14}/cm^2$ (b), respectively.The deviations are almost in proportion to the dose.To confirm the relation, we

1)Faculty of Science and Technology, Science Univ. of Tokyo

carried out the simulation for various doses and the result is shown in the Fig.2. The investigation of the periodicity of subsidiary maxima is in progress.

Forthcoming Research

Now we are going to research the annealing effect on the strain distribution of irradiated samples and,moreover, to clarify the performance of defects produced by MeV ion implantation into Si single crystals.

References

1)J.F.Ziegler,Nucl.Instrum.Methods.B6,(1985)270.
2)M.Tamura,N.Natsuaki,Y.Wada,and E.Mitani,J.Appl.Phys.59(1986)3417.
3)H.Tanaka et al.,JAERI TANDEM and V.D.G.Report 1992(1993)pp47-50.

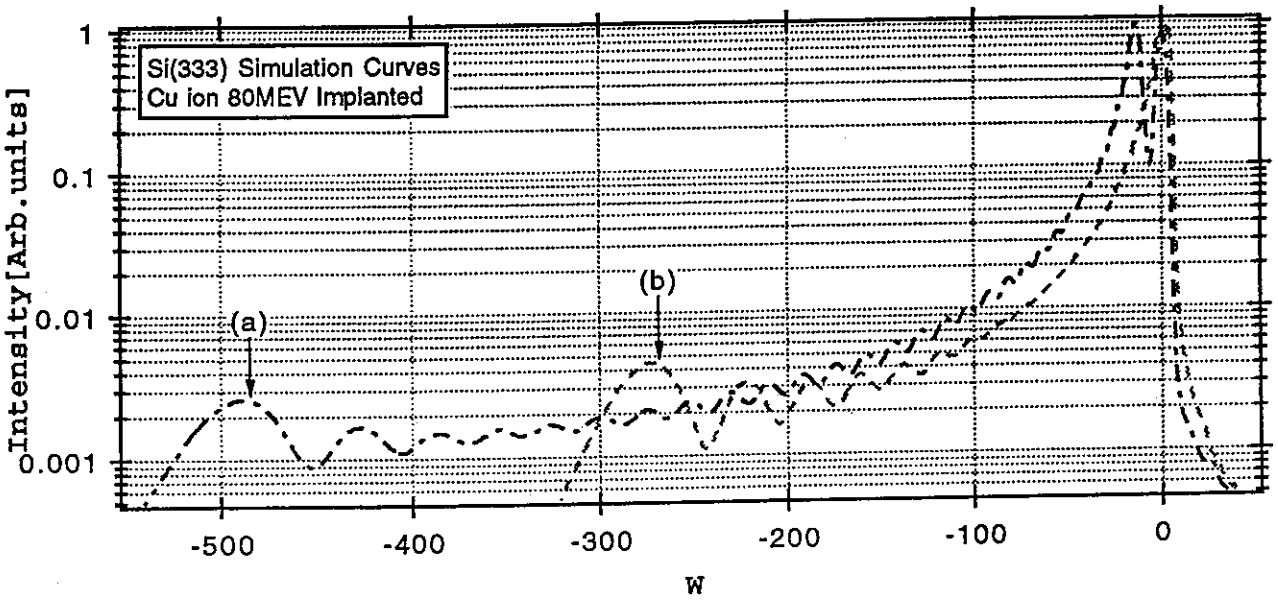

Fig.1 Experimental rocking curve from Si(333) implanted Cu ion 80MeV with dose rate of $2.0\times10^{14}/cm^2$ (a) and $5.0\times10^{14}/cm^2$ (b),where W=1.0 corresponds to θ=0.52[sec]

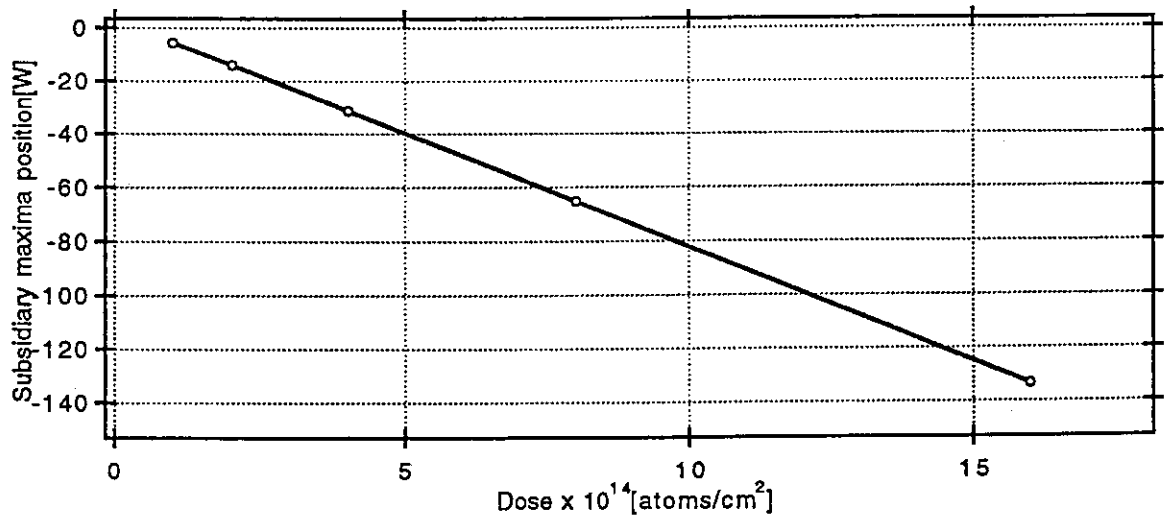

Fig.2 Simulation of Subsidiary maxima position [W] vs Dose

6.2 ELECTRICAL CONDUCTIVITY CHANGE OF SYNTHETIC SINGLE CRYSTAL DIAMOND BY ION IRRADIATION

K. HARUNA[1], H. MAETA, F. ONO[2], T. IWASITA[1], T. ODAJIMA[1] and K. OHASHI[1]

Diamond is very strong against radioactive rays and fits to the electron devices in the high temperature region owing to the wide energy gap. However, there are not yet n-type diamonds. In order to get n-type diamond , we selected the ion implantation method. We measured the temperature dependence of electrical conductivity for the as grown diamond crystal before and after the heavy ion irradiation. We report the following.

The synthetic diamond single crystals used in this experiment were purchased from Sumitomo Denko Co. Ltd. The specimens are p-type. These contain boron impurities. The crystal size is 3.5x3.5x0.3 mm^3 and surfaces of the specimens were oriented parallel to the (100) plane. The electrical conductivity is measured by Van der Pauw method. The measurement is performed at temperatures between 77 and 350 K.

In fig.1, open rectangulars show the temperature dependence of conductivity of boron doped synthetic diamond crystal. This result suggests that impurity conduction has three stages. That is, it is expressed as follows.

$$\sigma=\sigma_1\exp(-E_1/KT)+\sigma_2\exp(-E_2/KT)+\sigma_3\exp(-E_3/KT)$$

According to Mott and Twose and Davis and Compton[1], the first term is usual impurity conduction. The activation energy E_1 is the normal acceptor ionization energy. The second term is associated with conduction in an impurity band. This conduction takes place in acceptors charged by binding an extra hole jumping from one otherwise neutral

---

1.Faculty of Engineering,Tamagawa University

2.Liberal arts of Okayama University

center to another. Third term is most prominent for specimens with a relatively low impurity concentration. This conduction takes place by tunneling. Therefore, the activation energy is required to overcome the Coulomb barriers associated with the compensated impurities. These activation energies are as follows.

E_1 = 0.15eV E_2 = 0.065eV E_3 = 0.0037eV

The solid circle shows the conductivity of the boron doped diamond irradiated by P ion. It shows that there are three stages. The activation energies of these two samples are clearly different. At present, the reason is unknown why these samples have these differences. This analysis is being carried out. The result will be reported in the near future.

References

1) N.F.Mott and W.D.Twose: Adv. Phys. 10 (1961) 107-63.
E.A.Davis and W.D.Compton: Phys. Rev. 140 (1965) A2183-94.

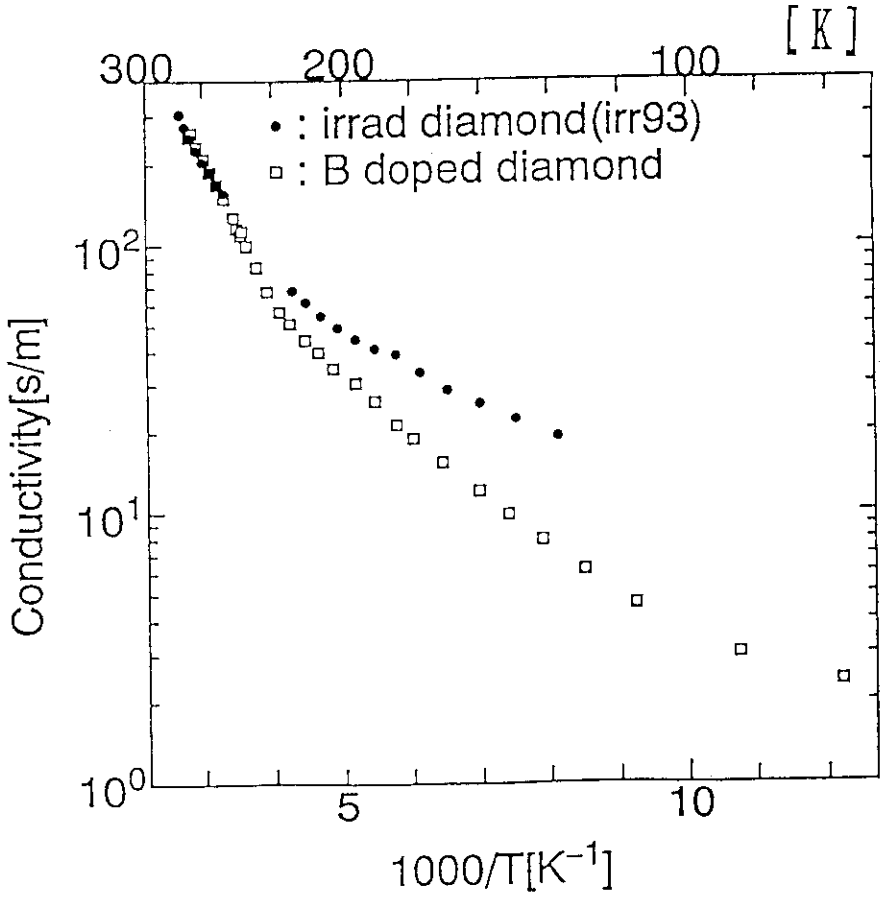

Fig.1 Temperature dependence of the conductivity for boron doped synthetic diamond single crystal before and after P ion irradiation.

6. 3 ELECTRICAL AND STRUCTURAL PROPERTIES OF Li-ION IRRADIATED β-LiAl

K. Kuriyama [1], Tomoharu Kato [1], M. Yahagi [2], H. Sugai, and Y. Maeta

LiAl alloy is an useful material for solid-blankets of nuclear fusion[1]. Electrical conductivity of β-LiAl below room temperature has been reported[2-4]. The important feature of the conduction mechanism for β-LiAl is governed by positive carriers(holes)[5, 6] in the valence band. The electrical conductivity based on these holes is affected considerably by the defect structure[7] in β-LiAl (about 48-56 at.% Li). The defect structure at room temperature consists of two types of defects: vacancies in the lithium sublattice (V_{Li}), and lithium anti-structure atoms in the aluminum sublattice (Li_{Al}). A heat-capacity anomaly relating to an abrupt change in the resistivity has been observed at around 95 K near the critical composition corresponding to the Li-deficient region[8]. The anomalous behavior is closely correlated with the lower temperature ordering or clustering of Li vacancies[8, 9]. The purpose of this work is (i) to measure the electrical resistivity of β-LiAl before and after heavy ion irradiation and (ii) to survey the modification of Li vacancies in Li-ion irradiated β-LiAl. In the previous report, we have studied the temperature dependence of the resistivity of β-LiAl before and after Li-ion irradiations. We suggested that the increase in resistivity is attributed to the transition from an ordered arrangement of Li vacancies to the partially

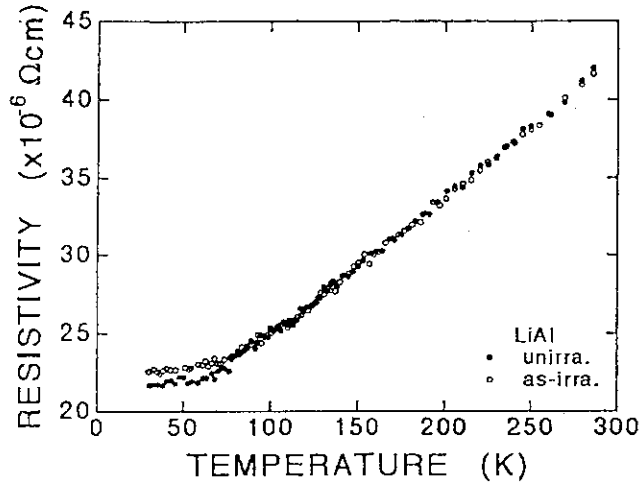

Fig.1. Temperature dependence of electrical resistivity of β-LiAl(~50 at.%Li) before and after Li-ion irradiation; Li dose is 1.2 x 10^{15} cm^{-2}.

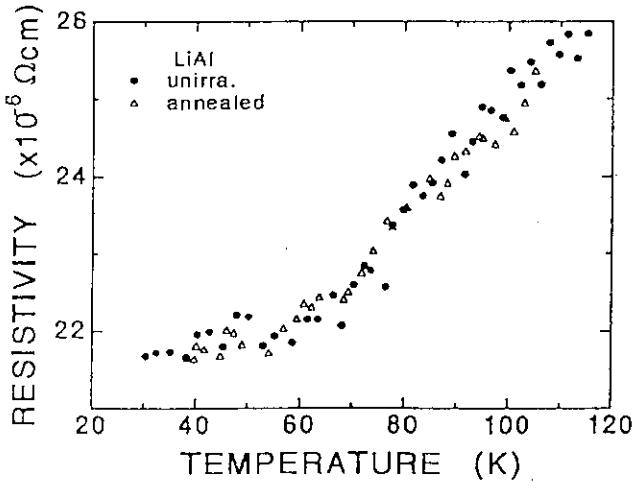

Fig.2. Temperature dependence of electrical resistivity of β-LiAl(~50 at.%Li) before and after annealing. The sample was annealed at a temperature above the ordering temperature. Li dose is 1.2 x 10^{15} cm^{-2}.

[1]College of Engineering and Research Center of Ion Beam Technology, Hosei University.
[2]Faculty of Engineering, Aomori University.

disordered arrangement of Li vacancies. In this report, we describe the detailed behavior of electrical resistivity of β-LiAl before and after Li-ion-irradiations.

Samples were prepared by a resistance furnace melting of 99.9% lithium and 99.999% aluminum. The details of sample preparation have been previously described[10]. Li-ion irradiations were performed by a tandem accelerator at JAERI. 60 MeV-$^{7}Li^{3+}$ ions were used in this study. The projected range of Li^{3+} evaluated using TRIM was 0.56 mm. The dimension of samples is about 5 x 5 x 1.5 mm^3.

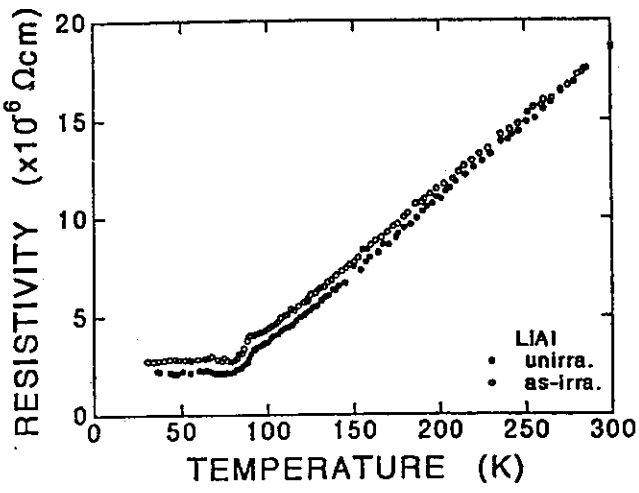

Fig.3. Temperature dependence of electrical resistivity of β-LiAl(~48 at.%Li) before and after Li-ion irradiation; Li dose is 4.9 x 10^{15} cm^{-2}.

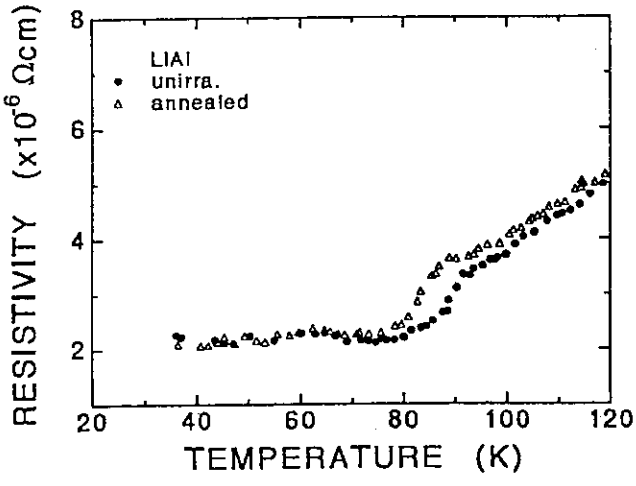

Fig.4. Temperature dependence of electrical resistivity of β-LiAl(~48 at.%Li) before and after annealing. The sample was annealed at a temperature above the ordering temperature. Li dose is 4.9 x 10^{15} cm^{-2}.

Figure 1 shows a temperature dependence of resistivity of β-LiAl(~50 at.%Li) before and after Li-ion irradiations. The Li dose is 1.2 x 10^{15} cm^{-2}. Before irradiation, one can observe an abrupt change in resistivity at around 70 K(see closed circles in Fig.1). This anomalous behavior has been associated with the lower temperature ordering[9] of Li vacancies. After irradiation, the resistivity increases at a temperature range below the ordering temperature (see open circles in Fig.1). This behavior is interpreted as the destruction of the ordered arrangement of Li vacancies due to the Li-ion irradiation. Figure 2 shows a temperature dependence of resistivity, whose data were taken after keeping at a temperature above the ordering temperature.

The resistivity after annealing was coincident with those before Li-ion irradiation. Therefore we conclude that the recovery of the ordered arrangement of Li vacancies occurs after the thermal annealing.

Following this experiment, a new sample with a Li content of ~48 at.%Li was irradiated with a dose of 4.9×10^{15} cm^{-2}, whose dose is about 4 times larger than that described earlier. Figure 3 shows a temperature dependence of resistivity of β-LiAl before and after Li-ion irradiations. After irradiation the resistivity increases at a temperature range below ~250 K, remaining an anomalous resistivity observed at around 90 K. This indicates that the ordering temperature of Li vacancies is not affected by the irradiation, but newly defects are introduced. However the defects annihilate almost by the thermal annealing(see Fig.4), accompanied with the slight shift of the ordering temperature.

The different behavior for Li irradiation may be attributed to the difference in Li vacancy concentration in β-LiAl used here.

References

1) J. R. Powell, F. T. Miles, A. Aronson and W. E. Winsche, *BNL-18236*, Bookhaven National Laboratory(1973).
2) K. Kuriyama, T. Kamijoh and T. Nozaki, Phys. Rev. B22, 470 (1980), K. Kuriyama, S. Yanada, T. Nozaki and T. Kamijoh, Phys. Rev. B24, 6158(1981).
3) T. Asai, M. Hiratani and S. Kawai, Solid State Communicat. **48**,173 (1983).
4) L. H. Hall, T. O. Brun, G. W. Crabtree, J. E. Robinson, S. Susman and T.Tokuhiro, Solid State Communicat. **48**, 547(1983).
5) K. Kuriyama, T. Nozaki and T. Kamijoh, Phys. Rev. B26, 2235(1982).
6) M.Yahagi, Phys. Rev. B24, 7401(1981).
7) K. Kishio and J. O. Brittain, J. Phys. Chem. Solids **40**, 993(1979).
8) K. Kuriyama, S. Yanada, T. Nozaki, and K. Kamijoh, Phys. Rev. B24, 6158 (1981).
9) T. O. Brun, S.Susman, R. Dejus, B. Granelli, and K.Skold, Solid State Communicat. **45**, 721 (1983).
10) K. Kuriyama, S. Saito and K. Iwamura, J. Phys. Chem. Solids **40**, 457(1979)457.

6.4 ION IRRADIATION EFFECTS ON $EuBa_2Cu_3O_y$ THIN FILMS

N.ISHIKAWA, A.IWASE, T.IWATA,
H.MAETA, K.TSURU[1] and O.MICHIKAMI[2]

When high-T_c cuprate superconductors are irradiated with energetic particles, they produce defects. The nature of these defects depends on the particle and the energy employed for irradiation. In general, irradiation causes decrease in the transition temperature, broadening of the transition width, and increase in the normal-state resistivity as a function of increasing fluence[1-3]. In order to elucidate these phenomena we need to obtain information on the defects themselves.

We investigated ion fluence dependence on c-axis lattice parameter of $EuBa_2Cu_3O_y$ superconductors when they were irradiated with He ions or Au ions. We prepared 300nm thick $EuBa_2Cu_3O_y$ epitaxial thin films. Critical temperature, T_c, was about 81K. The films were found to be c-axis oriented. 1MeV He ions and 120 MeV Au ions were irradiated in a direction parallel to c-axis of the materials at room temperature. Before and after the irradiation X-ray diffraction pattern was measured to determine c-axis lattice parameter. Temperature dependence on electrical resistivity was measured as well to investigate corresponding change of T_c. Fig.1 shows ion fluence dependence on c-axis lattice parameter. Both in the case of He ion irradiation and Au ion irradiation, c-axis lattice parameter increased as increasing fluence. Total defect production cross section can be estimated by assuming that increase of c-axis lattice parameter is proportional to the density of irradiation-produced defects[4]. As a result, total defect production cross section were estimated to be $10^{-18}cm^2$ for the He ion irradiation and $10^{-13}cm^2$ for the Au ion irradiation. This large difference of total defect production cross section may be attributed to the difference in dominant defect production process; i.e. elastic collision and electronic excitation.
Concerning the decrease of T_c due to irradiation, ion fluence necessary to make T_c zero was estimated to be $2*10^{16}cm^{-2}$ for He irradiation and $3*10^{12}cm^{-2}$ for Au irradiation, respectively. This result also indicates there is a large difference in defect production rate between the two irradiations.

---

[1]Electron Devices Laboratory, NTT Interdisciplinary Research Laboratories.

[2]Faculty of Engineering, Iwate University.

This great difference cannot be explained if assuming elastic collision alone contributes to the defect production[5]. Therefore, electronic excitation plays an important role of defect production when the samples were irradiated with Au ions.

References

1)See for example O.Meyer "Studies of High-Tc Superconductors", A.V.Narlikar ed.,Nova Science Publishers Inc NY (1989).
2)B.Roas, B.Hensel, G.Saemann-Ischenko, L.Schultz, Appl. Phys. Lett. 54 (1989) 1051.
3)J.Lesueur, L.Dumoulin, S.Quillet and J.Radcliffe, J. of Alloys and Compounds, 195 (1993) 527.
4)H.J.Wollenberger in : "Vacancies and Interstitials in Metals" ed. A.Seeger, D.Schumacher, W.Schilling and J.Diehl (North-Holland, Amsterdam, 1970)p.215.
5)T.Aruga, K.Nakata and S.Takamura, Nucl. Instrum. & Method B33(1988)748.

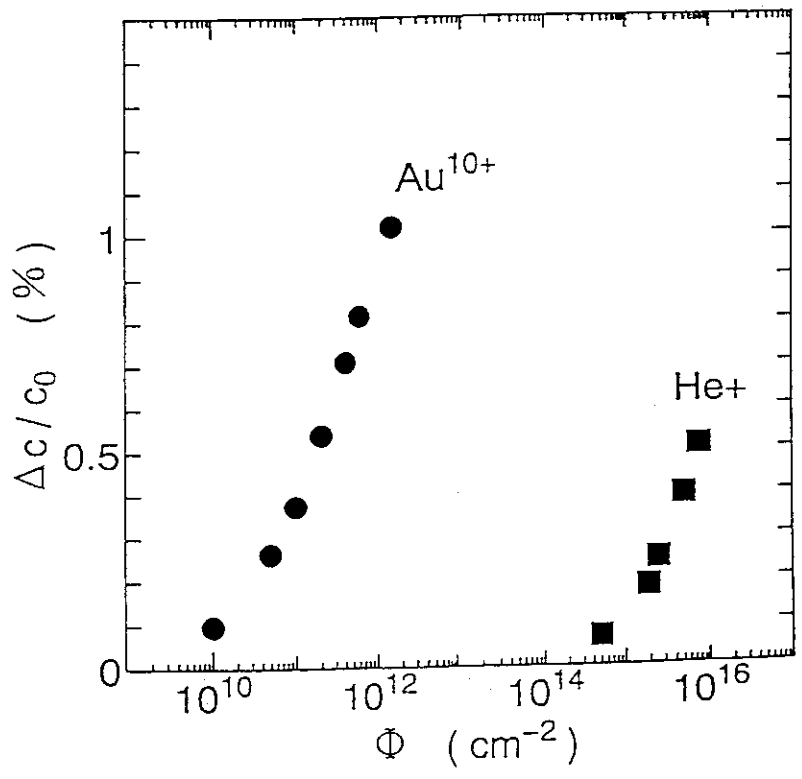

Fig.1. c-axis lattice parameter as a function of ion fluence when $EuBa_2Cu_3O_y$ thin films were irradiated with 120MeV Au ion (●) and 1MeV He ion (■). Δc is the increment of c-axis lattice parameter. c_0 is the value before irradiation. Φ is ion fluence.

6.5 EFFECTIVE ACTIVATION ENERGY OF PROTON IRRADIATED QMG-YBCO.

S. OKAYASU, Y. KAZUMATA, E. TESHIMA[1], M. TANAKA[1] and M. HASHIMOTO[1]

One possible expression of effective activation energies for QMG-YBCO high-Tc superconductors has been derived from a series of measurements of time decaying magnetizations. A comparison of the activation energies between 30MeV proton-irradiated (up to $3x10^{15}$ ions/cm^2) and unirradiated YBCO has been accomplished and the effect of the irradiation on the activation energy of YBCO has been investigated.

It is well known that critical current densities flowing within high-Tc superconducing materials exhibit a long time decay due to the creeping of vortices. These phenomena are related to pinning properties of vortices. Maley et. al. proposed a direct expression of the activation energy derived from time decaying magnetizations [1]:

$$U_{eff} = -T \{\ln(dM/dt) - C\}. \quad (1)$$

We assumed that the activation energy U_{eff} can be expressed as a product of three kind functions; G(T), F(H) and K(J). We determined each functions under two assumptions; U_{eff} must be a continuous function of the critical current density J and U_{eff} must diverge toward to a characteristic temperature T_X which is based on the vortex glass or collective pinning theory.

Long time decaying moment measurements were carried out with the following procedures;
1. Sample was cooled down to the target temperature in zero magnetic field.
2. Then external magnetic field was applied up to 5T and then to -5T. This field cycle ensures that the critical state is established within the sample.
3. The desired external field was applied and time decay of the magnetization was measured for a period of about $3x10^4$sec. From data thus obtained, we can derive the effective activation energy U_{eff} using eq. (1). Using Bean's model [2], the magnetization can be related to the critical current density Jc as [3]:

$$Jc=40M/L_1[1-L_1/3L_2], \quad (L_1<L_2) \quad (2)$$

where M (emu/cm^3) is magnetization, L_1 and L_2 (cm) are the sides of a rectangular crystal with the magnetic field applied perpendicular to that face. With the above procedures, we can obtain the relation between U_{eff} and J. However, the result of $U_{eff}(J)$ is not a continuous function because of no consideration of temperature-dependence of J [4]. To make $U_{eff}(J)$ as a continuous function of J and to reproduce a quasi-logarithmic T dependence of J(T), we introduced an appropriate temperature dependent function G(T) as

$$G(T) = [1-(T/T_X)^2]^{1/2}, \quad (3)$$

[1]Advanced Materials & Technology Research Laboratories, Nippon Steel Co.; 1618 Ida, Kawasaki, 211, Japan

where T_X is a characteristic temperature related to so-called the irreversibility temperature[5].

Fig. 1 shows the J-dependence of $U_{eff}(J)$ for both proton-irradiated and unirradiated YBCO-QMG sample. Unirradiated cases show two different power-dependence of J. The powers are about -1 at higher J-region and about -0.5 at lower J-region. On the other hand, the powers are about -1 for the proton-irradiated cases. Irradiation is not only just decrease of J but some contribution of the powers. It seems that the activation energy after the irradiation becomes larger than that of the unirradiated one at lower J region. This means that pinning for votices improves at high temperature and high field. Field dependence of U_{eff} is small for both cases except H_{ext}=0T.

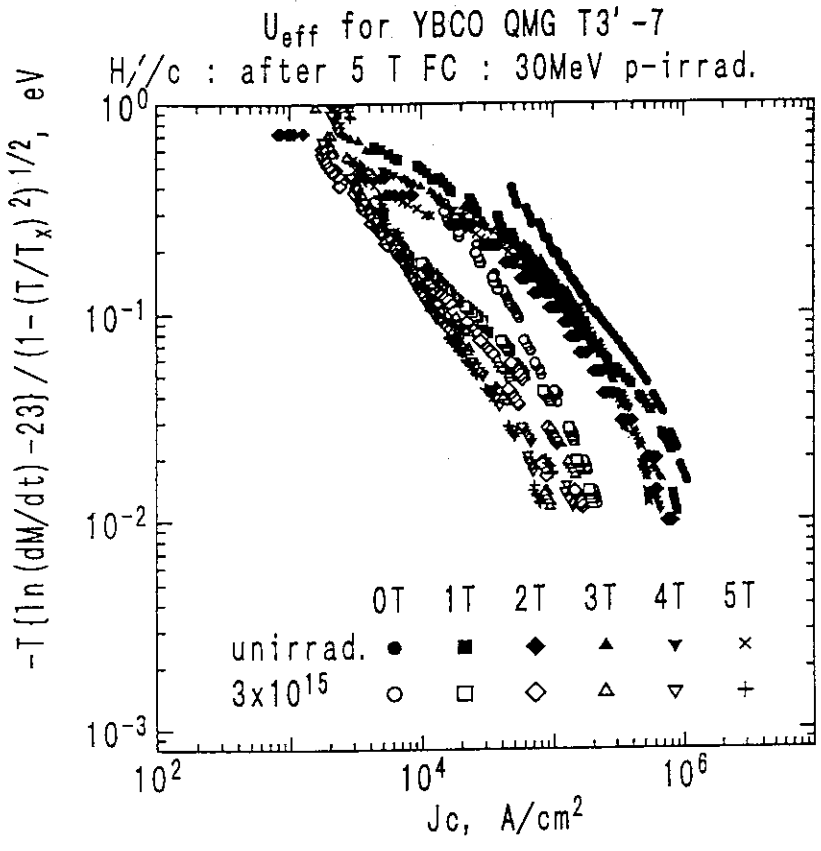

Fig. 1 Effective activation energy of QMG-YBCO with different external fields.

Reference
1) M. P. Maley, J. O. Willis, H. Lessure and M. E. McHenry, Phys. Rev. B42, 239 (1990)
2) C. P. Bean, Phys. Rev. Lett. 8, 250 (1962)
3) A. M. Campbell and J. E. Evetts, Adv. Phys. 21, 199 (1972)
4) M. E. McHenry, S. Simizu, H. Lessure, M. P. Maley, Y. C. Coulter, I. Tanaka and K. Kojima, Phys. Rev. B44, 7614 (1991)
5) P. J. Kung, M. P. Maley, M. E. McHenry and J. O.. Willis, Phys. Rev. B48, 13922 (1993)

6. 6
EFFECT OF 180MeV Cu^{11+} IRRADIATION ON $YBa_2Cu_3O_x$ AND $Bi_2Sr_2CaCu_2O_y$

H. KUMAKURA[1], H. KITAGUCHI[1], K. TOGANO[1], S. OKAYASU and Y. KAZUMATA

It was reported by several authors that high energy heavy ion irradiation introduces columnar defects in $YBa_2Cu_3O_x$(Y-123) and $Bi_2Sr_2CaCu_2O_y$(Bi-2212). However, littel comparison of the effect of ion irradiation was made between Bi-2212 and Y-123 using the samples irradiated under the same conditions. Such a comparison should be useful for the comprehensive understanding of flux pinning characteristics of oxide superconductors. Before, we demonstrated that 180MeV Cu^{11+} irradiation to Bi-2212 films introduced columnar defects and that the defects are effective to enhance flux pinning characteristics[1,2]. In this report, we performed Cu^{11+} irradiation on Y-123 and the obtained results were compared to those of the Bi-2212.

Samples were grain oriented polycrystalline Y-123 thick films prepared by a doctor blade method[3]. Transistion temperature T_c was measured by a four probe resistive method before and after the irradiation. Figure 1 shows the comparison of the fluence dependence of T_c for the Y-123 and the Bi-2212 films. In this figure, midpoint of the resistive transition and the transition width were plotted as a function of fluence. T_c of the Y-123 is much less sensitive to irradiation than that of Bi-2212. For Y-123 about an order of magnitude higher fluence is required to obtain the degradation of T_c. This is due to the smaller lattice distortion in irradiated Y-123 than that in Bi-2212[4].

D.C. magnetization curves were measured using a vibrating sample magnetometer(VSM). For Y-123, substantial enhancement of the magnetic hysteresis ΔM was obtained for a fluence larger than $5x10^{11}$ions/cm^2. Above this fluence, ΔM significantly increased with incresing fluence, and then, rapidly decreased for higher fluence. This behavior is similar to that of the irradiated Bi-2212. However, the fluence which gives maximum ΔM for Y-123 is an order of magnitude larger than that for Bi-2212. This is consistent with the difference of fluence dependence of T_c between Y-123 and Bi-2212, indicating that the decrease in ΔM at larger fluence is primarily due to the decrease of T_c shown in Fig. 1. Maximum of the enhancement factor ΔM(irrad.)/ΔM(No irrad.) of Bi-2212 is larger than that of Y-123. This is not due to large ΔM(irrad.) of Bi-2212 but is due to large ΔM(No irrad.) of Y-123, as discussed below.

ΔM was dominantly attributed to the intragrain critical current. Intragrain J_c was calculated using Bean's model. Figure 2 shows the typical J_c-B cuves of irradiated and non-irradiated Y-123 at various temperatures. Fluence of the Cu^{11+} was $9x10^{11}$ions/cm^2. Irradiation increases J_c values in all magnetic fields and temperatures. At low temperatures, enhancement of J_c is comparatively small, which is similar to Cu^{11+} irradiated Bi-2212. At 77K, an order of magnitude larger

[1]1st Research Group, National Research Institute for Metals

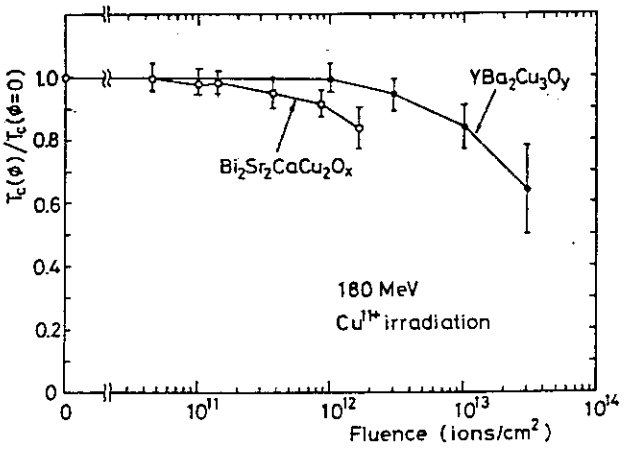

Fig. 1 Fluence dependence of T_c for Cu^{11+} irradiated Y-123 and Bi-2212.

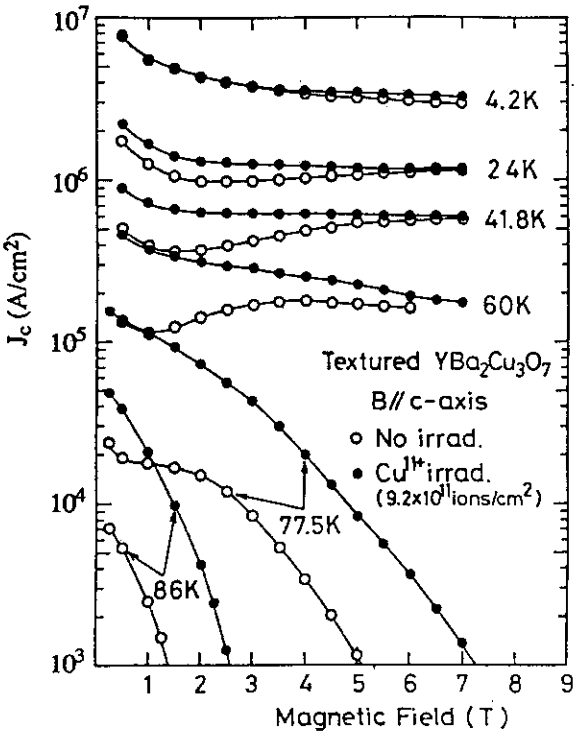

Fig. 2 Temperature dependence of J_c for Cu^{11+} irradiated and non-irradiated Y-123.

J_c is obtained. In case of Y-123, enhancement factor of J_c by the irradiation, J_c(irrad.)/J_c(No irrad.), increases with temperature up to T_c. This result is in contrast to Cu^{11+} irradiated Bi-2212, where enhancement factor of J_c becomes maximum at around 60K and the factor rapidly decreases at higher temperatures. However, at temperatures below 60K the enhancement factor of Y-123 is much smaller than that of Bi-2212 where one or two orders of magnitude larger enhancement factor is obtained for equivalent fluence of 10^{12}ions/cm^2. These results do not mean that the defects in Y-123 introduced by the irradiation act as less effective pinning centers than those introduced in Bi-2212. In case of Bi-2212, pinning strength before the irradiation is so weak that the large enhancement of pinning is obtained after the irradiation. For Y-123, on the other hand, relatively strong pinning centers have already existed, and smaller enhancement factors of J_c are obtained by the irradiation.

References

1) B. Chenevier, S. Ikeda, H. Kumakura, K. Togano, S. Okayasu and Y. Kazumata, Jpn. J. Appl. Phys. 31(1992)L777.
2) H. Kumakura, H. Kitaguchi, K. Togano, H. Maeda, J. Shimoyama, S. Okayasu and Y. Kazumata, J. Appl. Phys. 74(1993)451.
3) M. Suzuki, S. Kondoh, E. Yanagisawa, J. Shimoyama, N. Irisawa and T. Morimoto, Jpn. J. Appl. Phys. 29(1990)L67.
4) H. Kumakura, K. Togano, N. Tomita, S. Okayasu and Y. Kazumata, manuscript in preparation.

6.7 Bi2212 TAPES IRRADIATED BY 120 MeV OXYGEN IONS

Y. KAZUMATA, S. OKAYASU, H. KUMAKURA[1] and K. TOGANO[1]

Two kind of defects by ion irradiation are found in high T_c superconductors, which are point-like defects including clustered defects and columnar defects. The former defects are produced by nuclear collisions between target atoms and energetic incident particles, while the latter are introduced by electronic excitations due to high energy heavy ions[1-3].
In this paper we described the influence of point defects to critical current density (ΔM). The correlation between current density and the activation energy is obtained.
Specimens used in this experiment were grain-oriented polycrystalline Bi-2212 tapes of which thickness is 15 μm. Irradiations were carried out at 100 K by the Tandem accelerator in JAERI. Projected range of 120 MeV oxygen ions is estimated to be 65 μm so that projectiles pass through the specimen. The amount of defects created by this ion bombardment is estimated to be 10^{-6}dpa for the fluence of 10^{12} O^+/cm^2, which is equivalent to 1 ppm defect concentration. Transition temperature (T_c) before irradiation is 82 K and it is reduced to 76.9 K at the fluence of $1.3\times10^{15}O^+/cm^2$. Magnetic measurements were made by using a Quantum Design model MPMS SQUID magnetometer.

Fig.1 represents the temperature dependence of ΔM of before and after irradiation of a fluence of obtained from hysteresis loops. The ordinate in this figure is normalized by unit area of the specimens. ΔM at 5 K in 0.5 T field at $1.3\times10^{15}O^+/cm^2$ is only about 1.6 times as much as that before irradiation, while the increase of ΔM at 35 K at the same fluence amounts to 9.5 and 164 times at the fields of 0.2 and 0.5 T, respectively. This result indicates that the irradiation effects are dominant at high temperatures and also high fields.
Irreversibility lines obtained from hysteresis loops are shown in Fig.2 before and after the irradiation, respectively. Irreversibility fields are increased with an increase of the fluence. As seen in this figure, irreversibility fields are formulated by

$$H_{irr}=H_0\exp(-T/T_X). \qquad (1)$$

This formula is different from the well-known relation of the irreversibility line, $H_{irr}=a[1-(T/T_c)^2]^n$ derived from the flux creep theory. From Fig.2, the parameter of H_0 and T_X in eq.(1) are obtained to be 18.1 tesla and 10.3 K for the unirradiated specimen and 27.9 tesla and 12.9 K for 1.3×10^{15} O^+/cm^2, respectively.
From the measurements of magnetic relaxation, effective activation energies for motion of flux were obtained from the following formula (1)[4].

$$U/k=-T(\ln|dM/dt|+C) \qquad (2)$$

Temperature scaling function of U is chosen as

$$G(T)=[1-(T/T_X)^2]^{3/2}. \qquad (3)$$

The parameters C and T_X in eqs.(1) and (2) are chosen so as to obtain smoothest continuous curves. The results are shown in Fig.4 together with the

---

[1]National Research Institute for Metals, 1-2-1 Sengen, Tsukuba, Ibaraki-ken

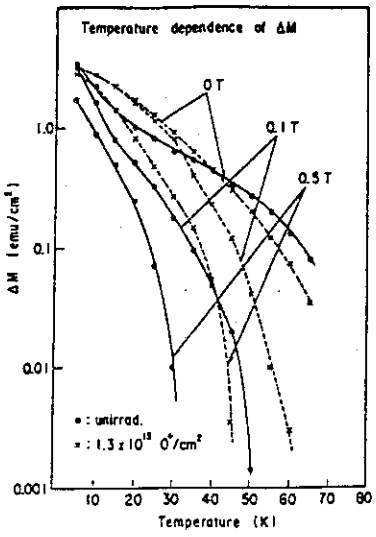

Fig.1 Temperature dependence of ΔM obtained from hysteresis loops.

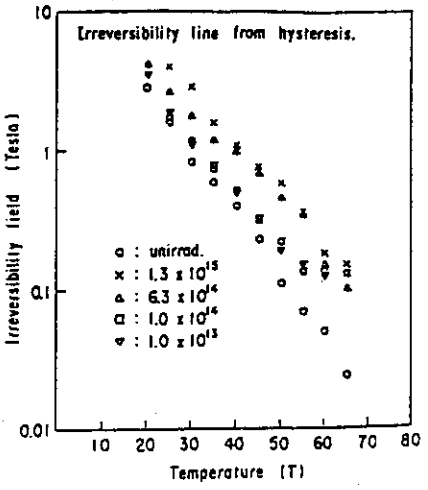

Fig.2 Irreversibility lines before and after irradiation.

parameters obtained. Activation energies after irradiation increase at high temperature.Since small size point defects will be effective only at low temperatures, clustered defects produced by irradiation will be responsible to the increase of activation energies and ΔM.

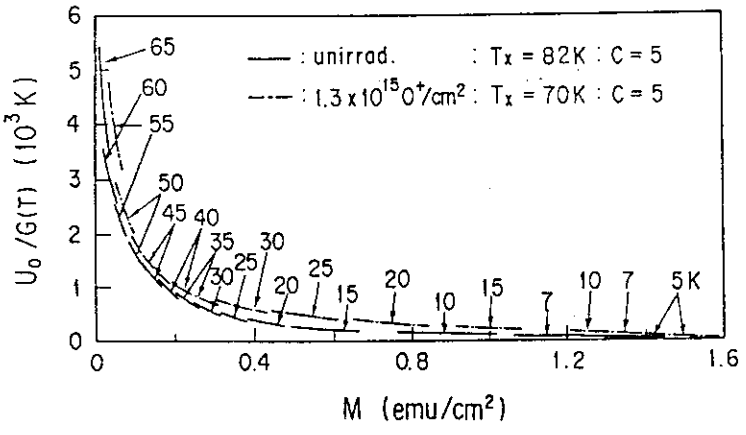

Fig.3 Flux-creep activation energybefore and after irradiation.

References

1) L. Civale, A.D. Marwick, T.K. Worthington, M.A. Kirk, J.R. Thompson, L. Krusin-Elbaum, Y. Sun, J.R. Clem and F. Holtsberg; Phys. Rev. Lett. 67(1991)6488.
2) W. Gerhauser, G. Ries, H.W. Neumuller, W. Schmidt, O. Eibl, G.Saemann-Ischenko and S. Klaummunzer; Phys. Rev. Lett. 68(1992))879.
3) H. Kumakura, H. Kitaguchi, K. Togano, H. Maeda,J. Shimoyama, S. Okayasu and Y. Kazumata; J. Appl. Phys. 74(1663)451
4) M.P. Maley, J.O. Wills, H. Lessure and M.E. McHenry; Phys.Rev. B42(1990)2639.

6. 8 RADIATION DAMAGE OF UO_2 IMPLANTED WITH 100 MeV IODINE IONS UP TO FLUENCES OVER AN EXTENDED RANGE

K.HAYASHI, H.KIKUCHI and K.FUKUDA

Using the Tandem Accelerator, we have been studying the radiation damage of UO_2 by implantation of heavy ions with 100 MeV, which is in the same energy level as that for fission fragments. This work is related with the so-called "rim effect", which is a microstructural change of the UO_2 fuel at the peripheral region of the fuel pellet of light water reactors at increased burnups above 50-70 GWd/t.

In the previous experiment [1,2], UO_2 specimens were irradiated with 100 MeV iodine ions to a limited range of fluences of $1.0x10^{18}$-$3.1x10^{20}$ions/m^2. And an increasing tendency of the lattice parameter with increasing fluence was observed. However, the behavior at higher fluences with apparent saturation as well as the threshold fluence at the lower side to observe the lattice parameter increase was not clear. In the present experiment, irradiation was made to a wider fluence range of $1x10^{16}$-$1.8x10^{20}$ions/m^2, using the same ion species, i.e., iodine with 100 MeV, as in the previous experiment.

Specimen preparation and ion implantation were made in the same way as before [1,2], except that the specimens were annealed at 1400°C for 2 h before implantation, and except that the specimen temperature was monitored by an infrared pyrometer [3] during implantation. The measured temperatures were found to be lower than 200°C, which is the lower detection limit of the pyrometer. The irradiated specimens were analyzed by X-ray diffractometry [3].

The lattice parameter change due to irradiation is plotted in fig. 1 as a function of the ion fluence. In this figure, the threshold fluence for the lattice parameter increase can be seen around $5x10^{16}$ions/m^2. At fluences below this value, the lattice parameter change falls into a range of the experimental error.
Above the threshold, the parameter change increases monotonously with increasing fluence. However, the shoulder of the curve found by Nakae et al. [4] for their in-pile experiment can not be observed in the present figure.
Instead, the slope of the curve tends to gradually decline at higher fluences above 10^{19} ions/m^2. It is noticed that the values of the lattice parameter change are significantly larger than those in the previous data. Furthermore, unlike the previous, the present data do not indicate a definite tendency of saturation at the higher fluences.

The overall features for the present experiment suggest that the radiation-induced lattice defects detectable by the X-ray diffraction were effectively accumulated without more effective recovery during ion implantation. The difference in the saturation behavior between the present and previous experiments is considered to be attributable to the difference in the target temperature under ion-beam heating. The temperature was kept below 200°C for the present experiment with lower ion fluxes below $5x10^{15}$ions/m^{2}s, while the temperature is estimated to be around 300°C for the previous, with higher fluxes of 8-$9x10^{15}$ions/m^{2}s.

The saturation behavior described above suggests that the recovery of the lattice defects of UO_2 is sensitive to the temperature around 200°C. As a next step in the research scope, a study on the recovery process of the radiation-induced lattice defects is under planning.

The authors are indebted to Mr. H. Serizawa and Mr. T. Shiratori of JAERI and Mr. K. Maejima of Tokyo Nuclear Service, Ltd. for their helpful advice, as well as for their experimental assistance in the Tandem irradiation and the X-ray diffraction measurement.

References

[1] K.Hayashi et al., JAERI-M 92-124 (1992) p.71.
[2] K.Hayashi, H.Kikuchi and K.Fukuda, J. Alloys and Compounds (1994), in press.
[3] K.Hayashi et al., JAERI-M 93-173 (1993) p.63.
[4] N.Nakae, A.Harada and T.Kirihara, J. Nucl. Mater. 71 (1978) 314.

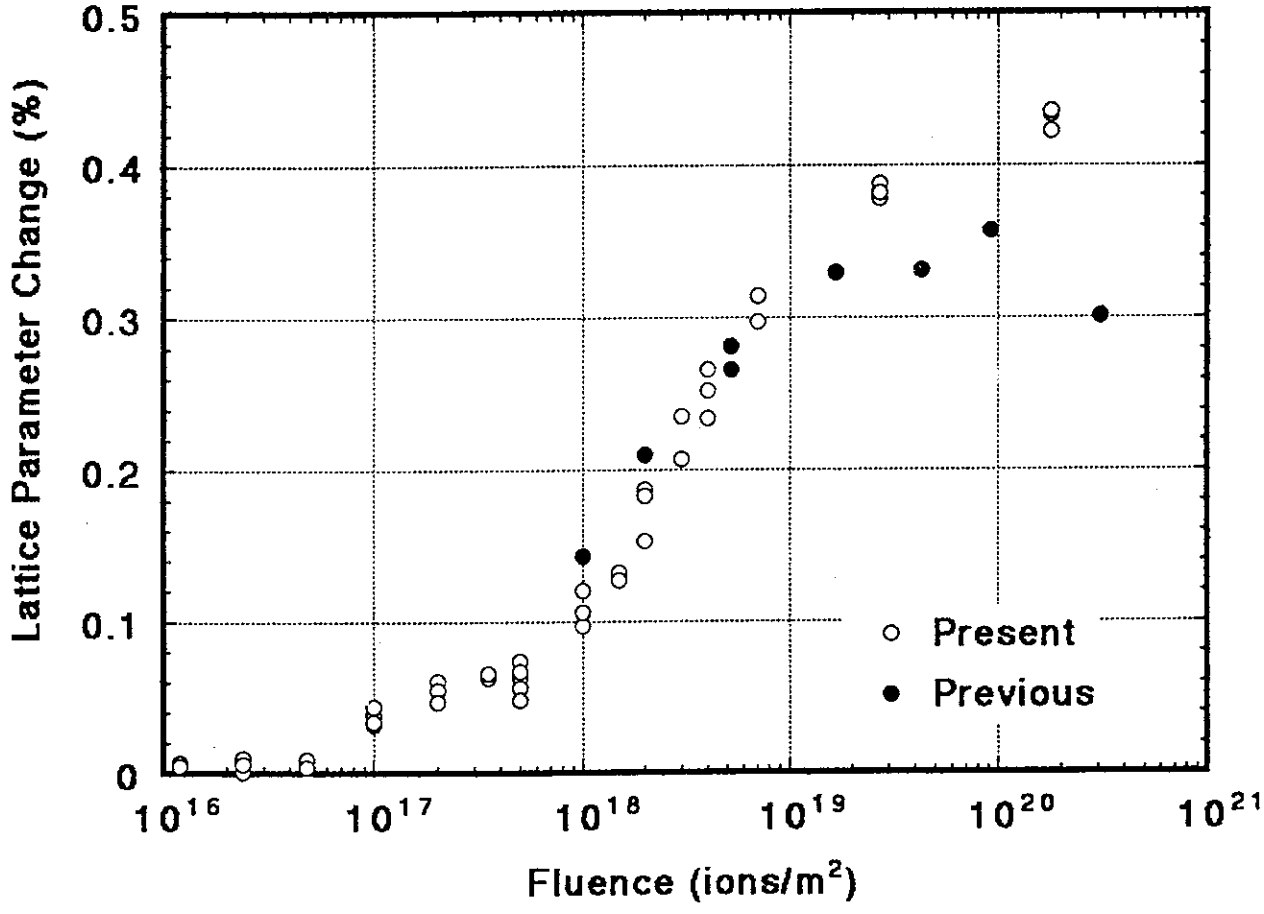

Fig.1 Lattice parameter change of UO_2 implanted with 100 MeV iodine ions as a function of ion fluence.

6. 9 Radiation Dameges in Li_4SiO_4 irradiated by High Energy Oxygen Ions

T. Nakazawa and K. Noda

Ceramic breeders in fusion blankets are exposed to severe neutronic environments during the operation of fusion reactors and changes in the properties of the ceramic breeders at high burnups may effect their performance in a fusion blanket application. Radiation damage in Li_4SiO_4 irradiated with high energy oxygen ions has been investigated by ionic conductivity measurements, Raman spectroscopy and Fourier transform infrared photoacostic spectroscopy (FT-IR PAS), in order to obtain fundamental information on irradiation defect and decomposition due to high energy neutron irradiation [1,2]. A further radiation damage study is being carried out to investigate ion energy dependence on radiation damage which can provide information on radiation damage due to primary knock-on atoms with various energies in high energy neutron irradiation.

In the present paper, a recent radiation damage study for Li_4SiO_4 using high energy oxygen ion irradiation are described.

Li_4SiO_4 was irradiated at the ambient temperature with 120MeV oxygen ions by a tandem accelerator at Japan Atomic Energy Research Institute (JAERI). Using the Fourier transform infrared photo-acoustic spectroscopy (FT-IR PAS), the specimens irradiated to 10^{19} ions/m^2 were characterized. The FT-IR PAS is very powerful tool for the nondestructive investigation of the structure changes of ceramics irradiated [2,3]. Especially, information on structural change can be obtained as a function of specimen depth through alteration of the modulation frequency by controlling the optical path difference (OPD) velocity. A FT-IR PAS spectrum of nonirradiated Li_4SiO_4 was shown in fig. 1. The spectrum was decomposed into eleven Gaussian/Lorentzan mixed curves. In those curves, the seven curves between 1050 and 750 cm^{-1} were assigned to be the bands of stretching Si-O vibrations. The three bands of the Si-O vibrations at high frequencies are considered to correspond to the triply degenerate vibration of the SiO_4 group, while the bands at lower frequencies are thought to be related to its holosymmetric vibration [4].

For Li_4SiO_4 irradiated, the spectra were also decomposed into above- mentioned curves. Fig. 2 shows ratios of individual peak area of the curves to total peak area (i.e., peak area ratios) for the spectra obtained by controlling the OPD velocity. In the case of data on the Si-O vibration at 1000 cm^{-1} for OPD velocity of 0.20 cm/s, the peak area ratios reflect structural information at the specimen depth of 30 μm. On the other hand, the structural information in the region of about 50 μm in depth is obtained from the vibration data at 1000 cm^{-1} in the spectra measured with the OPD velocity of 0.05 cm/s. The peak area ratio for the vibration at 1000 cm^{-1} before irradiation was substantially changed by the irradiation. The changes due to the irradiation depended on the specimen depth. The energy of incident ions at the position of 30 μm in depth is much higher than that of 50 μm in depth. Thus, the ion energy dependence on radiation damage such as decomposition and oxygen-lattice site defects of SiO_4 etc. can be studied using FT-IR PAS by controlling the OPD velocity. When irradiation is carried out with component ions, the ion energy dependence can provide information on primary knock-on atom (PKA) spectrum effects on radiation damage. In high energy ion irradiation of ceramic materials, the ratio between electronic excitation and elastic displacement due to nuclear collision also changes extensively with depth. For some ceramic materials, electronic excitation can contribute to production of displacement damage especially at high ion energies [5]. Consequently, FT-IR PAS with controlling the OPD velocity can be also applied to investigate contribution of electronic excitation process to damage production as a function of incident ion

energy, and therefore, it can provide information on electronic excitation effects due to PKA with high energy which can be generated in fusion reactor neutronic environment.

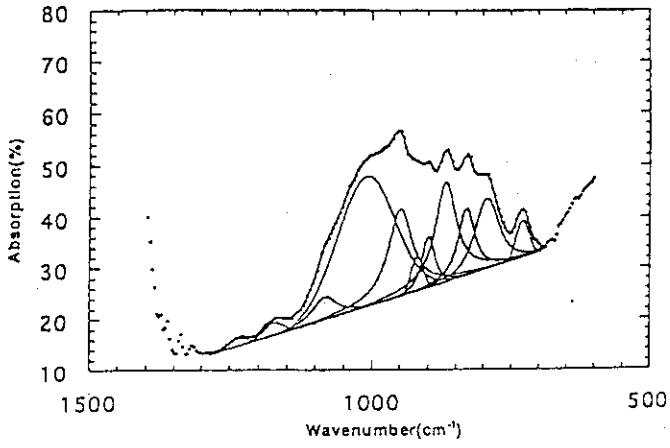

Fig. 1 A FT-IR PAS spectrum of nonirradiated Li_4SiO_4

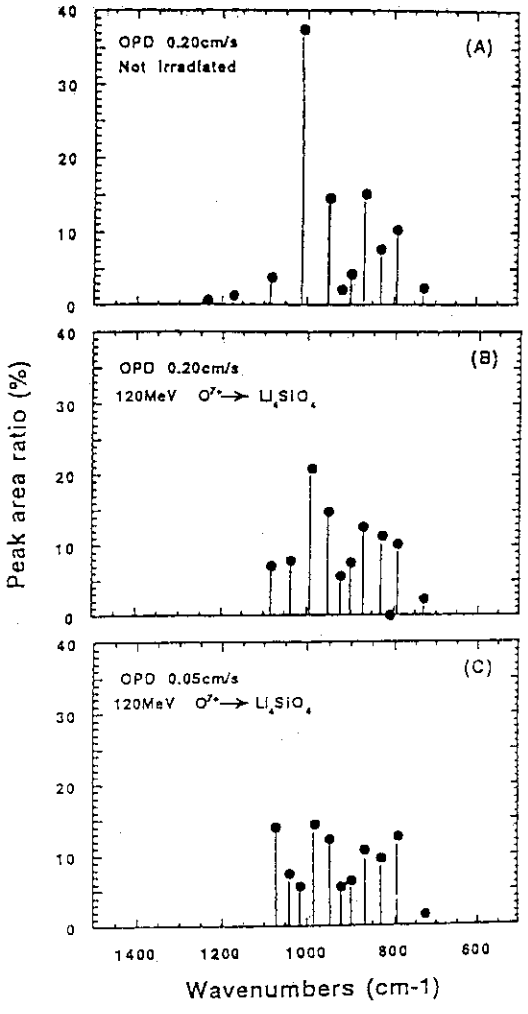

Fig. 2 Ratio of individual peak area of the curve to total peak area for the spectra obatined by controlling the OPD velocity

References

1) K. Noda, Y. Ishii, T. Nakazawa, H. Matsui, N. Igawa, D. Vollath, H. Ohno and H. Watanabe, J. Nucl. Mater. 191-194 (1992) 248.
2) T. Nakazawa, K. Noda, Y. Ishii, H. Matsui, N. Igawa, D. Vollath, H. Ohno and H. Watanabe, Proc. 17th Sym. Fusion Technology, Sept. 14-18, 1992 (Rome) p.1444-1448.
3) N.Teramae and S.Tanaka, in:H. Ishida(Ed.), Fourier Transform Infrared Characterization of Polymers, Plenum Publishing Corporation, 1987, pp.315-340.
4) A.N.Lazarev, V.A.Kolesova,L.S.Solntseva and A.P.Mirgorodskii, Izv. Akad. Nauk SSSR, Neorgan. Mat., 9(1973)1969.
5) K. Noda, Y.Ishii, H. Matsui and H. Watanabe, Radiat. Eff. 97 (1986) 297.

6.10 Radiation Damages in Vitreous Silicas Induced by High Energy N^{+5} and Cu^{+12} Ions Irradiation

S.Nasu[1], S.Oonishi[1], H.Nanto[1], R.Yamamoto[1], T.Nakazawa, K.Noda, T.Igarashi[2] and Y.Morimoto[2]

The purposes of this study are (1) to clarify the effect of hydroxyl contents on radiation damages in vitreous silicas induced by high energy N^{+5} and Cu^{+12} ions irradiation and (2) to examine photostimulated luminescence phenomenon due to irradiation induced color centers and implanted transition elements.

Samples used were fine polished commercially available vitreous silicas of SUPRASIL-P20 and GE214, the hydroxyl contents of which are about 1200 wppm and below 1 wppm respectively, and their dimension is 10x10x1mm^3. Three samples were irradiated at room temperature as shown below.

SUPRASIL-P20, N^{+5}, 85MeV, 3×10^{15} ions/cm^2 *
SUPRASIL-P20, N^{+5}, 85MeV, 3×10^{14} ions/cm^2
GE214, Cu^{+12}, 195MeV, 1×10^{15} ions/cm^2

An absorption peak at 215nm (5.77eV) and a shoulder at 245nm (5.06eV) were observed in the visible and ultraviolet region for SUPRASIL-P20 after irradiation of 85MeV N^{+5} ions, while a shoulder at 5.77eV and a peak at 5.06eV were observed for GE214 after irradiation of 195MeV Cu^{+12} ions, as shown in Fig.1.

Three steady state photoluminescence peaks at 290nm (4.3eV), 460nm (2.7eV) and 560nm (2.2eV) were observed for SUPRASIL-P20 aftre irradiation, while none of these peaks appeared before irradiation as shown in Fig.2 together with its excitation data.

Four luminescence peaks were observed at 4.3eV, 400nm (3.1eV), 2.7eV and 2.2eV for GE214 after irradiation of 195MeV Cu^{+12} ions, while three peaks were observed at 4.3eV, 3.1eV and 2.2eV before irradiation.

That is, a luminescence peak at 2.7eV appeared and the peak at 3.1eV decreased after high energy Cu^{+12} ions irradiation.

Strain profile measurements showed the maximum strain at about 500μm below the irradiated surface for SUPRASIL-P20 after irradiation of 85MeV N^{+5} ions.

It is interesting to note that the estimated depth of the implanted nitrogen atoms in vitreous silica is 100μm based on the calculation of the stopping cross section.

Several authors have reported that the absorption peak at 5.77eV and the luminescence peak at 4.3eV are attributed to the E'center [1], while the absorption peak at 5.6eV and the luminescence peak at 4.3eV are attributed to the $B_2\alpha$ band, and the absorption peak at 5.16eV and the luminescence peak at 3.1eV are attributed to the $B_2\beta$ band [2,3].

Therefore, it is concluded that high energy ion irradiation could form the E'center and the $B_2\alpha$ band and annihilate the $B_2\beta$ band in vitreous silicas.

---

1. Department of Electrical Engneering, Kanazawa Institute of Technology
2. Usio Inc.

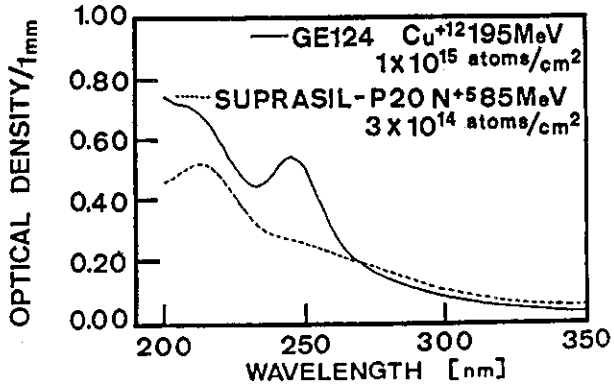

Fig.1 Ultraviolet optical absorption spectra of SUPRASIL-P20 and GE214 after N^{+5} and Cu^{+12} irradiation respectively.

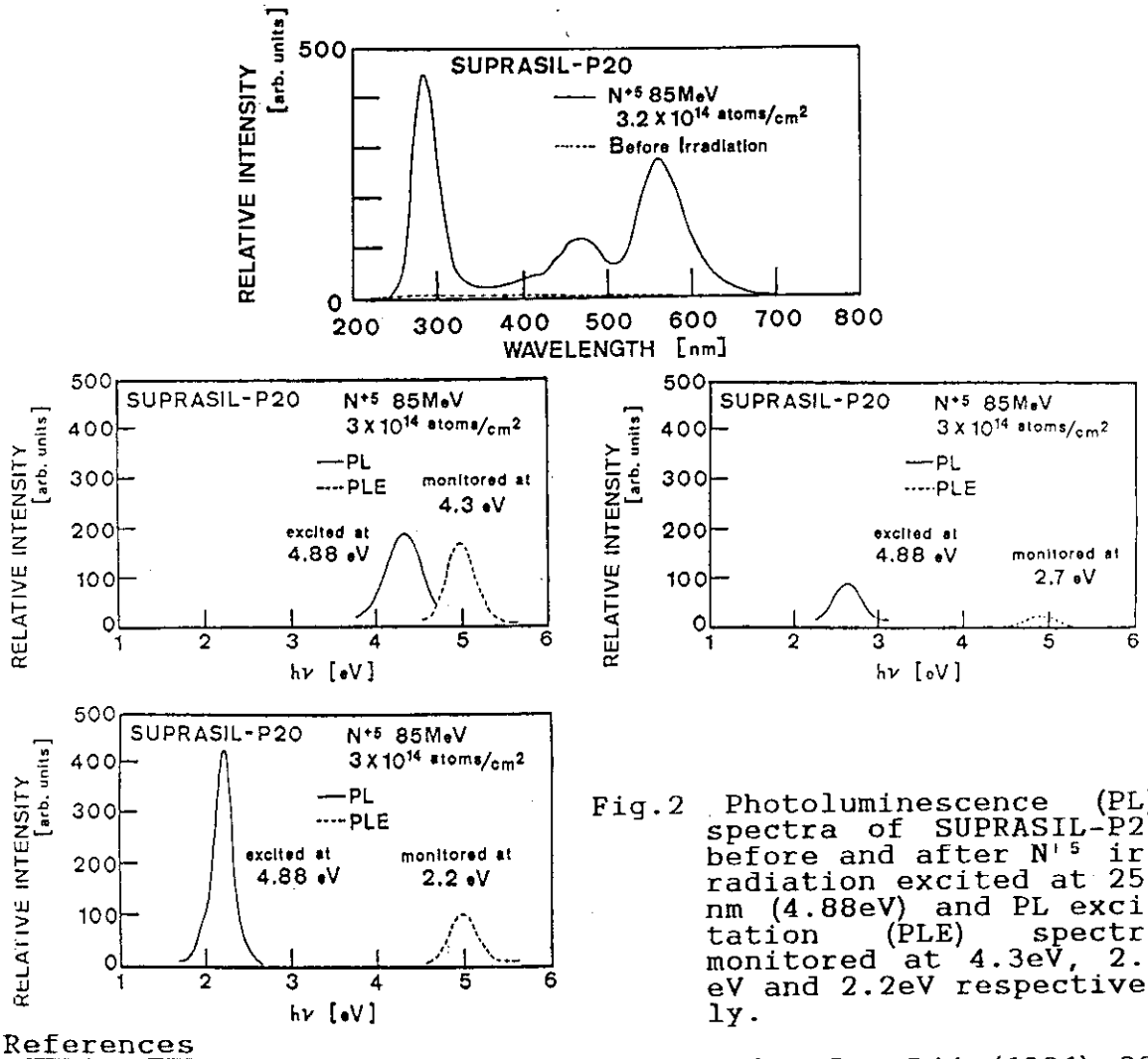

Fig.2 Photoluminescence (PL) spectra of SUPRASIL-P20 before and after N^{+5} irradiation excited at 254 nm (4.88eV) and PL excitation (PLE) spectra monitored at 4.3eV, 2.7 eV and 2.2eV respectively.

References
1) N.Kuzuu, Y.Komatsu and M.Murahara, Phys.Rev.B44 (1991),9265.
2) M.Kohketsu, K.Awazu, H.Kawazoe and M.Yamane, J.Appl.Phys. 28 (1989) 615.
3) R.Tohmon, H.Mizuno, Y.Ohki, K.Sasagane, K.Nagasawa and Y.Hama, Phys.Rev. B39 (1989) 1337.

* The SUPRASIL-P20 specimen with the higher dose has still been kept in Materials Inovation Laboratory in JAERI because of its high activity due to the H-N reaction.

6.11 SINGLE EVENT EFFECT IN POWER MOSFETS BY HIGH-ENERGY CARBON ION

S. MATSUDA[1], I. NASIYAMA, T. HIRAO, S. KUBOYAMA[1], T. HADA[1], T. KANNO[1], T. HIROSE[2], H. OHIRA[2]

Power MOSFETs are essential devices for power switching in electric circuits. However, they have a possible catastrophic failure mode known as Single Event Burn-Out(SEB) triggered upon incidence of high-energy ions. Since this is an annoying phenomenon to be considered in space electronic applications, it is necessity to improve the immunity from the SEB for the commercial devices.

To study the SEB mechanism, a spectrum of charge collected in the device was measured by a pulse-height analyzer system with a modified charge-sensitive amplifier. In the previous work for Power MOSFETs, it was suggested that SEB was triggered when a collected charge exceeded some threshold charge Q_{TH}.[1)]

High-energy ions from TANDEM accelerator were utilized this year to analyze the dependence of Q_{TH} on BV_{DS}. Figure 1 shows the charge spectra of the Power MOSFETs applied step-up drain voltage. The data were obtained using 105.3MeV Carbon ion from TANDEM accelerator. The effect of single event occurred at the drain voltage higher than V_{DS}=280V, which is consistent with other experimental results.[1)]

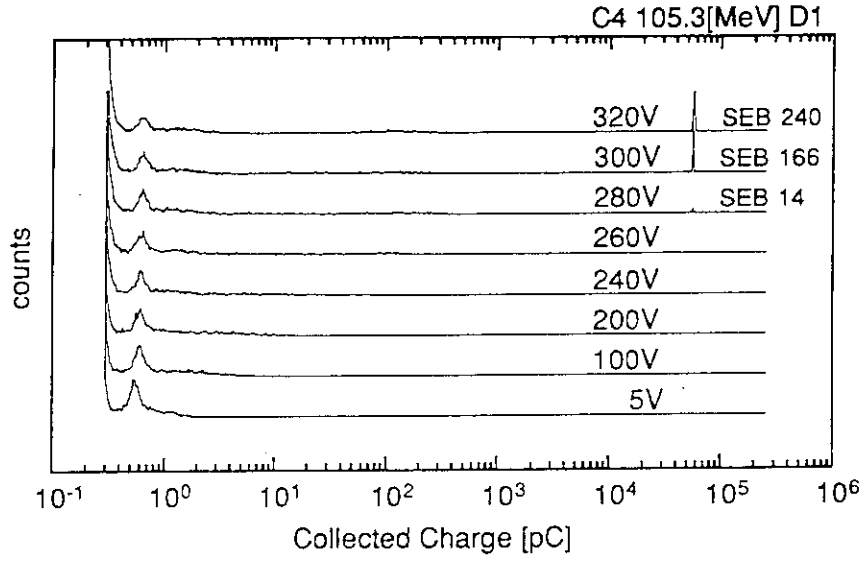

Fig. 1. The charge spectra of the Power MOSFETs applied step-up drain voltage.

Reference

1) S. Kuboyama et al.: IEEE Trans. Nucl. Sci., NS-39, No6, 1698 (1992).

---

[1]Parts and Material Technology Laboratory, Space Subsystems and Technology Department, Office of Research and Development, National Space Development Agency of Japan.
[2]Components Engineering Section, Engineering Dept., RYOEI TECHNICA Corporation.

6.12 RESPONSE OF SILICON SURFACE BARRIER DETECTOR TO HEAVY IONS

I. KANNO[1], S. KANAZAWA[1], K. NISHIO[1], T. MIKAWA[1],
M. MIYOSHI[1], T. INBE[1], I. KIMURA[1] and S. HAMADA

Silicon surface barrier detectors (SSBD) are widely used for charged particle measurements. The plasma delay, which is defined as the time delay between the charged particle injection and the pulse output, is an important phenomena in the timing property of SSBD. Typical results of the plasma delay were reported by Bohne *et al.*[1] They proposed an empirical formula for the plasma delay but did not discuss the physical explanation of the phenomena. One of the authors proposed a model of plasma column erosion.[2] In this model, the plasma delay was defined as the time interval between the plasma column formation and the beginning of the plasma column erosion, and the results of Bohne *et al.* were clearly explained except the resistivity dependence of the plasma delay.

With the development project of large scale accelerator in Europe, the resistivity change of silicon by parasitic neutrons became a theme of intensive study. The resistivity dependence of the plasma delay is one of the important theme of study associated with the accelerator project.

We carried out the measurements of the plasma delay for the study of its resistivity dependence. Oxygen ions were accelerated and scattered by a gold target foil of $100\mu g/cm^2$ in thickness. The scattered oxygen ions were extracted into the flight path of 105cm in length with the angle of 45 degrees. In the flight path, a micro-channel-plate detector (MCPD) was placed. The SSBDs with resistivities of 362Ωcm and 2100Ωcm were set at the end of the flight path. The time-of-flight measurement was carried out between the MCPD and the SSBD, with changing the applied bias voltages of the SSBDs. The plasma delay was obtained following the method of Bohne *et al.*[1] and are shown in Fig. 1.

In the model of the plasma column erosion[2], two forces compete each other : the carrier attracting force which is proportional to the electric field strength F and the plasma column compressing force which is proportional to F^2 (for low energy heavy ions such as ^{129}Xe with 166MeV in energy, F). In a high electric field strength, the plasma column radius hardly expands due to the strong compressing force. The electron-hole density in the plasma column remains high and the electric field strength hardly penetrates the plasma column. On the other hand, the electrons and holes are strongly attracted towards the positive and negative electrodes. With these competing forces, the plasma delay shows complicated behavior to have a peak value as a function of inverse electric field strength. In the former model described above, the effective electric field strength F_{eff} (the electric field strength at

[1]Department of Nuclear Engineering, Kyoto University.

the 2/3 of the plasma column length) was employed as a representative value. The plasma column has dielectric property when it begins to erode. The electric field strength inside the plasma column F_{in} is depressed by the ratio of dielectric constants of silicon (ϵ) and the plasma column (ϵ').

$$F_{in}(x) = \frac{\epsilon}{\epsilon'} F_{out}(x). \tag{1}$$

Here, d is the depletion layer thickness, x the distance from the backside of the entrance window and $F_{out}(x)$ the electric field strength outside of the plasma column. On the other hand, $F_{out}(x)$ is enhanced so that the electric potential of the depletion layer is kept constant.

$$F_{out}(x) = \frac{2V(d-x)}{(d-l)^2 + \frac{\epsilon}{\epsilon'} l(2d-l)}, \tag{2}$$

where, l is the plasma column length. In Fig. 2, the electric field strengths are plotted for 362Ωcm and 2100Ωcm SSBDs with the same F_{eff} for the plasma column length of 30μm and the ratio of dielectric constants, 1/10. The electric field strength in the side of the plasma column has no influence with the presence of the plasma column and remains unchanged. We conclude here that we should employ the enhanced electric field strength F_{out} for the estimation of the attractive force, and F_{eff} for the compressing force. The plasma delays for two different resistivity SSBDs were calculated and were normalized at the experimental data of 362Ωcm SSBD with 0.5cm/kV inversed field strength as shown in Fig. 1. This improved model of the plasma column erosion showed a simple and clear explanation for the resistivity dependence of the plasma delay in a SSBD.

This study was partly supported by the Grant-in-Aid of Scientific Research from the Ministry of Education, Science and Culture of Japan.

References

1) W. Bohne, W. Galster, K. Grabisch, and H. Morgenstern, Nucl. Instrum. Methods **A240**, 145 (1985).

2) I. Kanno, Rev. Sci. Instrum. **61**, 129 (1990).

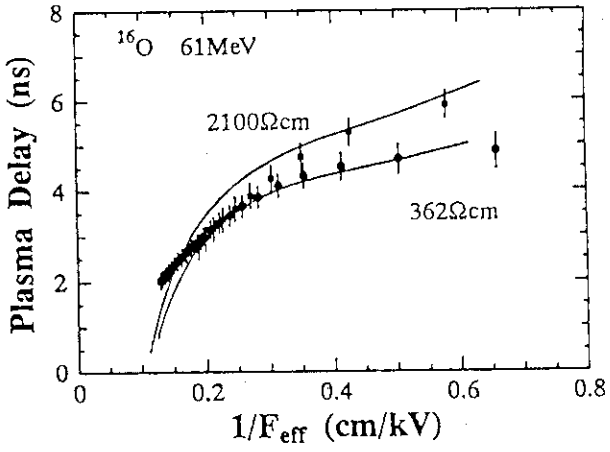

Fig.1 Measured and calculated plasma delay for SSBDs with different resistitities.

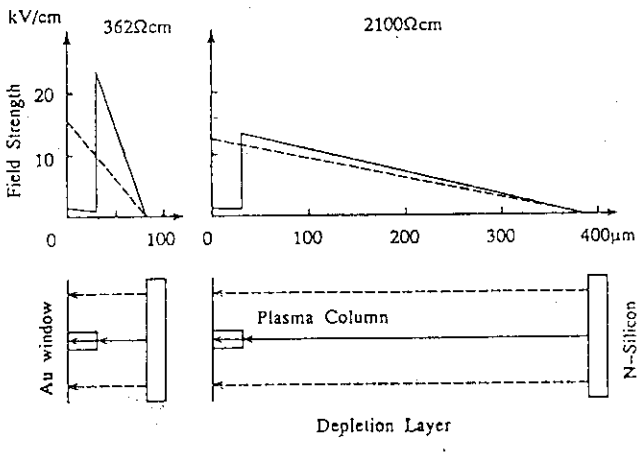

Fig.2 Electric field strengths for SSBDs with different resistivities.

6.13 EFFECT OF GAMMA-RAY ON ETCHING OF HEAVY ION TRACK IN POLYIMIDE(2)

Y. KOMAKI, N. ISHIKAWA, K. FURUKAWA and T. SAKURAI

Polyimide films were subjected to heavy ion for the purpose of making the microfilter of high resistivity to radiation and examining the etchability of the track formed in a polymer of high resistivity to radiation(~10^{10}Rad)[1]. As the previous tentative examination by ^{107}Ag and ^{59}Ni ions presented[2]only an insufficient consideration, the second examination has been carried out.

The 12.4μm thick and 13 mm diameter polyimide films(UPILEX, UBE Industry Co.Ltd.)irradiated by defocussed beams fixed $3\times10^{8}/cm^{2}$ of heavy ions were etched in a 10%NaClO solution at 60°C. The pore size formed was measured by gaseous transmittance through the holes.

Figure 1 shows the growth of the hole diameter with the etching time. Numerical values on the curves show doses of gamma-ray. The figure shows that the gaseous transmittance is not detected until the etched tracks from both surfaces of the film are bonded in the film. Consequently, the etching time which the gaseous transmittance occurs is the time necessary to connect the track,(V_t). As the degree of each slope was considered to be the same and related to the radial etching rate,(V_g) in the holes, the gamma-ray irradiation was found to give no effect on V_g. The etching time necessary to obtain the hole diameter of a certain size decreases down to one third with the increase in dose.
In Table 1, the effect of gamma-ray irradiation on the V_t and V_g are shown for several kinds of ion. The Table indicates that (1)in the film irradiated by the heavier ions the etching time necessary to obtain the hole of the same size is shorter, (2)the effect of gamma-ray exposure is more remarkable on the film irradiated by the lighter ions than the one by the heavier ions, (3)the effect converges on a region of a certain small V_t at more than 4×10^{8}Rad, regardless of ions, (4) V_g is not effected by any kind of ions and by dose up to 4×10^{8}Rad, and (5) V_t/V_g ratio increases two orders of magnitude. Additionally the track by C ions has not been etched even after irradiation at 4×10^{8}Rad in dose. Exposure to gamma-ray of dose up to 4×10^{8}Rad was found not to cause any changes on the characteristic of the microfilter of polyimide. The bulk polyimide having high radiation resistivity and the small chemical solubility shows the considerable radiation damage only in tracks by the heavy ions. In tracks the molecules scissred along the pass of ions bond with O_2 during gamma-ray irradiation and yield some oxygenated bonds, and this results in increase in the solubility. The mechanism of solubility must be considered to relate to the progressive formation of new bonding with O_2 every scission.[1]

References

1) T. Sasuga.: POLYMER. 29 (1988) 1562.
2) Y. Komaki, et al.: JAERI-M 92-124 (1992) 122-125.

Table 1 Effect of gamma-ray on the etching rates in the films irradiated by the heavy ions

Dose (Rad)	^{64}Cu			^{79}Br			^{107}Ag		
	V_t (μm/h)	V_g	V_t/V_g	V_t (μm/h)	V_g	V_t/V_g	V_t (μm/h)	V_g	V_t/V_g
0	0.23		7.7	0.46		15	0.78		26
$1x10^7$	0.35		12	0.70		23	0.97		32
$1x10^8$	0.80	0.03	27	1.8	0.03	59	1.4	0.03	47
$4x10^8$	1.6		54	2.1		71	2.3		77

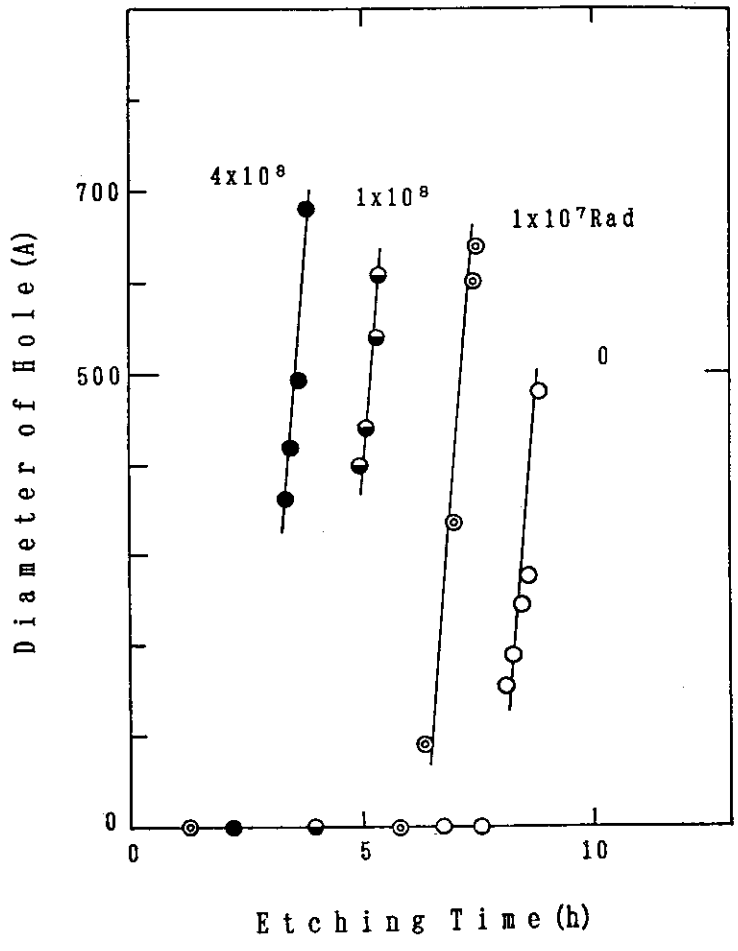

Figure 1 Effect of gamma-ray on the growth of holes in the films irradiated by the Ag ion

7. Publication in Journals and Proceedings, and Contributions to Scietific Meetings

7. Publication in Journals and Proceedings, and Contributions to Scietific Meetings

ACCELERATOR OPERATION AND DEVELOPMENT

Journal/Proceedings

Hanashima, S., Shozi, T., Shiozaki, Y., Saito, M., Oogane, Y. and Sekiguchi, S.
The Control System for the JAERI Tandem Particle Accelerator using Transputers, Transputer and OCCAM Engineering Series Vol.35 (Proceedings of the 5th Transputer/OCCAM International Conference 1993 Osaka, Japan) IOS Press, pp.69-81.

Shibata, M., Takeuchi, S., Ishii, T., Kanazawa, S., Yoshida, T. and Sugiyama, Y.
RF Performances of Superconducting Resonators for the JAERI Tandem Booster
Proceedings of the 6th Workshop on RF superconductivity, CEBAF, Washington D.C., 1993

Shibata, M., Ishii, T. and Takeuchi, S.
Off-Line Tests of Superconducting Resonators of the JAERI Tandem Booster
Proceedings of the 18th Linear Accelerator Meeting in JAPAN, KEK, Tsukuba, Japan, July, 1993, pp. 296-298.

Takeuchi, S.
Superconducting Tandem-Booster
Proc. of The Fifth Japan-China Joint Symposium, Osaka (Oct., 1993) p189.

Takeuchi, S., Shibata, M., Ishii, T. and Other Booster Project Members
Development of JAERI Tandem Superconducting Booster
Proceedings of the 9th Symposium on Accelerator Science and Technology, KEK, Tsukuba, Japan, 1993, pp. 437-439.

Meetings

Shibata, M.
RF Performances of Superconducting Resonators for JAERI Tandem Booster
Sixth Workshop on RF Superconductivity, CEBAF(Oct. 1993)

Shibata, M.
Superconducting RF Activities at JAERI
Sixth Workshop on RF Superconductivity, CEBAF(Oct. 1993)

Takeuchi, S.
Status and Future of Heavy Ion Accelerator Development at JAERI Tokai
Symposium on Heavy Ion Accelerators, RIKEN(July, 1993)

NUCLEAR STRUCTURES

Journal/Proceedings

Ferragut, A., Gono, Y., Murakami, T., Morikawa, T., Zhang, Y.H., Morita, K., Yoshida, A., Oshima, M., Kusakari, H., Sugawara, M., Ogawa, M., Nakajima, M., Mitarai S., Odahara, A., Ideguchi, E., Shizuma, T., Kidera, M., Kim, J.C., Chae, S.J., Min, B.J. and Kumagai, H.
A New High-Spin Isomer in ^{145}Sm.
J. of Phys. Soc. Japan, Vol.62(1993)3343.

Gono, Y., Murakami, T., Morikawa, T., Ferragut, A., Zhang, Y.H., Morita, K., Yoshida, A., Oshima, M., Kusakari, H., Sugawara, M., Ogawa, M., Nakajima, M., Mitarai, S., Odahara, A., Ideguchi, E., Shizuma, T., Kidera, M., Kim, J.C., Chae, S.J. and Min, B.J.
High-Spin Isomers and High-Spin Isomer Beams.
Nucl. Phys., A557(1993)341c.

Gono, Y., Murakami, T., Morikawa, T., Ferragut, A., Zhang, Y.H., Morita, K., Yoshida, A., Oshima, M., Kusakari, H., Sugawara, M., Ogawa, M., Nakajima, M., Mitarai, S., Odahara, A., Ideguchi, E., Shizuma, T., Kidera, M., Kim, J.C., Chae, S.J. and Min, B.J.
High-Spin Isomers and High-Spin Isomer Beams.
Proc. 6th Franco-Japanese Colloquium,
"Nuclear Structure and Interdisciplinary Topics"
N. Alamanos, S. Fortier and F. Dykstra, (Eds.)(Saint-Malo, France, 1993)p7.

Gono, Y., Murakami, T., Morikawa, T., Ferragut, A., Zhang, Y.H., Morita, K., Yoshida, A., Oshima, M., Kusakari, H., Sugawara, M., Ogawa, M., Nakajima, M., Mitarai, S., Odahara, A., Ideguchi, E., Shizuma, T., Kidera, M., Kim, J.C., Chae, S.J. and Min, B.J.

Physics on/with Extremely High-Spin Isomers.
Conf. Proc. Vol.38, "Perspectives in Heavy Ion Physics"
M. Di Toro and E. Migneco (Eds.)(SIF, Bolognia, 1993)p85.

Ishii, T., Makishima, A., Koganemaru, K., Saito, Y., Ogawa, M. and Ishii, M.
High-Spin States in ^{107}Sn
Z. Phys. A, 347(1993)41.

Katakura, J., Oshima, M., Kitao, K. and Iimura, H.
Nuclear Data Sheets for A=125.
Nucl. Data Sheets, 70(1993)217.

Murakami T., Gono, Y., Ferragut, A., Zhang, Y.H., Morita, K., Yoshida, A., Ogawa, M., Nakajima, M., Min, B.J., Kumagai, H., Oshima, M., Morikawa, T., Sugawara, M. and Kusakari, H.
High-Spin Isomeric State in ^{144}Pm.
Z. Phys., A345(1993)123.

Oshima, M., Morikawa, T., Kusakari, H., Kobayashi, N., Sugawara, M., Zhang, Y.H., Ferragut, A., Ichikawa, S., Shinohara, N., Nagame, Y., Shibata, M., Gono, Y. and Inamura, T.
Double-γ Vibrational States in ^{168}Er and ^{192}Os.
Nucl. Phys., A557(1993) 635c.

Oshima, M.
High Spin Isomer Beam and its Application
"Report of Specialist Research Meeting on the Nuclear Physics and Solid State Physics by a Radioactive Nuclear Beam" (KURRI-TR-377)(Kyoto, 1993) p22.

Meetings

Gono, Y., Shibata, M., Ideguchi, E., Odahara, A., Kidera, M., Mitarai, S., Morikawa, T., Oshima, M., Hatsukawa, Y., Iimura, H., Shibata, H. and Hamada, S.
High-Spin State of ^{147}Eu.
Spring Meeting of the Physical Society of Japan in Kochi(March, 1994).

Hatsukawa, Y., Tsukada, K., Shinohara, N., Nagame, Y., Magara, M.,
Decay Property of ^{245}Cf(2).
The 37th Symposium on Radiochemistry(Oct.6-8, 1993)

Ideguchi, E., Morikawa, T., Gono, Y., Mitarai, S., Odahara, A., Shizuma, T., Kidera, M., Narimatsu, K., Shibata, M., Nishimoto, S. and Oshima, M.
High-Spin Isomer of ^{146,147}Eu.
Fall Meeting of the Physical Society of Japan in Kochi(October, 1993).

Ideguchi, E., Odahara, A., Shizuma, T., Kidera, M., Shibata, M., Mitarai, S., Gono, Y., Morikawa, T., Oshima, M., Hatsukawa, Y. and Hamada, S.
High Spin Isomer of ^{146}Eu.
Spring Meeting of the Physical Society of Japan in Fukuoka(March, 1994).

Ideguchi, E., Morikawa, T., Gono, Y., Mitarai, S., Odahara, A., Sizuma, T., Kidera, M., Narimatsu, K., Shibata, M., Nishimoto, S., Kishida, T., Morita, K., Yoshida, A., Murakami, T., Oshima, M., Ogawa, M., Kusakari, H., Sugawara, M., Shin, S.A., Kim, J.C., Chae, S.J. and Min, B.J.
Simulation of a γ-Ray Spectrum for a Segmented Ge Detector.
Fall Meeting of the Physical Society of Japan in Kochi(October, 1993).

Ideguchi, E., Morikawa, T., Gono, Y., Mitarai, S., Odahara, A., Sizuma, T., Kidera, M., Narimatsu, K., Shibata, M., Nishimoto, S. and Oshima, M.
High-Spin Isomer of ^{148}Tb.
Fall Meeting of the Physical Society of Japan in Kochi(October, 1993).

Ishii, T., Makishima, A., Shibata, M., Koganemaru, K., Ogawa, M. and Ishii, M.
Nuclear Structure of ^{109}Sb
Fall Meeting of Physical Society of Japan in Kochi(Oct.3-6, 1993)

Makishima, A., Ishii, T., Shibata, M., Koganemaru, K., Ogawa, M. and Ishii, M.
Electromagnetic Properties of 6^+, 10^+ and 14^- States in ^{106,108}Sn
Fall Meeting of Physical Society of Japan in Kochi(Oct.3-6, 1993)

Morikawa, T., Kishida, T., Morita, K., Yoshida, A., Gono, Y., Mitarai, S., Odahara, A., Idegichi, E., Shizuma, T., Kidera, M., Narimatsu, K., Shibata, M., Nishimoto, S., Murakami, T., Ogawa, M., Oshima, M., Kusakari, H.,

Sugawara, M., Shin, S.A., Kim, J.C. and Chae, S.J.
Fall Meeting of the Physical Society of Japan in Kochi(October, 1993).

Morikawa, T.
Coulomb Excitation of ^{178}Hf
"JAERI Workshop on Joint Spectroscopy Experimants with Tandem-Boaster Accelerator" (JAERI, November, 1993).

Morikawa, T., Gono, Y., Kishida, T., Ideguchi, E., Morita, K., Yoshida, A., Ferragut, A., Kumagai, H., Zhang, Y.H., Murakami, T., Oshima, M., Sugawara, M., Kusakari, H., Ogawa, M., Nakajima, M., Mitarai, S., Odahara, A., Kidera, M., Shibata, M., Kim, J.C. and Chae, S.J.
Development of High-Spin Isomer Beam.
Int. Sympo. on Frontiers of Nuclear Structure Physics in Tokyo(March, 1994).

Odahara, A., Gono, Y., Mitarai, S., Tomura, H., Ideguchi, E., Shizuma, T., El-Badry, A.M., Kidera, M., Narimatsu, K., Shibata, M., Morikawa, T., Kishida, T., Zhang, Y.H., Ferragut, A., Morita, K., Yoshida, A., Murakami, T., Ogawa, M., Nakajima, M., Oshima, M., Kusakari, H., Sugawara, M., Min, B.J., Kim, J.C. and Chae, S.J.
High-Spin Isomer and Level Structure of ^{145}Sm.
Fall Meeting of the Physical Society of Japan in Kochi(October, 1993).

Odahara, A., Gono, Y., Mitarai, S., Ideguchi, E., Kidera, M., Sibata, M., Morikawa, T., Kishida, T., Zhang, Y.H., Ferragut, A., Morita, K., Yoshida, A., Murakami, T., Ogawa, M., Oshima, M., Kusakari, H., Sugawara, M., Min, B.J., Kim, J.C. and Chae, S.J.
High-Spin Isomer and Level Structure of ^{145}SmⅡ.
Spring Meeting of the Physical Society of Japan in Fukuoka(March, 1994).

Odahara, A., Gono, Y., Mitarai S., Ideguchi, E., Kidera, M., Shibata, M., Morikawa, T., Kishida, T., Morita, K., Yoshida, A., Kumagai, H., Zhang, Y.H., Ferragut, A., Murakami, T., Oshima, M., Kusakari, H., Sugawara, M., Ogawa, M., Nakajima, M., Min, B.J., Kim, J.C. and Chae, S.J.
High-Spin Isomer and Level Structure of ^{145}Sm.
Int. Sympo. on Frontiers of Nuclear Structure Physics in Tokyo(March, 1994).

Oshima, M., Morikawa, T., Hatsukawa, Y., Iimura, H., Ishii, T., Kusakari, H., Kobayashi, N., Taki, M., Sugawara, M., Ideguchi, E., Kidera, M. and

Gono, Y.
Two-Phonon γ-Vibrational States in Deformed Nuclei.
Int. Sympo. on Frontiers of Nuclear Structure Physics in Tokyo(March, 1994).

Oshima, M.
Spectroscopic Study of Unstable Nuclei through Tandem and Booster Accelerator.
INS symposium on Science of Short-lived Nuclear Beam '93 in Tokyo(December, 1993).

Oshima, M.
Study of Vibrational Excitation in Heavy Nuclei
"JAERI Workshop on Joint Spectroscopy Experiments with Tandem-Booster Accelerator " in Tokai(November,1993)

NUCLEAR REACTIONS
Journal/Proceedings

Ikezoe, H., Nagame, Y., Nishikawa, I., Sugiyama, Y., Tomita, Y., Ideno, K., Hamada, S., Shikazono, N., Iwamoto, A. and Ohtsuki. T.
Prescission and Postscission Charged Particle Emission from the $^{19}F+^{159}Tb$ Reaction
Phys. Rev. C 49(1994) 968.

Ikezoe, H., Shikazono, N., Nagame, Y., Ohtsuki, T., Sugiyama, Y., Tomita, Y., Ideno, K., Nishinaka, I., Qi, B.J., Kim, H.J., and Iwamoto, A.
Charged Particle Multiplicities in Heavy-Ion Induced Fission
Societa Italiana di Physica, Conf. Proc., Vol.38, "Perspective in Heavy-Ion Physics, SIF, Bologna(1993)p119.

Nagame, Y., Baba, S. and Saito, T.
Isomeric Yield Ratio for the $^{95}Mo(p, n)^{95m,g}Tc$ Reaction
Appl. Radiat. Isot. 45((1994)281

Nakahara, H., Sueki, K., Nishinaka, I., Nagame, Y., Ikezoe, H. and Ohtsuki, T.
Bimodal Nature of Nuclear Fission
Proceedings of RIKEN International Workshop on HEAVY-ION REACTIONS WITH

NEUTRON-RICH BEAMS, World Scientific(1993)p.114

Ohtsuki T., Nakahara H. and Nagame Y.
Systematic Variation of Fission Barrier Heights for Symmetric and Asymmetric Mass Divisions.
Phys. Rev. C48(1993)1667.

Pu, Y.H., Lee, S.M., Jeong, S.C., Fujiwara, H., Mizota, T., Futami, Y., Nakagawa, T., Ikezoe, H. and Nagame, Y.
The Competition between Fusion-Fission and Deeply Inelastic Reactions in the Medium Mass Systems
Proceedings of RIKEN International Workshop on HEAVY-ION REACTIONS WITH NEUTRON-RICH BEAMS, World Scientific(1993)p.154

Sugiyama, Y., Tomita, Y., Ikezoe, H., Yamanouchi, Y., Ideno, K., Hamada, S., Sugimitsu, T., Hijiya, M. and Kondo, Y.
Observation of Airy Oscillation for the $^{16}O+^{16}O$ System at E_{lab}=145MeV
Phys. Lett. B312(1993)35.

Sugiyama, Y., Tomita, Y., Ikezoe, H., Yamanouchi, Y., Ideno, K., Hamada, S., Sugimitsu, T., Hijiya, M., Mukae, T., Nakamoto, K., Utsunomiya, K., Okamoto, T., Mitsuoka, S., Matsuo, M. and Fujita, H.
New Approach to Spin Assignments of Intermediate Structure in $^{12}C(^{16}O, ^{12}C(2_1^+))^{16}O$
Phys. Rev. C49(1994)3305.

Meetings

Fujita, H.
Magnetic Substate Population of $^{12}C(2^+)$ in $^{12}C+^{16}O$ Inelastic Scattering
Kiken Meeting in Kyoto (Nov. 11, 1994)

Hijiya, M., Fujita, H., Mukae, T., Nakamoto, K., Utsunomiya, K., Sugimitsu, T., Okamoto, T., Ikeda, N., Morinobu, S., Sugiyama, Y., Ikezoe, H., Ideno, K., Tomita, Y., Yamanouchi, Y. and Hamada, S.
Measurement for $^{12}C(2^+)$ Spin Alignment Following $^{16}O+^{12}C$ Collision
Fall Meeting of the Physical Society of Japan in Kochi (Oct. 5, 1994)

Iimura, H., Kubota, M., Nakahara, Y., Ichikawa, S. and Horiguchi, T.
Measurements of Hyperfine Structure in ^{143}Pr ($T_{1/2}$ = 13.6 d) by Collinear Laser-Ion-Beam Spectroscopy
Fall Meeting of the Physical Society of Japan in Kochi (Oct. 3, 1993)

Iimura, H., Kubota, M., Nakahara, Y., Ichikawa, S. and Horiguchi, T.
Laser Spectroscopy of Radioactive Pr Isotopes
Spring Meeting of the Physical Society of Japan in Fukuoka(Mar. 30, 1994)

Ikezoe, H.
Charged Particle Emissions in Fission Process
Scientific Meeting of "Dynamics of Highly Excited Nuclei" in Sendai, March 17, 1994

Nagame, Y., Ikezoe, H., Tsukada, K., Hatsukawa, Y., Magara, M., Shinohara, N., Oshima, M., Ohtsuki, T., Sasaki, R., Aoki, Y., Kasagi, J. and Nishinaka, I.
Sub-Barrier Energy Heavy-Ion-Induced Fission in Heavy Actinides
The 37th Symposium on Radiochemistry in Kanazawa(Oct. 6-8, 1993).

Meetings

Nishinaka, I., Nagame, Y., Ikezoe, H., Ohtsuki, H., Tanikawa, M., Tsukada, K., Sueki, K. and Nakahara, H.
Fragment Mass and Kinetic Energy Distributions from Fission of Light Actinides
ACTINIDES-93 International Conference, Santa Fe (Sep. 19-24, 1993)

Nishinaka, I., Tanikawa, M., Sueki, K., Nakahara, H., Tsukada, K., Magara, M., Shinohara, N. and Nagame, Y.
Isotopic Distribution of Fission Products from Neutron-Deficient Compound Nuclei in Light Actinide Region
ACTINIDES-93 International Conference, Santa Fe(Sep. 19-24, 1993)

Nishinaka, I., Miyamoto, S., Kobayashi, K., Sueki, K., Nakahara, H., Tsukada, K., Magara, M., Hatsukawa, Y., Nagame, Y., Ikezoe, H., Ohtsuki, T. and Tanikawa, M.
Nuclear Fission of Neutron-Deficient Nuclei in Light Actinide Region

The 37th Symposium on Radiochemistry in Kanazawa(Oct. 6-8, 1993)

Ohtsuki, T., Nagame, Y., Ikezoe, H., Sueki, K. and Nakahara, H.
Bimodal Nature of Actinide Fission
ACTINIDES-93 International Conference, Santa Fe(Sep. 19-24, 1993)

Sueki, K., Nishinaka, I., Tanikawa, M., Tsukada., K. and Nakahara, H.
Kinetic Energies of Cs Isotopes Produced by $^{16}O+^{209}Bi$ Nuclear Fission Measured by Differential Range Method
ACTINIDES-93 International Conference, Santa Fe(Sep. 19-24, 1993)

Sugiyama, Y.
Heavy-Ion Nuclear Reactions around the Coulomb Barrier
INS Symposium on Toward a Unified Understandings of Elastic and Inelastic Scattering and Transfer Reactions, INS, University of Tokyo(1994)

Sugiyama, Y., Tomita, Y., Ikezoe, H., Yamanouchi, Y., Ideno, K., Hamada, S., Sugimitsu, T., Hijiya, M. and Kondo, Y.
Nuclear Rainbow Scattering Observed in $^{16}O+^{16}O$ Elastic Scattering at E_{lab} =145MeV
Fall Meeting of the Physical Society of Japan in Kochi(Sep. 30, 1993)

Sugiyama, Y., Tomita, Y., Ikezoe, H., Yamanouchi, Y., Ideno, K., Hamada, S., Sugimitsu, T., Hijiya, M., et al.
Elastic and Inelastic Scattering of $^{58}Ni+^{60}Ni$ and $^{58}Ni+^{90,94}Zr$ near the Coulomb Barrier
Workshop on Heavy-Ion Fusion (1994) Italy

Sugiyama, Y., Tomita, Y., Ikezoe, H., Yamanouchi, Y., Ideno, K., Hamada, S., Sugimitsu, T., Hijiya, M. and Kondo, Y.
Observation of Nuclear Rainbow Scattering in the $^{16}O+^{16}O$ System at E_{lab} =124MeV and 145MeV
5th Intern. Conf. on Nucleus Nucleus Collision (1994) Italy

Tanikawa, M., Miyamoto, S., Nishinaka, I., Sueki, K., Nakahara, H., Kobayashi, T., Tsukada, T. and Nomura, T.
Influence of the Angular Momentum on the Fission Process of the Compound Nucleus ^{210}Po (2)
The 37th Symposium on Radiochemistry in Kanazawa(Oct. 6-8, 1993).

Teshigawara M., Konashi K., Yamamoto T., Kayano H., Aratono Y., Furukawa K., and Tachikawa E.
Measurement of D-D fusion in TiD Target under Irradiation of Heavy Ion
Fourth International Conference on Cold Fusion, Hawaii(December 7, 1993)

Teshigawara M., Konashi K., Yamamoto T., Kayano H., Aratono Y., Furukawa K., and Tachikawa E.
Heavy Ion Induced D-D Fusion in Deuteride Compound
Spring Meeting of the Physical Society of Japan, Fukuoka(March 29, 1994)

Tsukada, K., Shinohara, N., Nagame, Y., Magara, M., Ichikawa, S., Hoshi, M., Nakahara, H., Sueki, K., Tanikawa, M., Nishinaka, I., Kobayashi, T. and Ohtsuki, T.
Mass Yield and Angular Distributions of Rare Earth Elements Produced on Proton Induced Fission of Actinides
ACTINIDES-93 International Conference, Santa Fe(Sep. 19-24, 1993)

Tsukada, K., Nagame, Y., Shinohara, N., Ichikawa, S., Magara, M., Sueki, K., Nishinaka, I., Nakahara, H. and Ohtsuki, T.
Extremery Asymmetric Mass Division Products in Low-Energy Proton-Induced Fission of Actinides(3)
The 37th Symposium on Radiochemistry in Kanazawa(Oct. 6-8, 1993).

Uno, Y., Meigo, S., Chiba, S., Fukahori, T., Kasugai, Y. and Ikeda, Y.
Measurements of Activation Cross Sections at 18-30 MeV by Using the ^{7}Li(p, n) Quasi-Monoenergetic Neutron Source at JAERI-TANDEM
Spring Meeting of the Atomic Energy Society of Japan in Tokai(Mar., 1994)
Watanabe, Y., Chadwick, M.B. and Hodgson, P.E.

FKK Model Analysis of Preequilibrium Nucleon Emission from Nucleon-Induced Reactions at Incident Energies below 30MeV
Spring Meeting of the Atomic Energy Society of Japan in Tsukuba (Mar.29-31, 1993)

NUCLEAR THEORY
Journal/Proceedings

Bonasera, A. and Maruyama, T.

Kaon Production in Proton-Nucleus and Deuteron-Nucleus Collisions near the Kinematical Threshold.
Prog. Theor.Phys.90(1993)1155.

Iwamoto, A.
Nuclear Fission Process Studied with Charged-Particle Emission
Soryuushironn-kennkyuu 87 (1993) C163.

Iwamoto, A.
Semiclassical Methods for the Multi-Dimensional Quantum Decay
Proc. RIKEN Int. Workshop on Heavy-Ion Reactions with Neutron-Rich Beams, 1993, Wako(1993)p131.

Sugita, M., Gelberg, A. and Otsuka, T.
E2 Selection Rules of γ-Rigid and γ-Unstable Rotors,
Nucl. Phys.A567(1994)33.

Sugita, M. and Otsuka, T.
Double-γ Phonon Excitation in the Os Nuclei,
Nucl. Phys.A557(1993)643c.

Ono, A., Horiuchi, H., Maruyama, T., and Ohnishi, A.
Momentum Distribution of Fragments in Heavy-Ion Reactions:Dependence on the Stochastic Collision Process.
Phys. Rev. C47 (1993)2652.

Ono, A., Horiuchi, H. and Maruyama, T.
Nucleon Flow and Fragment Flow in Heavy Ion Reactions.
Phys. Rev. C48(1993)2946.

Meetings

Iwamoto, A.
Multi-Dimensional Tunneling and Nuclear Fission Process
2nd Int. Conf. on Atomic and Nuclear Clusters '93 in Santorini(June 28, 1993)

Iwamoto, A.
Quantum Tunneling in Nuclear Fission
Sicentific Meeting Quantum Tunneling in Multi-Freedom System, Tokyo(Aug. 24, 1993)

Iwamoto, A.
Nuclear Fission and Quantuim Tunneling Effect
Sicentific Meeting on Quantum Tunneling in Multi-Freedom System, Izu(Nov. 21, 1993)

Iwamoto, A.
Generalization of Nucleus-Nucleus Potential
RIKEN Sympo. on Dynamics of Hot Nuclei, Wako(Feb. 22, 1994)

Maruyama, T. and Bonasera, A.
Kaon Production in Proton-Nucleus and Deuteron-Nucleus Collisions.
Fall Meeting of the Physical Society of Japan in Kochi(Oct. 3, 1993)

Maruyama, T.
Current Status of the QMD Method
First Symposium on Simulation of Hadron Many-body System at JAERI(Oct. 18, 1993)

Niita, K.
Review and Perspective of Microscopic Simulations for Heavy Ion Collisions
First Symposium on Simulation of Hadron Many-body System.
at JAERI(18-20 October 1993)

ATOMIC PHYSICS

Journal/Proceedings

Kawatsura, K., Nakae, T., Shimatani, N., Maeda, K., Arai, S., Mitamura, T., Terasawa, M., Iwasaki, H., Uchida, H., Koterazawa, K., Hirono, Y., Mokuno, Y., Fujii, K., Satou, M., Sataka, M., Imai, M. and Maeta, H.
PIXI and RBS Study of Radiation-Induced Segregation in Single Crystal Austenitic Stainless Steel SUS304
Nucl. Instr. and Meth. B75(1993)367.

Sataka, M., Imai, M., Yamazaki, Y., Komaki, K., Kawatsura, K., Kanai, Y. and Tawara, H.
Binary Peak Electrons Observed at 0° for 2-4MeV/u F^{q+}, Si^{q+} and Ni^{q+} Ions in Collisions with a He Target
Nucl. Instr. and Meth. B79(1993)81.

Meetings

Imai, M. and Stataka, M.
Charge State distribution of Neon Recoil Ion by Carbon Ion Impact in Coincidence with Projectile Final State
XVth Int. Conf. on Physics of Electronic and Atomic Collisions in Auhus(July 1993).

Sataka, M., Imai, M., Yamazaki, Y., Komaki, K., Kawatsura, K., Kanai, Y. and Tawara, H., Schultz, D.R. and Reinhold, C.O.
Binary Peak Electrons Observed at 0 Degree for Au Ion Impact on He
Fall Meeting of the Physical Society of Japan in Okayama(October 12-15, 1993)

SOLID STATE

Journal/Proceedings

Chenevier, B., Ikeda, S., Kumakura, H., Togano, K., Okayasu, S. and Kazumata, Y.,
HREM Observation of Effects of 180MeV Cu^{11+} Ion-Irradiation on the Crystal Structure of $Bi_2Sr_2CaCu_2O_x$
Materials Science Forum 129(1993)17.

Haruna, K., Maeta, H.
Thermal Expansion of Synthetic Diamond Single Crystal at Low Temperatures
Diamond and Related Materials 2(1993)859-861

Ishikawa, N., Iwase, A., Iwata, T., Maeta, T., Tsuru, K. and Michikami, O.
Ion Irradiation Effects in $EuBa_2Cu_3O_y$ Thin Film
J. Supercond., 7(1994)241

Iwase, A. and Iwata, T.
Effect of Electron Excitation on Radiation Damage in FCC Metals Nucl. Instrm. Method B90(1994)322

Kanno, I., Kanazawa, S. and Kimura, I.
Energy Response Characteristics of Silicon Surface Barrier Detector
Proc. of the Seventh Workshop on Radiation Detectors and Their Uses
KEK Proceedings 93-8, p.31.

Kazumata, Y., Okayasu, S. and Aruga, T.
$YBa_2Cu_3O_x$ Films Irradiated by 120MeV Oxygen Ions
Jpn. J. Appl. Phys. 33(1994)1012

Kumakura, H., Kitaguchi, H., Togano, K., Maeda, H., Shimoyama, J., Okayasu, S. and Kazumata, Y.,
Effect of High-Energy Ion Irradiation and Electron Irradiation on Textured $Bi_2Sr_2CaCu_2O_x$ —180MeV Cu^{11+} and Br^{11+} Irradiations and 3MeV Electron Irradiation
J. Appl. Phys., 74(1993)451.

Maeta, H., Haruna, K., Bang, Lu and Ono, F.
X-Ray Diffraction Studies of Self-Ion Irradiated Synthetic Single Crystal Diamond
Nucl. Instr. and Meth. in Phys. Res. B80/81(1993)1477-1479

Matsumoto, N., Bang, Lu, Maeta, H., Jakubovics, J.P., Haruna, K. and Maeta, H.
Effect of Ion Beam Irradiation in Amorphous Ferromagnetics Alloys
Nucl. Instr. and Meth. in Phys. Res. B80/81(1993)428-431

Matsumoto, Y., Matsuura, Y., Hibino, Y., Kawakami K., Komaki Y., Ishikawa, N., Sakurai, T. and Tachikawa, E.
Microchannel Formation in Polyimide by Heavy Ion Irradiation. (for the Electric Packaging Board)
JAERI-M 93-196

Tanaka, H.
X-Ray Study of Strain Distribution in High Energy Ion Implantated Si(111) Wafers

Thesis of Master of Science(Physics)
(Science Univ. Tokyo)(March, 1993)

Meetings

Hayashi, K., Kikuchi, H. and Fukuda, K.
Radiation Damage of UO_2 Implanted with 100MeV Iodine Ions
Actinides-93, Sept. 19-24, 1993, Santa Fe, USA.

Ishikawa, N., Iwase, A., Iwata T., Maeta, T., Tsuru, K. and Michikami, O.
Ion Irradiation Effects in $EuBa_2Cu_3O_y$ Thin Film
Physics and Chemistry of Molecular & Oxide Superconductors
Satellite Conference to LT20(July 27, 1993)

Ishikawa, N., Iwase, A., Iwata, T., Maeta, T., Tsuru, K. and Michikami, O.
Ion Irradiation Effects of $EuBa_2Cu_3O_y$ Thin Film
The 3rd IUMRS International Conference on Advanced Materials(Sept. 2, 1993)

Kanno, I., Inbe, T., Kanazawa, S. and Kimura, I.
Recombination Effect in Silicon Surface Barrier Detector
Fall Meeting of the Atomic Energy Society of Japan in Kobe(October 10, 1993).

Kanno, I., Nishio, K., Kimura, I., Nakagome, Y. and Kobayashi, K.
Resistivity Change of Irradiated Si Surface Barrier Detector
Fall Meeting of the Atomic Energy Society of Japan in Kobe(October 10, 1993).

Kanno, I., Kanazawa, S. and Kimura, I.
Response Characteristics of Silicon Surface Barrier Detector
8th. Workshop on Radiation Detectors and Their Uses(at KEK, January, 26, 1994).

Kanno, I., Inbe, T., Kanazawa, S. and Kimura I.
Resistivity Dependence of Plasma Delay in Si Surface Barrier Detector
Annual Meeting of the Atomic Energy Society of Japan in Tsukuba(March 31, 1994).

Kasuga, R., Yamaguchi, T., Yano, D., Yokoyama, A., Takahashi, N., Baba, H. and Shinohara, N.

Fission of the ^{238}U + p System in the Region Near E_x=14MeV
The 37th Symposium on Radiochemistry, Kanazawa(Oct. 6-8, 1993).

Kasuga, R., Yamaguchi, T., Yano, D., Yokoyama, A., Takahashi, N., Baba, H. and Shinohara, N.
Dependence of Excitation Energies Observed in the Proton-Induced Fission of ^{238}U
Spring Annual Meeting of the Chemical Society of Japan, Tokyo(March 29-April 1, 1994)

Kazumata, Y., Okayasu, S., Kumakura, H. and Togano, K.
Ion Irradiation Effects of High Tc Superconductors(IV)
Spring Meeting of the Physical Society of Japan in Sendai(April 1. 1993)

Kazumata, Y., Okayasu, S. and Michigami, O
Ion Irradiation Effects of $EuBa_2Cu_3O_x$
The 3rd IUMRS International Conf. on Advanced Materials in Tokyo(August 31, 1993)

Kumakura, H., Togano, K., Suzuki, M., Tomita, N., Okayasu, S. and Kazumata, Y.
Effects of 180MeV Cu^{11+} on C-Axis Grain Oriented $YBa_2Cu_3O_y$,
Spring Meeting of the Cryogenic Engineering Society of Japan in Tsukuba, Ibaraki(May 20, 1993).

Nasu, S., Oonishi, S., Nanto, H., Yamamoto, R., Tanifuji T., Nakazawa, T., Noda, K., Igarashi, T. and Matsushima, T.
Radiation Damages of wet Amorphuos Silica by Pile and Irradiation
The 41th Spring Meeting of the Japan Society of Applied Physics and Related Societies in Kanagawa(Mar. 28～31, 1994)

Okayasu, S., Kazumata, Y., Teshima, E., Tanaka, M., and Hashimoto, M.
Irradiation Effects on QMG-YBCO Samples
Spring Meeting of the Physical Society of Japan in Fukuoka(March 28, 1994)

Tanaka, H., Tomita, H., Kanamaru, T., Kuribayashi, M., Tsuji, E., Katoh, H., Ishida, K., Tomimitu, H., Kazumata, Y.
Study of the Strain Distributions in Ion-Implanted Perfect Crystals Spring. Meet Jpn. Phys. Soc.(Sendai)(Mar. 1993)

8. Personnel and Committees

(1) Personnel (FY 1993)

Department of Reactor Engineering

	Toru Hiraoka	Director
	Hiroyuki Yoshida	Deputy Director
	Yasuo Suzuki	Deputy Director
	Nobuaki Ogino	Administrative Manager

Accelerators Division

Scientific Staff	Chiaki Kobayashi *
	Suehiro Takeuchi
	Susumu Hanashima
	Michihiro Shibata
Technical Staff	Tadashi Yoshida
(Tandem V.D.G.)	Isao Ohuchi
	Susumu Kanda
	Katsuzo Horie
	Yoshihiro Tsukihashi
	Shinichi Abe
	Shuhei Kanazawa

Nuuclear Data Center

	Yasuyuki Kikuchi *
	Satoshi Chiba
	Tokio Fukahori

Thermal Reactor Physics Laboratory

	Tsuyoshi Yamane
	Shinichiro Meigo
	Kazuo Hasegawa

Fusion Neutronics Laboratory

	Hiroshi Maekawa *
	Yujiro Ikeda

* Head

Accelerator Engineering Laboratory
Motoharu Mizumoto *

Advanced Science Research Center
Tadao Iwata
Research Group for Exotic Heavy Nuclei
Hiroshi Ikezoe *
Yasuharu Sugiyama
Masumi Ohshima
Yoshiaki Tomita
Kazumi Ideno
Yoshimaro Yamanouchi
Michiaki Sugita
Tetsuro Ishii
Shingo Hamada

Research Group for Hadron Transport Theory
Akira Iwamoto *
Toshiki Maruyama
Koji Niita

Research Group for Low-Temperature Radiation Effects
Akihiro Iwase *
Norito Ishikawa

Department of Health Physics
Masamitsu Kikuchi

Radiation Control Division II
Yasunori Harada
Akira Endo

Department of Materials Science and Engineering
Material Innovation Laboratory
Tetsuya Nakazawa

* Head or Leader

Material Processing and Qualification Laboratory
Masami Shindo *

Radiation Effects and Analysis Laboratory
Akimichi Hishinuma *
Takeo Aruga
Shozo Hamada
Tomotsugu Sawai
Katsumaro Fukai

Solid State Physics Laboratory
Yukio Kazumata *
Satoru Okayasu

Neutron Scattering Laboratory
Hiroshi Tomimitsu
Kazunari Aizawa

Radiation and Solid States Laboratory
Hiroshi Maeta *
Masao Sataka

Department of Chemistry and Fuel Research
Analytical Chemistry Laboratory
Michio Hoshi *

Physical Chemistry Laboratory
Mutsuhide Komaki
Jiro Ishikawa

Laser Chemistry Laboratory
Koji Shiraishi *
Katsutoshi Furukawa

Department of Radioisotopes
Isotope Research and Development Division
Nobuo Shinohara

* Head

Yuichiro Nagame
Shin-ichi Ichikawa
Yuichi Hatsukawa
Kazuaki Tsukada
Hideki Iimura
Hiroyuki Sugai

* Head

(2) Tandem Steering Committee

(Chairman)	Tatsuo	Kondo	(Deputy Director General, Tokai Research Establishment)
	Muneyuki	Date	(Director, Advanced Science Research Center)
	Satoru	Funahashi	(Director, Department of Materials Science and Engineering)
	Toru	Hiraoka	(Director, Department of Reactor Engineering)
	Enzo	Tachikawa	(Director, Department of Chemistry and Fuel Research)
	Hisamichi	Yamabayashi	(Director, Department of Radio Isotopes)
(Secretary)	Chiaki	Kobayasi	(Head, Accelerators Division)
(Secretary)	Nobuaki	Ogino	(Administative Manager, Department of Reactor Engineering)

(3) Tandem Consultative Committee

(Chairman)	Shojiro	Matsuura	(Director General, Tokai Research Establishment)
(Vice Chairman)	Tatsuo	Kondo	(Deputy Director General, Tokai Research Establishment)
(Vice Chairman)	Toru	Hiraoka	(Director, Department of Reactor Engineering)
	Mamoru	Akiyama	(Professor, University of Tokyo)
	Hiroyasu	Ejiri	(Professor, Osaka University)
	Ichiro	Fujiwara	(Professor, Otemon Gakuin University)
	Naohiro	Hirakawa	(Professor, Tohoku University)
	Nobutsugu	Imanishi	(Professor, Kyoto University)
	Masayasu	Ishihara	(Research Scientist, Institute of Physical and Chemical Research)
	Shiori	Ishino	(Professor, University of Tokyo)
	Yasuo	Ito	(Associate professor, University of Tokyo)
	Kohzoh	Masuda	(Professor, University of Tsukuba)
	Shunpei	Morinobu	(Professor, Kyushu University)
	Hiromichi	Nakahara	(Professor, Tokyo Metropolitan University)
	Koji	Nakai	(Professor, National Laboratory for High Energy Physics)
	Akito	Takahashi	(Professor, Osaka University)

	Hiroyuki	Tawara	(Associate Professor, Institute of Plasma Physics, Nagoya University)
	Hirosuke	Yagi	(Professor, University of Tsukuba)
	Sadaei	Yamaguchi	(Professor, The Research Institute for Iron Steel and Other Metals, Tohoku University)
(Secretary)	Yasuo	Suzuki	(Deputy Director, Depertment of Reactor Engineering)
(Secretary)	Akihiro	Iwase	(Head, Research Group for Low-Temperature Radiation Effects, Advanced Science Research Center)
(Secretary)	Hiroshi	Ikezoe	(Head, Research Group for Exotic Heavy Nuclei, Advanced Science Research Center)
(Secretary)	Akira	Iwamato	(Head, Research Group for Hadron Transport Theory, Advanced Science Research Center)
(Secretary)	Chiaki	Kobayashi	(Head, Accelerators Division)
(Secretary)	Hiroshi	Maeta	(Head, Radiation and Solid States Laboratory, Depertment of Materials Science and Engineering)
(Secretary)	Kenji	Noda	(Head, Material Innovation Laboratory, Depertment of Materials Science and Engineering)
(Secretary)	Nobuaki	Ogino	(Administrative Manager, Depertment of Reactor Engineering)
(Secretary)	Toshiaki	Sekine	(Department of Radio Isotopes)

9. Cooperative Researches

	Title	Contact person Organization
1.	Study of Neutron-Rich Nuclei Produced by Multi-Nucleon Transfer Reactions	Toru NOMURA Institute for Nuclear Study University of Tokyo
2.	Atomic Collision Research Using Highly Charged Ions	Ken-ichiro KOMAKI Institute of Physics, College of Arts and Sciences, University of Tokyo
3.	Gamma-Ray Spectroscopy in the Neighbour Nuclei of ^{100}Sn	Masao OGAWA Tokyo Institute of Technology
4.	Radiation Effects of High T_c Materials	Hiroaki KUMAKURA National Research Institute for Metals
5.	X-Ray Study of Irradiation Defects Caused by MeV Ion Implantation in Si Perfect Crystals.	Kohtaro ISHIDA Faculty at Science Science University of Tokyo
6.	Study of Higher-Order Effect in Nuclear Collective Motion through Coulomb Excitation	Hideshige KUSAKARI Faculty of Education, Chiba University
7.	Study of Amgulan Momentum Effect on Nuclar Fission	Hiromichi NAKAHARA Faculty of Science, Tokyo Metropolitan University
8.	Study of Total Kinetic Energy Distributions in the Fission Process of the Lead-Bismuth Region.	Jirota KASAGI Laboratory of Nuclear Science Tohoku University
9.	Study of Nuclear Interactions in Heavy-Ion Reaction	Takao NAKAJIMA Department of Physics, Kyushu

		University
10.	Search for High-Spin Isomers in Deformed Potential	Yasuyuki Gōno Faculty of Science Kyushu University
11.	Study of Responce of Semi-Conducter Detector Irradiated by Heavy-Ions	Itsurō KIMURA Faculty of Engineering Kyoto University
12.	Radiation Damage of Materials for Environment Resistance Devices	Kazutoshi OHASHI Faculty of Engineering, Tamagawa University
13.	Irradiation Effect on Electrical Property of LiAl with Li and Other Heavy Ions	Kazuo KURIYAMA Research Center of Ion Beam Technology, Hosei University
14.	Radiation Effects of Li_2O	Shōichi NASU Kanazawa Institute of Technology
15.	Measurement of Double-Differential (n, xα) Reaction Cross Sections for Structual Materials of the Fusion Reactor	Mamoru BABA Faculty of Engineering Tohoku University
16.	Study of Phase Transition on Nuclear Fission Phenomenon	Hiroshi BABA Faculty of Science, Osaka University
17.	Study of D-D Fusion in Solid Using Heary-Ion	Hideo KAYANO Institute for Material Research, Tohoku University